Solid Circulation Rate and Gas Leakage of a Novel Internally Circulating Bubbling Fluidized Bed for Pressurized Chemical Looping

Amanda Alain

Thesis submitted to the University of Ottawa

in partial fulfillment of the requirements for the

Master's of Applied Sciences in Chemical Engineering

Department of Chemical and Biological Engineering

Faculty of Engineering

University of Ottawa

Abstract

To achieve net-zero emissions by the year 2050, carbon capture, utilization and storage technologies must be implemented to decarbonize sectors with hard-to-abate emissions. Pressurized chemical looping (PCL) with a novel reactor design called a plug flow with internal recirculation (PFIR) fluidized bed reactor is proposed as an attractive carbon capture technology to decarbonize small- and medium-scale emitters. The objective of this work was to examine solid circulation rate, gas leakage between reactors, and purge gas fate in a cold flow chemical looping facility. These parameters were used to better understand the PFIR reactor and will be used to validate a computational particle fluid dynamic (CPFD) model of the PFIR reactor to inform the reactor operation and design for a hot flow PCL pilot plant. An energy balance across the fuel reactor was used to determine the solid circulation rate of the bed material, while helium and argon tracer gases were used to determine the amount of gas leaking between reactor sections and the fate of the purge gas, respectively. Statistical analyses were completed to determine the statistical significance of the data.

At the base case condition, the solid circulation rate was 3000 kg/h. Approximately 10% of the fluidizing gas that entered the air reactor moved to the fuel reactor indicating that, with reacting flow, there will be nitrogen infiltrating the fuel reactor, decreasing the purity of the carbon dioxide effluent stream. Furthermore, approximately 31% of the fluidizing gas entering the fuel reactor moved to the air reactor, indicating that, with reacting flow, there will be natural gas leaking into the air reactor, which will increase carbon dioxide emissions. Finally, over half of the purge gases move to the adjacent reactor, which helps prevent gas leakage between reactor sections.

The effect of static bed height, weir opening height and purge configuration on solid circulation rate, gas leakage and purge fate were investigated. The bed height has a small effect on the solid circulation rate and no effect of gas leakage, over the range of bed heights tested. Furthermore, increasing the weir opening height increases both solid circulation rate and gas leakage until the top of the circulation zone is reached. After this point, there is no change in either solid circulation rate or gas leakage. In terms of purge configuration, there appears to be no benefit for having two purge rows. Either one purge row or having a row of blanked tuyeres appear to be optimal as they decrease gas leakage, while having little effect on solid circulation rate. At the jet velocity tested, the vertical purge configuration prevented the solids from circulating, so it is not recommended for this purge configuration to be used in a PFIR reactor without further testing of different jet velocities. Across all configurations, it was shown that as more purge gas moves into the adjacent reactor section, less gas leakage between reactor sections occurs. It

was also determined that the primary method of gas movement between the reactor sections is likely via bubbles and/or jets.

The next step is to complete the validation of CPFD model of the PFIR reactor using the data presented herein. Additional conditions can also be run in the cold flow chemical looping pilot facility to fill in any gaps that are found during the CPFD model validation, or to fill in research gaps in better understanding the PFIR reactor.

Sommaire

Pour atteindre des émissions nettes nulles en 2050, des technologies de capture, d'utilisation et de stockage du carbone doivent être mises en œuvre pour décarboner les secteurs dont les émissions sont difficiles à réduire. La boucle chimique sous pression (PCL) avec une nouvelle conception de lit fluidisé appelée réacteur à recirculation interne à écoulement piston (PFIR) est proposée comme une technologie attrayante de capture du carbone pour décarboniser les émetteurs à petite et moyenne échelle. L'objectif de ce travail était d'examiner le taux de circulation des solides, les fuites de gaz entre les réacteurs et le sort des gaz de purge dans une installation de bouclage chimique à flux froid. Ces paramètres ont été utilisés pour mieux comprendre le réacteur PFIR et seront utilisés pour valider un modèle de dynamique des fluides et particules (CPFD) du réacteur PFIR afin d'informer le fonctionnement et la conception du réacteur pour une usine pilote PCL à flux chaud. Un bilan énergétique à travers le réacteur à combustible a été utilisé pour déterminer le taux de circulation solide du matériau du lit, tandis que les gaz traceurs d'hélium et d'argon ont été utilisés pour déterminer la quantité de gaz qui fuit entre les sections du réacteur et le sort du gaz de purge, respectivement. Des analyses statistiques ont été effectuées pour déterminer la signification statistique des données.

Dans les conditions de base, le débit de circulation solide était de 3000 kg/h. Environ 10% du gaz de fluidisation qui est entré dans le réacteur à air s'est déplacé vers le réacteur à combustible indiquant qu'avec le flux de réaction, il y aura de l'azote s'infiltrant dans le réacteur à combustible, diminuant la pureté du flux d'effluent de dioxyde de carbone. En outre, environ 31 % du gaz de fluidisation entrant dans le réacteur à combustible se sont déplacés vers le réacteur à air, ce qui indique qu'avec le flux de réaction, il y aura une fuite de gaz naturel dans le réacteur à air, ce qui augmentera les émissions de dioxyde de carbone. Enfin, 66,5 % du gaz de purge AR/FR se sont déplacés vers le réacteur à combustible, tandis que 81,1 % du gaz de purge FR/AR se sont déplacés vers le réacteur à air. Ces résultats indiquent que plus de la moitié des gaz de purge se déplacent vers le réacteur adjacent, ce qui aide à prévenir les fuites de gaz entre les sections du réacteur.

L'effet de la hauteur statique du lit, de la hauteur d'ouverture du déversoir et de la configuration de la purge sur le taux de circulation des solides, les fuites de gaz et le sort de la purge a été étudié. La hauteur du lit a un petit effet sur le taux de circulation solide et aucun effet de fuite de gaz, sur la plage de hauteurs de lit testées. De plus, l'augmentation de la hauteur d'ouverture du déversoir augmente à la fois le taux de circulation solide et les fuites de gaz jusqu'à ce que le haut de la zone de circulation soit atteint. Après ce point, il n'y a aucun changement ni dans le taux de circulation solide ni dans les fuites de gaz. En termes

de configuration de purge, il semble n'y avoir aucun avantage à avoir deux rangées de purge. Une rangée de purge ou une rangée de tuyères obturées semblent être optimales car elles diminuent les fuites de gaz, tout en ayant peu d'effet sur le taux de circulation des solides. À la vitesse de jet testée, la configuration de purge verticale a empêché les solides de circuler, et il n'est donc pas recommandé d'utiliser cette configuration de purge dans un réacteur PFIR sans tester davantage les différentes vitesses de jet. Dans toutes les configurations, il a été démontré que plus le gaz de purge se déplace dans la section de réacteur adjacente, moins il se produit de fuite de gaz entre les sections de réacteur. Il a également été déterminé que la principale méthode de mouvement du gaz entre les sections du réacteur est probablement via des bulles et/ou des jets.

La prochaine étape consiste à terminer la validation du modèle CPFD du réacteur PFIR en utilisant les données présentées ici. Des conditions supplémentaires peuvent également être exécutées dans l'installation pilote de boucle chimique à flux froid pour combler les lacunes qui sont trouvées lors de la validation du modèle CPFD, ou pour combler les lacunes de la recherche afin de mieux comprendre le réacteur PFIR.

Statement of contributions

I am the sole author of this thesis. My supervisor, Dr. Arturo Macchi, along with colleagues at CanmetENERGY-Ottawa, Dr. Robin Hughes and Scott Champagne, guided me in my research and provided editorial comments on this thesis. The cold flow chemical looping facility was designed by Scott Champagne and Nicole Bond. The patent for the plug flow with internal recirculation (PFIR) reactor design was by Hatch Ltd. The solid circulation measurement methodology was developed by me, Scott Champagne, and Nicole Bond. The gas composition analysis via gas chromatography was done by the Characterization Lab at CanmetENERGY-Ottawa. All other experimental work was led and completed by me, with help from several colleagues at CanmetENERGY-Ottawa. All post-processing of the data and analysis described in this thesis is my own work.

List of Tables

Table 1. Overview of varied parameters. 8
Table 2. Difference in solid circulation rate between heater configurations at a heater power of 2200 W (± 150 W). 14
Table 3. Difference in solid circulation rate between temperature measurement at three different air flowrates. 16
Table 4. Measurement error for instrumentation used in solid circulation rate analysis. 16
Table 5. Uncertainties used in gas leakage and purge fate analysis. 20
Table 6. Results of Tukey's HSD test for the effect of bed height on the mean solid circulation rate. 24
Table 7. Results of Tukey's HSD test for the effect of weir opening height on the mean solid circulation rate. 26
Table 8. Results of Tukey's HSD test for the effect of purge configuration on the mean solid circulation rate. 27
Table 9. Results of Tukey's HSD test for the effect of weir opening height on the air reactor to fuel reactor gas leakage. 32
Table 10. Results of Tukey's HSD test for the effect of purge configuration on the fuel reactor to air reactor gas leakage. 35
Table 11. Results of Tukey's HSD test for the effect of weir opening height on the percent of AR/FR purge gas that moved into the fuel reactor. 38
Table 12. Results of Tukey's HSD test for the effect of weir opening height on the percent of AR/FR purge gas that moved into the fuel reactor. 39
Table 13. Results of Tukey's HSD test for the effect of purge configuration on the air reactor to fuel reactor gas leakage. 40
Table 14. Results of Tukey's HSD test for the effect of purge configuration on the fuel reactor to air reactor gas leakage. 41
Table 15. Highest coefficient of variation seen in timeseries for all key parameters. 46
Table 16. Mean and population standard deviation of timeseries for solid circulation rate across all conditions. 108
Table 17. Mean and population standard deviation of timeseries for absolute gas leakage across all conditions. 109
Table 18. Mean and population standard deviation of timeseries for percent of gas leakage across all conditions. 110

Table 19. Mean and population standard deviation of timeseries for absolute AR/FR purge gas fate across all conditions. 110
Table 20. Mean and population standard deviation of timeseries for percent AR/FR purge gas fate across all conditions. 111
Table 21. Mean and population standard deviation of timeseries for absolute FR/AR purge gas fate across all conditions. 111
Table 22. Mean and population standard deviation of timeseries for percent FR/AR purge gas fate across all conditions. 112
Table 23. In-depth results from Tukey's HSD test for multiple comparisons comparing the effect of static bed height on solid circulation rate. The p value is reported, followed by the 95% confidence interval in square brackets. 112
Table 24. In-depth results from Tukey's HSD test for multiple comparisons comparing the effect of weir opening height on solid circulation rate. The p value is reported, followed by the 95% confidence interval in square brackets. 113
Table 25. In-depth results from Tukey's HSD test for multiple comparisons comparing the effect of purge configuration on solid circulation rate. The p value is reported, followed by the 95% confidence interval in square brackets. 113
Table 26. In-depth results from Tukey's HSD test for multiple comparisons comparing the effect of weir opening height on air to fuel reactor gas leakage. The p value is reported, followed by the 95% confidence interval in square brackets 114
Table 27. In-depth results from Tukey's HSD test for multiple comparisons comparing the effect of purge configuration on fuel reactor to air reactor gas leakage. The p value is reported, followed by the 95% confidence interval in square brackets. 114
Table 28. In-depth results from Tukey's HSD test for multiple comparisons comparing the effect of weir opening height on percent of AR/FR purge gas that moved into the fuel reactor. The p value is reported, followed by the 95% confidence interval in square brackets. 115
Table 29. In-depth results from Tukey's HSD test for multiple comparisons comparing the effect of weir opening height on percent of FR/AR purge gas that moved into the air reactor. The p value is reported, followed by the 95% confidence interval in square brackets. 115
Table 30. In-depth results from Tukey's HSD test for multiple comparisons comparing the effect of purge fate on percent of AR/FR purge gas that moved into the fuel reactor. The p value is reported, followed by the 95% confidence interval in square brackets. 116

Table 31. In-depth results from Tukey's HSD test for multiple comparisons comparing the effect of purge fate on percent of FR/AR purge gas that moved into the air reactor. The p value is reported, followed by the 95% confidence interval in square brackets. 116

List of Figures

Figure 1. Schematic of the chemical looping process. 2
Figure 2. Simplified diagram of the PFIR reactor, showing (A) the top-down view, (B) side view at one of the weirs, and (C) 3D view[13]. 3
Figure 3. Annotated diagram showing the top-down view of the cold flow PFIR column with important measurements. 6
Figure 4. Tuyere layout in the cold flow PFIR column. 7
Figure 5.Diagrams of purge tuyere configurations: (A) no purge row configuration, (B) blanked purge row configuration, (C) one purge row configuration, (D) two AR/FR purge row configuration, (E) one vertical purge row configuration. 9
Figure 6. Experimental concept for quantifying solid circulation rate. FT indicates the location of flowmeters and TE indicates the location of the type AA RTDs. The control volume is indicated by the red dashed box. 10
Figure 7. Solids and gas temperatures at a typical test condition. 11
Figure 8. The average differential temperature (out – in) of the solids and the gas throughout a typical test condition. 12
Figure 9. In-bed electric heater configurations, showing the three cartridge heater (A,B) and the seven cartridge heater (C,D). A front view diagram of the three-cartridge heater holder is shown in (A), with a photo of the top-down view in (B). A front view diagram of the seven-cartridge heater holder is shown in (C), with a photo of the top-down view in (D). 13
Figure 10. Photos of (A) the three vertical RTDs configuration and (B) the two-point RTD configuration. The approximate solids temperature measurement locations are indicated on the photos by yellow stars. 15
Figure 11. Experimental concept for quantifying gas bypassing for helium injection into the fuel reactor. FT indicates the location of flowmeters and AP indicates the location where the gas bag sample are taken from 17
Figure 12. Representative timeseries graphs for solid circulation rate. 21
Figure 13. Representative timeseries graphs for gas leakage. 22
Figure 14. Representative timeseries graphs for purge gas fate. 22
Figure 15. The effect of static bed height on solid circulation rate. The base case is indicated by the data points with a black outline. 24

Figure 16. The effect of weir opening height on solid circulation rate. The base case is indicated by the data points with a black outline. 25
Figure 17. The effect of purge configuration on solid circulation rate. The base case is indicated by the data points with a black outline. 27
Figure 18. The effect of static bed height on gas leakage between reactor sections as a function of (A) gas flow rate and (B) percent of the gas entering the reactor section in the air reactor or fuel reactor. The base case is indicated by the data points with a black outline. 29
Figure 19. The effect of weir opening height on gas leakage between reactor sections as a function of (A) gas flow rate and (B) percent of the gas entering the reactor section in the air reactor or fuel reactor. The base case is indicated by the data points with a black outline. 31
Figure 20. The effect of purge configuration on gas leakage between reactor sections as a function of (A) gas flow rate and (B) percent of the gas entering the reactor section in the air reactor or fuel reactor. The base case is indicated by the data points with a black outline. 34
Figure 21. The effect of static bed height on AR/FR purge gas fate. The base case is indicated by the data points with a black outline. 36
Figure 22. The effect of static bed height on FR/AR purge gas fate. The base case is indicated by the data points with a black outline. 37
Figure 23. The effect of weir opening height on AR/FR purge gas fate. The base case is indicated by the data points with a black outline. 38
Figure 24. The effect of weir opening height on FR/AR purge gas fate. The base case is indicated by the data points with a black outline. 39
Figure 25. The effect of purge configuration on AR/FR purge gas fate. The base case is indicated by the data points with a black outline. 40
Figure 26. The effect of purge configuration on FR/AR purge gas fate. The base case is indicated by the data points with a black outline. 41
Figure 27. Relationship between solid circulation rate and gas leakage across the base case and all bed height and weir height conditions. 43
Figure 28. Relationship between solid circulation rate and the amount of purge gas that moved to adjacent reactor across the base case and all bed height and weir height conditions. 44
Figure 29. Relationship between the amount of purge gas that moved to adjacent reactor and gas leakage across the base case and all bed height and weir height conditions. 45
Figure 30. Timeseries graphs for solid circulation rate at the base case condition (first repeat). 50

Figure 31. Timeseries graphs for solid circulation rate at the base case condition (second repeat). 50
Figure 32. Timeseries graphs for solid circulation rate at the base case condition (third repeat). 51
Figure 33. Timeseries graphs for solid circulation rate at the base case condition (forth repeat). 51
Figure 34. Timeseries graphs for solid circulation rate at the base case condition (fifth repeat). 51
Figure 35. Timeseries graphs for air reactor to fuel reactor gas leakage at the base case condition (first repeat)..... 52
Figure 36. Timeseries graphs for air reactor to fuel reactor gas leakage at the base case condition (second repeat)..... 52
Figure 37. Timeseries graphs for air reactor to fuel reactor gas leakage at the base case condition (third repeat)..... 52
Figure 38. Timeseries graphs for fuel reactor to air reactor gas leakage at the base case condition (first repeat)..... 53
Figure 39. Timeseries graphs for fuel reactor to air reactor gas leakage at the base case condition (second repeat)..... 53
Figure 40. Timeseries graphs fate of the amount of AR/FR purge gas that remained in the air reactor at the base case condition (first repeat). 54
Figure 41. Timeseries graphs fate of the amount of AR/FR purge gas that remained in the air reactor at the base case condition (second repeat). 54
Figure 42. Timeseries graphs fate of the amount of AR/FR purge gas that remained in the air reactor at the base case condition (third repeat)..... 55
Figure 43. Timeseries graphs fate of the amount of AR/FR purge gas that moved to the fuel reactor at the base case condition (first repeat). 55
Figure 44. Timeseries graphs fate of the amount of AR/FR purge gas that moved to the fuel reactor at the base case condition (second repeat). 56
Figure 45. Timeseries graphs fate of the amount of AR/FR purge gas that moved to the fuel reactor at the base case condition (third repeat). 56
Figure 46. Timeseries graphs fate of the amount of FR/AR purge gas that moved to air reactor at the base case condition (first repeat). 57
Figure 47. Timeseries graphs fate of the amount of FR/AR purge gas that moved to air reactor at the base case condition (second repeat). 57
Figure 48. Timeseries graphs fate of the amount of FR/AR purge gas that remained in the fuel reactor at the base case condition (first repeat). 58

Figure 49. Timeseries graphs fate of the amount of FR/AR purge gas that remained in the fuel reactor at the base case condition (second repeat). 58
Figure 50. Timeseries graphs for solid circulation rate at the 0.15 m bed height condition (first repeat). 59
Figure 51. Timeseries graphs for solid circulation rate at the 0.15 m bed height condition (second repeat). 59
Figure 52. Timeseries graphs for air reactor to fuel reactor gas leakage at the 0.15 m bed height condition. 59
Figure 53. Timeseries graphs for fuel reactor to air reactor gas leakage at the 0.15 m bed height condition. 60
Figure 54. Timeseries graphs fate of the amount of AR/FR purge gas that remained in the air reactor at the 0.15 m bed height condition. 60
Figure 55. Timeseries graphs fate of the amount of AR/FR purge gas that moved to the fuel reactor at the 0.15 m bed height condition. 61
Figure 56. Timeseries graphs fate of the amount of FR/AR purge gas that moved to the air reactor at the 0.15 m bed height condition. 61
Figure 57. Timeseries graphs fate of the amount of FR/AR purge gas that remained in the fuel reactor at the 0.15 m bed height condition. 62
Figure 58. Timeseries graphs for solid circulation rate at the 0.25 m bed height condition (first repeat). 62
Figure 59. Timeseries graphs for solid circulation rate at the 0.25 m bed height condition (second repeat). 63
Figure 60. Timeseries graphs for air reactor to fuel reactor gas leakage at the 0.25 m bed height condition. 63
Figure 61. Timeseries graphs for fuel reactor to air reactor gas leakage at the 0.25 m bed height condition. 63
Figure 62. Timeseries graphs fate of the amount of AR/FR purge gas that remained in the air reactor at the 0.25 m bed height condition. 64
Figure 63. Timeseries graphs fate of the amount of AR/FR purge gas that moved to the fuel reactor at the 0.25 m bed height condition. 64
Figure 64. Timeseries graphs fate of the amount of FR/AR purge gas that moved to the air reactor at the 0.25 m bed height condition. 65
Figure 65. Timeseries graphs fate of the amount of FR/AR purge gas that remained in the fuel reactor at the 0.25 m bed height condition. 65

Figure 66. Timeseries graphs for solid circulation rate at the 0.35 m bed height condition (first repeat). 66
Figure 67. Timeseries graphs for solid circulation rate at the 0.35 m bed height condition (second repeat). 66
Figure 68. Timeseries graphs for air reactor to fuel reactor gas leakage at the 0.35 m bed height condition. 66
Figure 69. Timeseries graphs for fuel reactor to air reactor gas leakage at the 0.35 m bed height condition. 67
Figure 70. Timeseries graphs fate of the amount of AR/FR purge gas that remained in the air reactor at the 0.35 m bed height condition. 67
Figure 71. Timeseries graphs fate of the amount of AR/FR purge gas that moved to the fuel reactor at the 0.35 m bed height condition. 68
Figure 72. Timeseries graphs fate of the amount of FR/AR purge gas that moved to the air reactor at the 0.35 m bed height condition. 68
Figure 73. Timeseries graphs fate of the amount of FR/AR purge gas that remained in the fuel reactor at the 0.35 m bed height condition. 69
Figure 74. Timeseries graphs for solid circulation rate at the 0.05 m weir opening height condition (first repeat)..... 69
Figure 75. Timeseries graphs for solid circulation rate at the 0.05 m weir opening height condition (second repeat)..... 70
Figure 76. Timeseries graphs for solid circulation rate at the 0.05 m weir opening height condition (third repeat)..... 70
Figure 77. Timeseries graphs for solid circulation rate at the 0.05 m weir opening height condition (forth repeat)..... 70
Figure 78. Timeseries graphs for air reactor to fuel reactor gas leakage at the 0.05 m weir opening height condition (first repeat). 71
Figure 79. Timeseries graphs for air reactor to fuel reactor gas leakage at the 0.05 m weir opening height condition (second repeat). 71
Figure 80. Timeseries graphs for fuel reactor to air reactor gas leakage at the 0.05 m weir opening height condition (first repeat). 72
Figure 81. Timeseries graphs for fuel reactor to air reactor gas leakage at the 0.05 m weir opening height condition (second repeat). 72

Figure 82. Timeseries graphs fate of the amount of AR/FR purge gas that remained in the air reactor at the 0.05 m weir opening height condition (first repeat). 73
Figure 83. Timeseries graphs fate of the amount of AR/FR purge gas that remained in the air reactor at the 0.05 m weir opening height condition (second repeat). 73
Figure 84. Timeseries graphs fate of the amount of AR/FR purge gas that moved to the fuel reactor at the 0.05 m weir opening height condition (first repeat). 74
Figure 85. Timeseries graphs fate of the amount of AR/FR purge gas that moved to the fuel reactor at the 0.05 m weir opening height condition (second repeat). 74
Figure 86. Timeseries graphs fate of the amount of FR/AR purge gas that moved to the air reactor at the 0.05 m weir opening height condition (first repeat). 75
Figure 87. Timeseries graphs fate of the amount of FR/AR purge gas that moved to the air reactor at the 0.05 m weir opening height condition (second repeat). 75
Figure 88. Timeseries graphs fate of the amount of FR/AR purge gas that remained in the fuel reactor at the 0.05 m weir opening height condition (first repeat). 76
Figure 89. Timeseries graphs fate of the amount of FR/AR purge gas that remained in the fuel reactor at the 0.05 m weir opening height condition (second repeat). 76
Figure 90. Timeseries graphs for solid circulation rate at the 0.125 m weir opening height condition (first repeat)..... 77
Figure 91. Timeseries graphs for solid circulation rate at the 0.125 m weir opening height condition (second repeat). 77
Figure 92. Timeseries graphs for solid circulation rate at the 0.125 m weir opening height condition (third repeat)..... 77
Figure 93. Timeseries graphs for air reactor to fuel reactor gas leakage at the 0.125 m weir opening height condition (first repeat). 78
Figure 94. Timeseries graphs for air reactor to fuel reactor gas leakage at the 0.125 m weir opening height condition (second repeat). 78
Figure 95. Timeseries graphs for fuel reactor to air reactor gas leakage at the 0.125 m weir opening height condition (first repeat). 79
Figure 96. Timeseries graphs for fuel reactor to air reactor gas leakage at the 0.125 m weir opening height condition (second repeat). 79
Figure 97. Timeseries graphs fate of the amount of AR/FR purge gas that remained in the air reactor at the 0.125 m weir opening height condition (first repeat). 80

Figure 98. Timeseries graphs fate of the amount of AR/FR purge gas that remained in the air reactor at the 0.125 m weir opening height condition (second repeat). 80
Figure 99. Timeseries graphs fate of the amount of AR/FR purge gas that moved to the fuel reactor at the 0.125 m weir opening height condition (first repeat). 81
Figure 100. Timeseries graphs fate of the amount of AR/FR purge gas that moved to the fuel reactor at the 0.125 m weir opening height condition (second repeat). 81
Figure 101. Timeseries graphs fate of the amount of FR/AR purge gas that moved to the air reactor at the 0.125 m weir opening height condition (first repeat). 82
Figure 102. Timeseries graphs fate of the amount of FR/AR purge gas that moved to the air reactor at the 0.125 m weir opening height condition (second repeat). 82
Figure 103. Timeseries graphs fate of the amount of FR/AR purge gas that remained in the fuel reactor at the 0.125 m weir opening height condition (first repeat). 83
Figure 104. Timeseries graphs fate of the amount of FR/AR purge gas that remained in the fuel reactor at the 0.125 m weir opening height condition (second repeat). 83
Figure 105. Timeseries graphs for solid circulation rate at the 0.15 m weir opening height condition (first repeat) 84
Figure 106. Timeseries graphs for solid circulation rate at the 0.15 m weir opening height condition (second repeat). 84
Figure 107. Timeseries graphs for air reactor to fuel reactor gas leakage at the 0.15 m weir opening height condition (first repeat). 84
Figure 108. Timeseries graphs for air reactor to fuel reactor gas leakage at the 0.15 m weir opening height condition (second repeat). 85
Figure 109. Timeseries graphs for fuel reactor to air reactor gas leakage at the 0.15 m weir opening height condition. 85
Figure 110. Timeseries graphs fate of the amount of AR/FR purge gas that remained in the air reactor at the 0.15 m weir opening height condition (first repeat). 86
Figure 111. Timeseries graphs fate of the amount of AR/FR purge gas that remained in the air reactor at the 0.15 m weir opening height condition (second repeat). 86
Figure 112. Timeseries graphs fate of the amount of AR/FR purge gas that moved to the fuel reactor at the 0.15 m weir opening height condition (first repeat). 87
Figure 113. Timeseries graphs fate of the amount of AR/FR purge gas that moved to the fuel reactor at the 0.15 m weir opening height condition (second repeat). 87

Figure 114. Timeseries graphs fate of the amount of FR/AR purge gas that moved to the air reactor at the 0.15 m weir opening height condition. 88
Figure 115. Timeseries graphs fate of the amount of FR/AR purge gas that remained in the fuel reactor at the 0.15 m weir opening height condition. 88
Figure 116. Timeseries graphs for solid circulation rate at the no purge tuyere condition (first repeat). . 89
Figure 117. Timeseries graphs for solid circulation rate at the no purge tuyere condition (second repeat). 89
Figure 118. Timeseries graphs for solid circulation rate at the no purge tuyere condition (third repeat). 89
Figure 119. Timeseries graphs for air reactor to fuel reactor gas leakage at the no purge tuyere condition (first repeat). 90
Figure 120. Timeseries graphs for air reactor to fuel reactor gas leakage at the no purge tuyere condition (second repeat). 90
Figure 121. Timeseries graphs for fuel reactor to air reactor gas leakage at the no purge tuyere condition (first repeat). 90
Figure 122. Timeseries graphs for fuel reactor to air reactor gas leakage at the no purge tuyere condition (second repeat). 91
Figure 123. Timeseries graphs for solid circulation rate at the blank purge tuyere condition (first repeat). 91
Figure 124. Timeseries graphs for solid circulation rate at the blank purge tuyere condition (second repeat)..... 91
Figure 125. Timeseries graphs for solid circulation rate at the blank purge tuyere condition (third repeat). 92
Figure 126. Timeseries graphs for solid circulation rate at the blank purge tuyere condition (forth repeat). 92
Figure 127. Timeseries graphs for air reactor to fuel reactor gas leakage at the blank purge tuyere condition (first repeat). 92
Figure 128. Timeseries graphs for air reactor to fuel reactor gas leakage at the blank purge tuyere condition (second repeat)..... 93
Figure 129. Timeseries graphs for fuel reactor to air reactor gas leakage at the blank purge tuyere condition (first repeat). 93
Figure 130. Timeseries graphs for fuel reactor to air reactor gas leakage at the blank purge tuyere condition (second repeat)..... 93

Figure 131. Timeseries graphs for solid circulation rate at the vertical purge tuyere condition (first repeat). 94
Figure 132. Timeseries graphs for solid circulation rate at the vertical purge tuyere condition (second repeat)..... 94
Figure 133. Timeseries graphs for solid circulation rate at the vertical purge tuyere condition (third repeat). 94
Figure 134. Timeseries graphs for solid circulation rate at the vertical purge tuyere condition (forth repeat)..... 95
Figure 135. Timeseries graphs for air reactor to fuel reactor gas leakage at the vertical purge tuyere condition (first repeat). 95
Figure 136. Timeseries graphs for air reactor to fuel reactor gas leakage at the vertical purge tuyere condition (second repeat)..... 95
Figure 137. Timeseries graphs for fuel reactor to air reactor gas leakage at the vertical purge tuyere condition (first repeat). 96
Figure 138. Timeseries graphs for fuel reactor to air reactor gas leakage at the vertical purge tuyere condition (second repeat)..... 96
Figure 139. Timeseries graphs fate of the amount of AR/FR purge gas that remained in the air reactor at the vertical purge tuyere condition (first repeat). 97
Figure 140. Timeseries graphs fate of the amount of AR/FR purge gas that remained in the air reactor at the vertical purge tuyere condition (second repeat). 97
Figure 141. Timeseries graphs fate of the amount of AR/FR purge gas that moved to the fuel reactor at the vertical purge tuyere condition (first repeat). 98
Figure 142. Timeseries graphs fate of the amount of AR/FR purge gas that moved to the fuel reactor at the vertical purge tuyere condition (second repeat). 98
Figure 143. Timeseries graphs fate of the amount of FR/AR purge gas that moved to the air reactor at the vertical purge tuyere condition (first repeat). 99
Figure 144. Timeseries graphs fate of the amount of FR/AR purge gas that moved to the air reactor at the vertical purge tuyere condition (second repeat). 99
Figure 145. Timeseries graphs fate of the amount of FR/AR purge gas that remained in the fuel reactor at vertical purge tuyere condition (first repeat). 100
Figure 146. Timeseries graphs fate of the amount of FR/AR purge gas that remained in the fuel reactor at vertical purge tuyere condition (first repeat). 100

Figure 147. Timeseries graphs for solid circulation rate at the two AR/FR purge tuyere condition (first repeat)..... 101
Figure 148. Timeseries graphs for solid circulation rate at the two AR/FR purge tuyere condition (second repeat)..... 101
Figure 149. Timeseries graphs for solid circulation rate at the two AR/FR purge tuyere condition (third repeat)..... 102
Figure 150. Timeseries graphs for solid circulation rate at the two AR/FR purge tuyere condition (forth repeat)..... 102
Figure 151. Timeseries graphs for air reactor to fuel reactor gas leakage at the two AR/FR purge tuyere condition (first repeat)..... 102
Figure 152. Timeseries graphs for air reactor to fuel reactor gas leakage at the two AR/FR purge tuyere condition (second repeat)..... 103
Figure 153. Timeseries graphs for fuel reactor to air reactor gas leakage at the two AR/FR purge tuyere condition (first repeat)..... 103
Figure 154. Timeseries graphs for fuel reactor to air reactor gas leakage at the two AR/FR purge tuyere condition (second repeat)..... 103
Figure 155. Timeseries graphs fate of the amount of AR/FR purge gas that remained in the air reactor at the two AR/FR purge tuyere condition (first repeat)..... 104
Figure 156. Timeseries graphs fate of the amount of AR/FR purge gas that remained in the air reactor at the two AR/FR purge tuyere condition (second repeat). 104
Figure 157. Timeseries graphs fate of the amount of AR/FR purge gas that moved to the fuel reactor at the two AR/FR purge tuyere condition (first repeat)..... 105
Figure 158. Timeseries graphs fate of the amount of AR/FR purge gas that moved to the fuel reactor at the two AR/FR purge tuyere condition (second repeat). 105
Figure 159. Timeseries graphs fate of the amount of FR/AR purge gas that moved to the air reactor at the two AR/FR purge tuyere condition (first repeat)..... 106
Figure 160. Timeseries graphs fate of the amount of FR/AR purge gas that moved to the air reactor at the two AR/FR purge tuyere condition (second repeat)..... 106
Figure 161. Timeseries graphs fate of the amount of FR/AR purge gas that remained in the fuel reactor at two AR/FR purge tuyere condition (first repeat)..... 107
Figure 162. Timeseries graphs fate of the amount of FR/AR purge gas that remained in the fuel reactor at two AR/FR purge tuyere condition (first repeat)..... 107

Nomenclature

Variables

C_p	Heat capacity [J/kgK]
c_4	Tabulated constant to estimate the population standard deviation
$\dot{m}$	Mass flowrate [kg/h]
s	Sample standard deviation [various]
P_{heater}	Heater power [W]
T	Temperature [°C or K]
x	Mass concentration [-]
y	Mol concentration [-]
μ	Average [various]
σ	Population standard deviation [various]

Subscripts

Ar	Argon
AR	Air reactor
AR→FR	Air reactor to fuel reactor
Ar+O_2	Argon and oxygen
FR	Fuel reactor
FR→AR	Fuel reactor to air reactor
He	Helium
N_2	Nitrogen
O_2	Oxygen
ref	Reference
solid	Bed material

Abbreviations

ANOVA	Analysis of variance
AR/FR	Air reactor-fuel reactor
CCUS	Carbon capture, utilization, and storage
CL	Control limit
CO_2	Carbon dioxide
CPFD	Computational particle fluid dynamic model
FR/AR	Fuel reactor-air reactor
HSD	Honest significant difference
PCL	Pressurized chemical looping
PFIR	Plug flow with internal recirculation
RTD	Resistance temperature detector

Acknowledgements

First and foremost, I would like to express my sincerest gratitude to my supervisor, Dr. Arturo Macchi, for his support and insight throughout my graduate studies in both professional and personal matters. Our weekly meetings were always something I looked forward to.

I wish to also thank all my colleagues in the Industrial Decarbonization team at CanmetENERGY-Ottawa, who offered support through good humour and baked goods, and without whom this work would not be possible. Specifically, I owe thanks to Dr. Robin Hughes who provided valuable guidance and encouraged me to become a better researcher. I am grateful to Scott Champagne for his mentorship. I would also like to thank Stephen Montero for his mechanical design expertise, and Christopher Mallon for his support in operating the cold flow chemical looping facility.

Furthermore, I owe thanks to the team at Hatch Ltd., including Sabrina Francey and Christopher McIntyre, for their guidance on development of the cold flow plug flow with internal recirculation (PFIR) reactor.

I am grateful to my family and friends for their support and encouragement. I am especially grateful to my husband, Brendan, who has been one of my biggest supporters and never fails to make me smile.

Finally, I would like to acknowledge the financial support I received from both the University of Ottawa and Natural Resources Canada for the completion of this research.

Table of contents

Abstract ii

Sommaire iv

Statement of contributions vi

List of Tables vii

List of Figures x

Nomenclature xx

Acknowledgements xxi

1 Introduction 1

1.1 Chemical looping 1

1.2 Plug flow with internal recirculation (PFIR) reactor 3

1.3 Research objectives 5

2 Experimental setup and methodology 5

2.1 Experimental setup of the PFIR column 5

2.2 Solid circulation rate methodology 10

2.2.1 Comparison of two heater configuration 12

2.2.2 Comparison of two temperature measurement configurations 14

2.2.3 Maximum measurement error in key measurements for calculating solid circulation rate 16

2.3 Gas leakage and purge gas fate methodology 16

2.3.1 Maximum measurement error in key measurements for calculating gas leakage and purge gas fate 20

2.4 Timeseries and statistical analysis 20

3 Results and discussion 23

3.1 Solid circulation rate 23

3.1.1 Varying the static bed height 23

3.1.2 Varying the weir opening height 25
3.1.3 Varying the purge configuration 26
3.2 Gas leakage 28
3.2.1 Varying static bed height 28
3.2.2 Varying the weir opening height 30
3.2.3 Varying the purge configuration 32
3.3 Purge gas fate 35
3.3.1 Varying the static bed height 36
3.3.2 Varying the weir opening height 37
3.3.3 Varying the purge configuration 40
3.4 Relationship between solid circulation rate, gas leakage and purge fate 42
4 Conclusions and recommendations 46
5 References 48
Appendix A: Additional data, tables, and figures 50
Timeseries graphs for all data points 50
Mean and population standard deviation for all data points 108
Tukey's HSD test results tables 112
Appendix B: Solid circulation rate methods that were considered 117

1 Introduction

The concentration of global atmospheric carbon dioxide (CO_2) has risen by about 76 ppm in the past 40 years, with an average concentration in 2022 of about 417 ppm [1]. These emissions are contributing to climate change and must be mitigated to prevent the worst impacts due to climate change [2]. Adopted in 2015, the Paris Agreement is an international treaty which has the goal to limit the global average temperature increase to below 2°C compared to pre-industrial levels, with efforts to limit the increase to 1.5°C [3]. To achieve the goal set out by the Paris Agreement, countries must transition to net-zero carbon dioxide emissions by the year 2050 [2]. To achieve net-zero emissions by 2050 in Canada, multiple approaches must be taken. Canada plans to have a 100% clean electrical grid by 2035. A clean electrical grid combined with electrification of end-use sectors are a big part of Canada's strategy to achieve net-zero emissions by 2050 [4]. Unfortunately, not all sectors can be easily electrified. In these situations, one option to mitigate carbon dioxide emissions is to implement carbon capture, utilisation, and storage (CCUS).

CCUS includes methods that remove carbon dioxide from emission sources, and either recycling the captured carbon dioxide for use in another process or storing the carbon dioxide permanently in reservoirs, such as saline aquafers [5]. All carbon capture technologies can be categorized into one of three groups: pre-combustion capture, post-combustion capture, and oxy-fuel combustion. Pre-combustion capture removes the carbon dioxide from the fuel feed stream. This happens through gasification and water-gas shift reactions where the fuel is converted to carbon dioxide and hydrogen [6]. The carbon dioxide and hydrogen can be separated, and the hydrogen can be used as a clean fuel. Post-combustion capture removes carbon dioxide from the flue gas streams. Carbon dioxide is separated from nitrogen in the flue gas using an additional unit such as an amine scrubber [6]. Oxy-fuel combustion uses high-purity oxygen to combust fuel. The flue gas does not contain nitrogen, so purifying the carbon in the flue gas stream is relatively easy compared to post-combustion capture.

1.1 Chemical looping

Chemical looping is a carbon capture technology that can be used to produce heat, steam, or hydrogen by intrinsically capturing carbon dioxide. It is considered an oxy-fuel combustion capture technology as it uses high-purity oxygen to combust fuel. Conventional oxy-fuel combustion obtains high-purity oxygen from an air separation unit, which is relatively costly and energy intensive [6]. With chemical looping, the oxygen is supplied via a solid oxygen carrier by undergoing cyclical oxidation and reduction reactions. The

oxygen carrier can be a synthetic or natural metal oxide, typically containing nickel, iron, manganese and/or copper [7].

A diagram of the chemical looping process is shown in Figure 1. Chemical looping typically operates as a dual fluidized bed with the oxygen carrier as the bed material. One of the reactors, called the air reactor, is fluidized with air. The other reactor, called the fuel reactor, is fluidized with fuel or an inert gas, if solid fuel is used. The oxygen from the air is transported from the air reactor to the fuel reactor via the oxygen carrier [8]. The oxygen carrier is oxidized by air in the air reactor and is reduced by the fuel in the fuel reactor. The oxygen carrier is transported back to the air reactor and the cycle repeats itself. The oxygen carrier allows for air and fuel streams to remain separate, which ideally yields a high-purity carbon dioxide flue gas from the fuel reactor after water condensation occurs, and vitiated air from the air reactor [8].

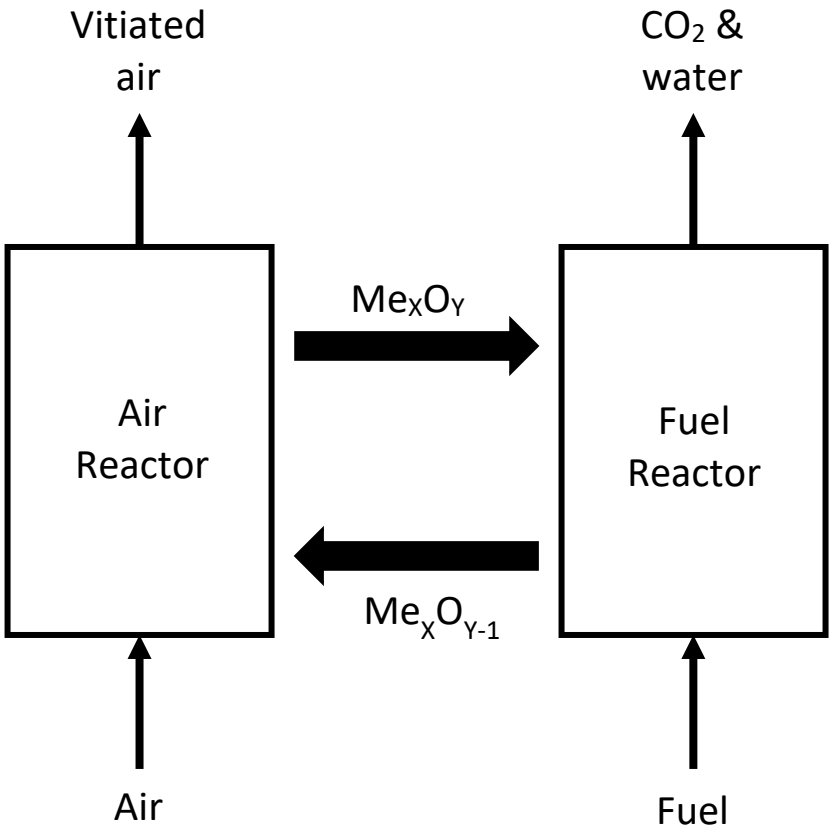

Figure 1. Schematic of the chemical looping process.

Pressurized chemical looping (PCL) offers some advantages over atmospheric operation. It improves the overall process efficiency by increasing reaction rates, lowering fresh water consumption due to water recovery during CO_2 processing, and enhancing latent heat recovery [9], [10]. Technoeconomic analyses

have determined that PCL may decrease costs compared to traditional systems. The cost of carbon dioxide captured could decrease to $44 CAD/t from $75 CAD/t when using pressurized chemical looping for steam assisted gravity drainage compared to atmospheric operation, using 2018 as the cost reference year [10]. Furthermore, it has been found that pressurized chemical looping for hydrogen production reduced fuel demand by 16% and water make-up by 42% compared to traditional steam methane reformers [11].

1.2 Plug flow with internal recirculation (PFIR) reactor

A novel reactor design concept patented by Hatch Ltd. [12], called the plug flow with internal recirculation (PFIR) reactor, is currently being developed for use in PCL as a collaboration between Hatch Ltd. and CanmetENERGY. The PFIR reactor is an annular dual fluidized bed reactor that allows for both the air reactor and the fuel reactor to be collocated in the same pressure vessel, shown in Figure 2. The air and fuel reactive zones are separated by weirs, with openings at the bottom of the weir closest to the distributor plate. The weir openings allow for internal solids transfer of oxygen carrier. Angled jets on the distributor plate induce angular momentum, which allows the oxygen carrier to be transported between reactor sections.

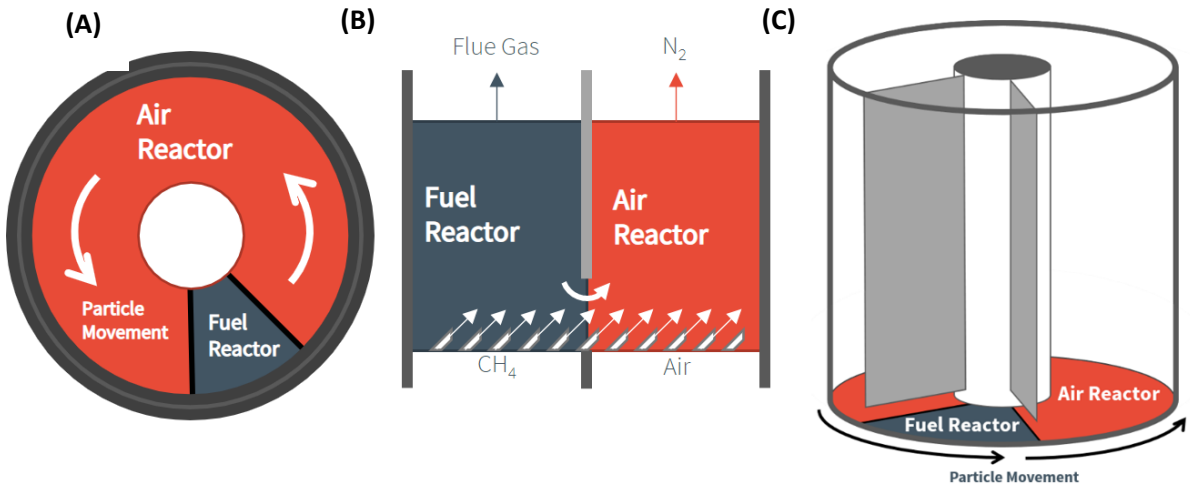

Figure 2. Simplified diagram of the PFIR reactor, showing (A) the top-down view, (B) side view at one of the weirs, and (C) 3D view[13].

Using a PFIR reactor for PCL instead of the traditional dual interconnected fluidized beds has a few advantages. Operational issues and downtime are expected to decrease with a PFIR reactor, since the reactor does not require external solids transfer. The PFIR reactor should be less prone to erosion from bed material, since it can be operated as a bubbling fluidized bed instead of circulating fluidized bed, and

there are no solids transfer lines between reactors. Finally, the PFIR reactor is more compact, which means it should be able to fit in existing facilities more easily compared to dual interconnected fluidized beds.

The solid circulation rate of oxygen carrier is a key parameter to characterize, as it will indicate if the PFIR reactor is suitable for PCL. The solid circulation rate needs to be sufficiently high to achieve the required fuel conversion and oxygen transport, and to ensure sufficient heat exchange between the reactors [8], [14]. CPFD modelling of the PFIR reactor indicated that solid circulation rate increases with the rate of fluid momentum entering the PFIR reactor through the distributor plate [15]. Understanding how different geometrical and operating parameters in the PFIR affect solid circulation rate is important in ensuring the success of a PFIR reactor for PCL.

To ensure optimal performance and carbon capture efficiency, air leaking into the fuel reactor or fuel leaking into the air reactor via the weir openings must be avoided as much as possible. Gaseous fuel leaking into the air reactor will combust in the air reactor, increasing carbon dioxide emissions. Air leaking into the fuel reactor will reduce the carbon dioxide purity [8]. With a more dilute carbon dioxide stream from the fuel reactor, the cost of carbon capture will increase to purify the carbon dioxide to achieve the desired composition specifications. Gas leakage in the PFIR reactor occurs when some of the fluidizing gas in one reactor section enters the other reactor section through the weir openings. Understanding how geometrical and operating parameters affect gas leakage is thus important to understand the economics of the PFIR for PCL as it will inform the amount of CO_2 purification that is needed downstream of the PFIR reactor.

Gas leakage between reactor sections of the PFIR reactor can occur in two ways: directly as the directional gas jets near the weir opening and indirectly as interstitial gas that circulates with the solids. To prevent gas leakage, the boundaries between the reactor sections can be purged with a condensable gas, such as steam. Some number of nozzles upstream of the solids outlet from the reactor section would be fed by purge gas. The goal of the purge gas is to sweep the fluidizing and product gas away from the boundary, preventing any of these gases from crossing the weir opening into the adjacent reactor section. Furthermore, understanding where the purge gas ends up is important for better understanding the PFIR reactor as it is a novel reactor configuration.

PCL with a PFIR reactor shows potential for decarbonizing small- and medium-scale industrial fired heaters and utility boilers. There are over 1300 of these sites across Canada emitting less than 115 000 t CO_2/year per facility [16]. Decarbonizing these facilities is required to achieve net-zero emissions by 2050, but most

research and development effort is focused on decarbonizing the larger emitters. Small- and medium-scale emitters pose some challenges as they generally do not have the space to retrofit an existing facility with post combustion capture, and oxy-fuel combustion is generally too expensive at this scale. PCL with a PFIR reactor will ensure a more economical, compact solution to decarbonizing these emitters.

To determine the suitability of the PFIR reactor for PCL, a 600 kW_{th} PCL pilot plant will be constructed at CanmetENERGY in Ottawa, Ontario as a collaboration between Hatch Ltd. and CanmetENERGY. A computational particle fluid dynamic (CPFD) model of the PFIR reactor was introduced by McIntyre [15], which used parameters from a validated CPFD model of a traditional bubbling fluidized bed. To ensure that the CPFD model of the PFIR reactor is modelling the hydrodynamics of the PFIR reactor properly, experimental data is required. A cold-flow pilot plant of the PFIR has been built at CanmetENERGY to obtain experimental data to better understand the PFIR reactor and to validate the CPFD model of the PFIR reactor. Once validated, the CPFD model can be used more confidently to design components of the PFIR reactor for the PCL pilot plant, such as the distributor plate.

1.3 Research objectives

The purpose of this thesis is to investigate key performance indicators of the PFIR reactor using a cold flow chemical looping pilot facility. These key performance indicators will be used to validate a CPFD model of the PFIR reactor to inform operating conditions and design of a hot flow PCL pilot facility. The specific objectives of the research are as follows:

1. Determine the effect of bed height, weir opening height and purge configuration on solid circulation rate in the PFIR reactor.
2. Determine the effect of bed height, weir opening height and purge configuration on gas leakage via the weir opening between reactor sections in the PFIR reactor.
3. Determine the fate of the purge gases after they are introduced into the PFIR reactor via the purge tuyeres on the distributor plate.

2 Experimental setup and methodology

2.1 Experimental setup of the PFIR column

The PFIR column consists of an annular vessel separated into two sections, representing the air reactor and fuel reactor in a pressurized chemical looping facility. The fuel reactor section is approximately 17% of the total cross-sectional area of the PFIR column, based on the expected reaction rates in the hot flow

PCL pilot plant. The separating walls have a small opening at the bottom to allow for solids transfer between sections. The inner process diameter of the PFIR is 0.114 m and the outer process diameter is 0.57 m. The outer wall is clear acrylic, while the inner wall is PVC. The column is 3.87 m tall. An overview of important measurements is shown in Figure 3.

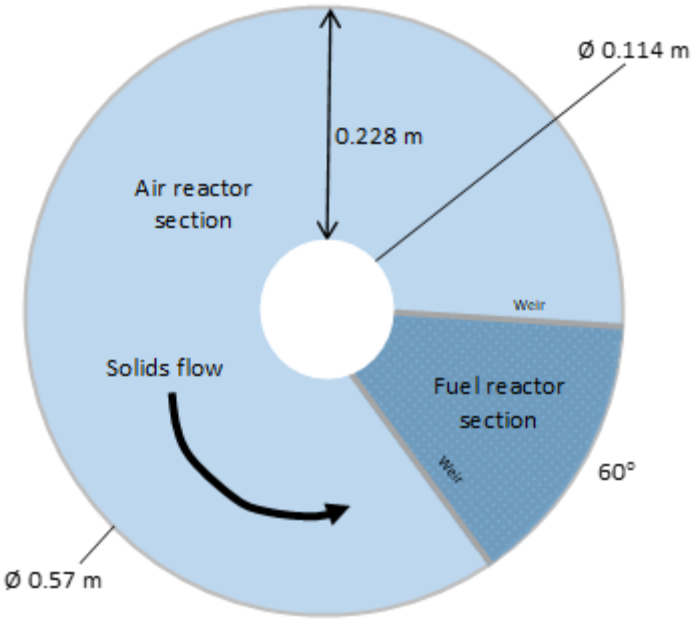

Figure 3. Annotated diagram showing the top-down view of the cold flow PFIR column with important measurements.

An in-bed electric heater is located approximately 0.1 m above the distributor plate in the middle of the fuel reactor for solid circulation rate measurements. The heater consists of three ¾" heating cartridges in a triangle formation, with a 0.045m centre-to-centre distance.

The bed material used for all tests was brown aluminum oxide with a particle density of 2987 kg/m^3 and a Sauter mean particle diameter of 251 µm. Air was used as the primary fluidizing gas. Helium and argon were used as tracer gases to determine gas leakage and the fate of the purge gases, respectively. The PFIR column was operated at near ambient temperature and atmospheric pressure. The windbox of the PFIR column was separated into the air reactor, fuel reactor and two purge sections, allowing for different gas compositions and flowrates.

Figure 4 shows a diagram of the distributor plate with a 0.056 m tuyere pitch. The distributor plate uses angled tuyeres to produce angled jets to induce angular momentum on the bed material. There are 70 nozzles in the air reactor and 14 nozzles in the fuel reactor. Of these nozzles, 0-8 of them can be used as purge nozzles in the air reactor, and 0-4 of them can be used as purge nozzles in the fuel reactor. One purge row is four nozzles. The jet velocity in the PFIR column was approximately 65 m/s. Gas flowrates of

approximately 3 U/U_{mf} were used to fluidize the air reactor and fuel reactor. Any purge gas that was introduced was in addition to this gas.

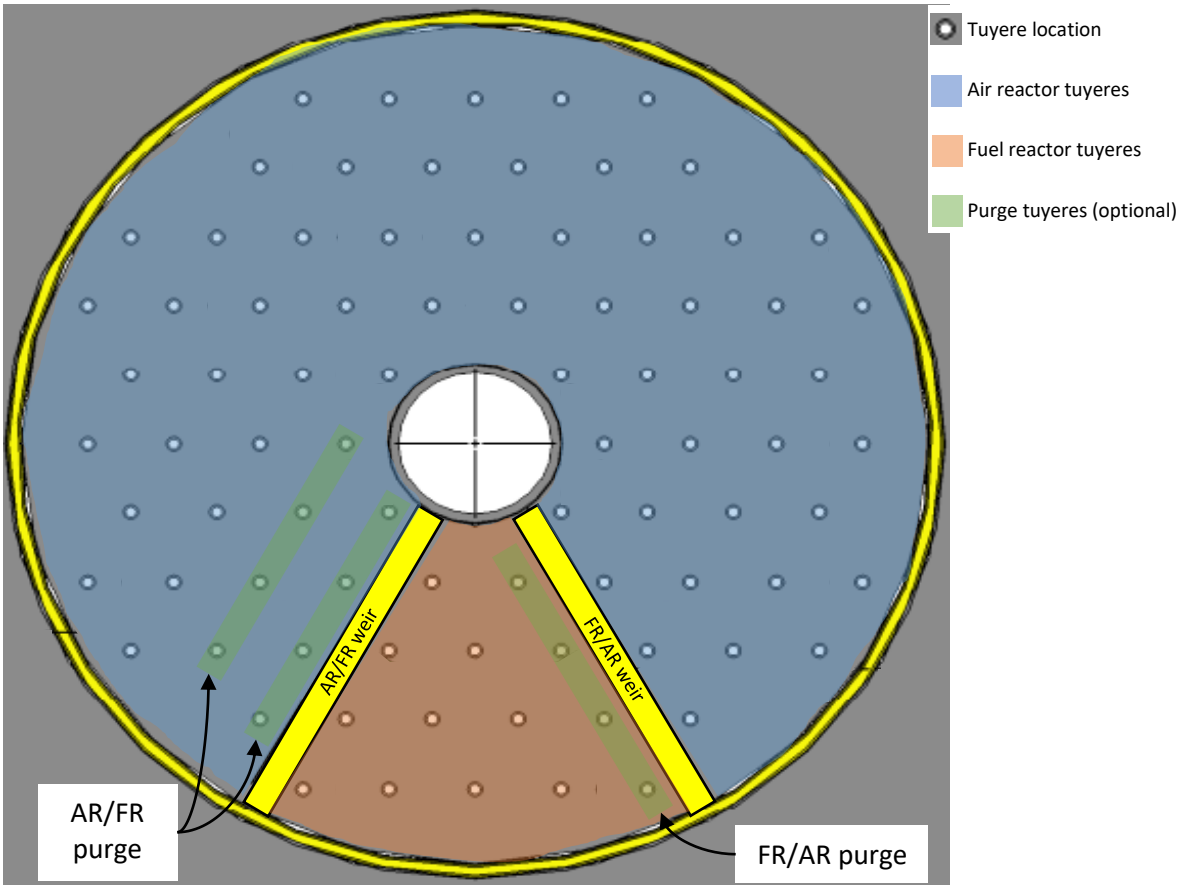

Figure 4. Tuyere layout in the cold flow PFIR column.

The geometrical and operating parameters that were varied are seen in Table 1. The static bed height was varied from 0.15 m to 0.5 m, with 0.5 m as the base case. The weir opening height was varied from 0.05 m to 0.15 m, with 0.1 m as the base case. The purge configuration was varied in several different ways including varying the number of purge rows and the type of purge row, shown in Figure 5. The no purge configuration is the condition where all tuyeres in the PFIR column will have fluidizing gas going through the tuyeres. It was expected that the no purge configuration will have the highest amount of gas leakage since there is no mechanism implemented to prevent it. The blanked purge row configuration is when the four nozzles at the outlet of both reactor sections have effectively been removed, so there is no gas introduced at these locations. This configuration was expected to decrease the gas leakage if the primary method of gas leakage is through bubbles, rather than within the emulsion. The one purge row configuration is the condition where the four nozzles at the outlet of both reactor sections have

representative purge gas flowing through them. This configuration was the base case, and was expected to decrease the gas leakage compared to the no purge configuration. The two AR/FR purge row configuration differs from the one purge row configuration as it adds an additional four purge nozzles to the purge located at the air reactor-fuel reactor boundary. A second purge row could not be added at the fuel reactor-air reactor boundary due to design constraints of the PFIR windbox. Adding a second purge row at the AR/FR boundary was expected to decrease the air reactor to fuel reactor gas leakage compared to the one purge row condition. Finally, the one vertical purge row is similar to the one purge row condition, but the angled purge tuyeres are replaced with vertical tuyeres. It was expected that vertical purge rows may be able to sweep the fluidizing gas from the emulsion, without inducing angular momentum at the weir opening. Only one parameter was varied per test condition, while all other parameters were at their base case.

Table 1. Overview of varied parameters.

Parameter	**Value/ configuration**	**Base case**
Static bed height (B1-B4)	0.15 m, 0.25 m, 0.35 m, 0.5 m	0.5 m
Weir opening height (W1-W4)	0.05 m, 0.1 m , 0.125 m, 0.15 m	0.1 m
Purge configuration (P1-P5)	No purge row	One purge row
	Blanked purge row	
	One purge row	
	Two AR/FR purge rows	
	One vertical purge row	

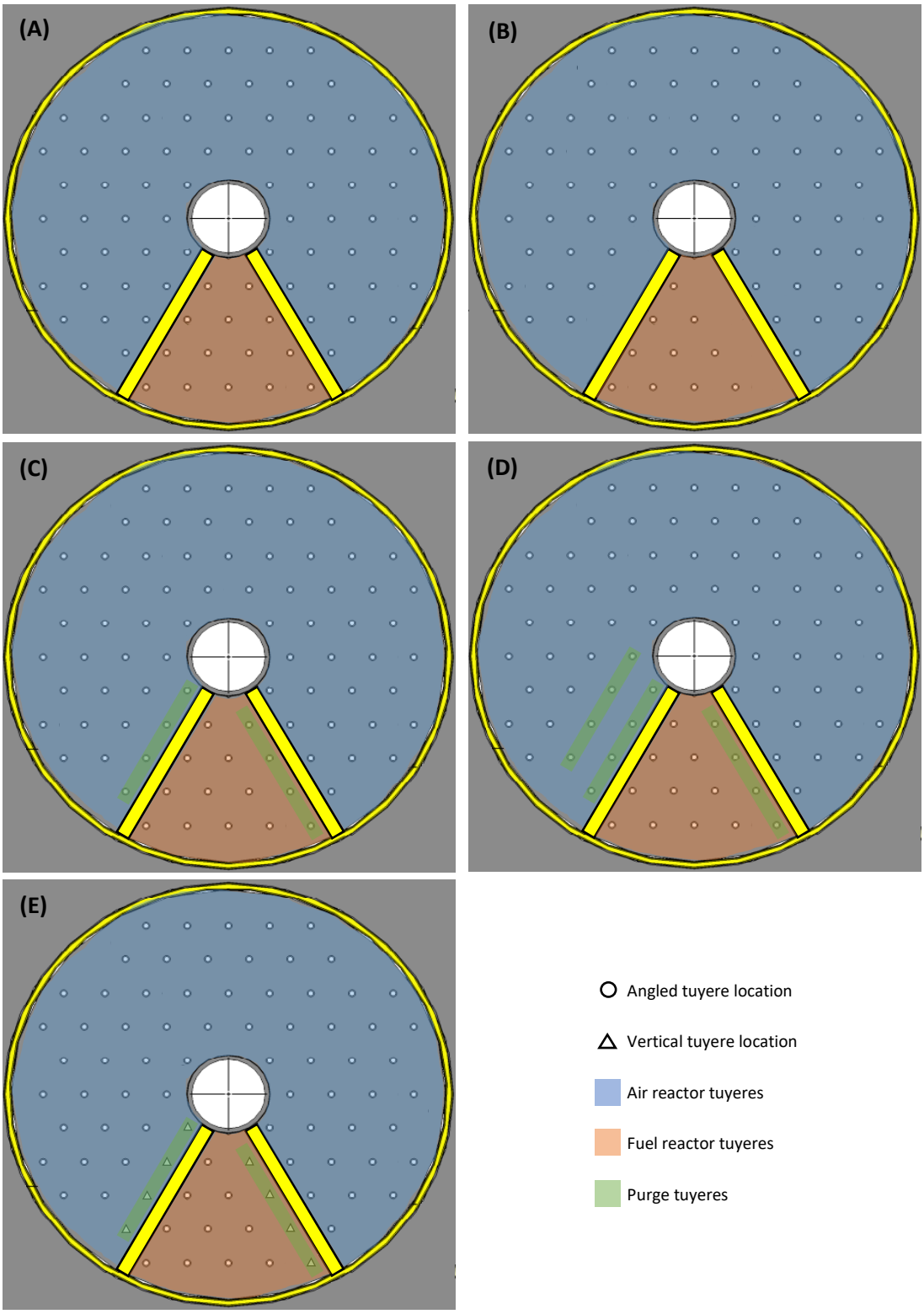

Figure 5.Diagrams of purge tuyere configurations: (A) no purge row configuration, (B) blanked purge row configuration, (C) one purge row configuration, (D) two AR/FR purge row configuration, (E) one vertical purge row configuration.

2.2 Solid circulation rate methodology

The solid circulation rate in the PFIR column was determined using a heat balance around the fuel reactor. The in-bed electric heater operated at 2800 W. Type AA resistance temperature detectors (RTDs) measured the gas temperature in the fuel reactor windbox and exiting the fuel reactor. The solids temperatures entering and exiting the fuel reactor were measured at the weir openings at two points, which were averaged to get the average solids temperature entering or exiting the fuel reactor. Heat loss to the environment was considered negligible, as it was less than 2% of the heater power at base case conditions. The environmental losses were low, since temperature gradients across the fuel reactor walls were small (less than 30°C), and the plastic walls have a relatively low heat conductivity compared to metal. A simplified overview of the experimental set up for solid circulation rate is shown in Figure 6.

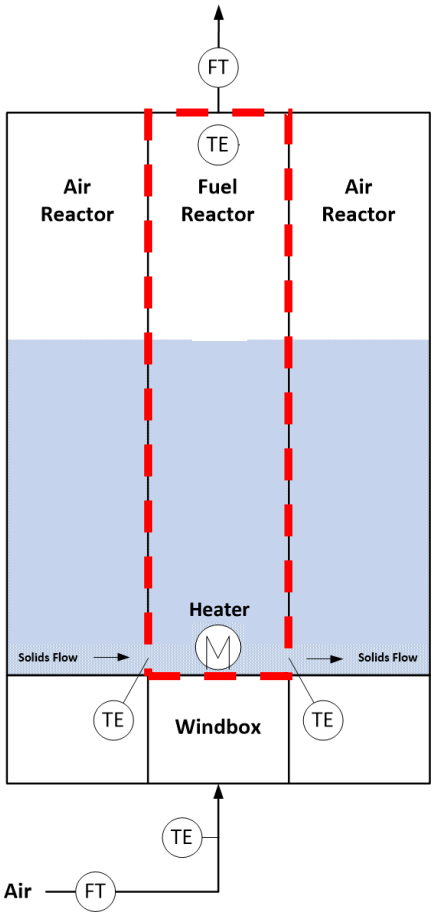

Figure 6. Experimental concept for quantifying solid circulation rate. FT indicates the location of flowmeters and TE indicates the location of the type AA RTDs. The control volume is indicated by the red dashed box.

The steady-state energy balance around the fuel reactor is shown in equation (1). Solid circulation rate can be calculated by substituting for known quantities and rearranging equation (1), shown in equation

(2). There were three assumptions: the RTDs in the bed are measuring the temperature of the solids despite being mostly wetted by the gas; the amount of solids entering the fuel reactor section was equal to the amount exiting the fuel reactor section; and the mass of air that circulated with the solids was negligible compared to the mass of the solids.

$$Heat\ In[gas] + Heat\ In[solids] + HeatIn[heater] = HeatOut[gas] + HeatOut[solids] + HeatOut[Env.Loss] \quad (1)$$

$$\dot{m}_{solid} = \frac{\dot{m}_{gas,FRout} C_{p,air}\left(T_{FR\ out} - T_{ref}\right) - \dot{m}_{gas,FRin} C_{p,air}\left(T_{FR\ in} - T_{ref}\right) - P_{Heater}}{C_{p,solid}\left(T_{solid,AR\rightarrow FR} - T_{solid,FR\rightarrow AR}\right)} \quad (2)$$

The system must be at steady state to calculate the solid circulation rate, but it was discovered that the heat introduced into the PFIR column via the in-bed heater cannot be dissipated sufficiently as the solids circulate in the air reactor section. As a result of this, a continual increase in solids and outlet gas temperature was seen, shown in Figure 7. The only temperature that remains relatively stable was the inlet gas temperature since it was not affected by the heater.

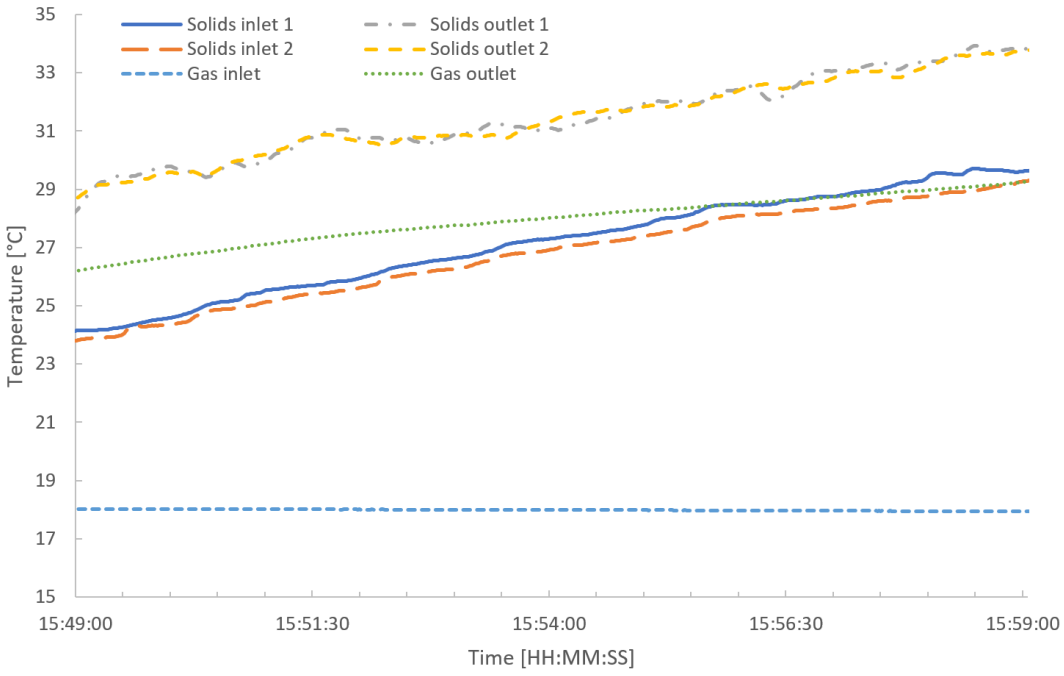

Figure 7. Solids and gas temperatures at a typical test condition.

It was not necessary that the temperatures reach steady state since the energy balance relies on a solids differential temperature. Further, considering that the amount of gas entering and exiting the fuel reactor was approximately equal, the gas contribution to the energy balance also relies on a gas differential

temperature. Thus, the energy balance can be calculated with increasing temperatures if the average differential temperatures have reached steady state (i.e., pseudo steady heat transfer). The average solid and gas differential temperatures are shown in Figure 8. The average solids differential temperature appeared to be at steady state from 15:54:00 to 15:59:00. The average gas differential temperature did continue to increase even while the solids differential temperature reached steady state.

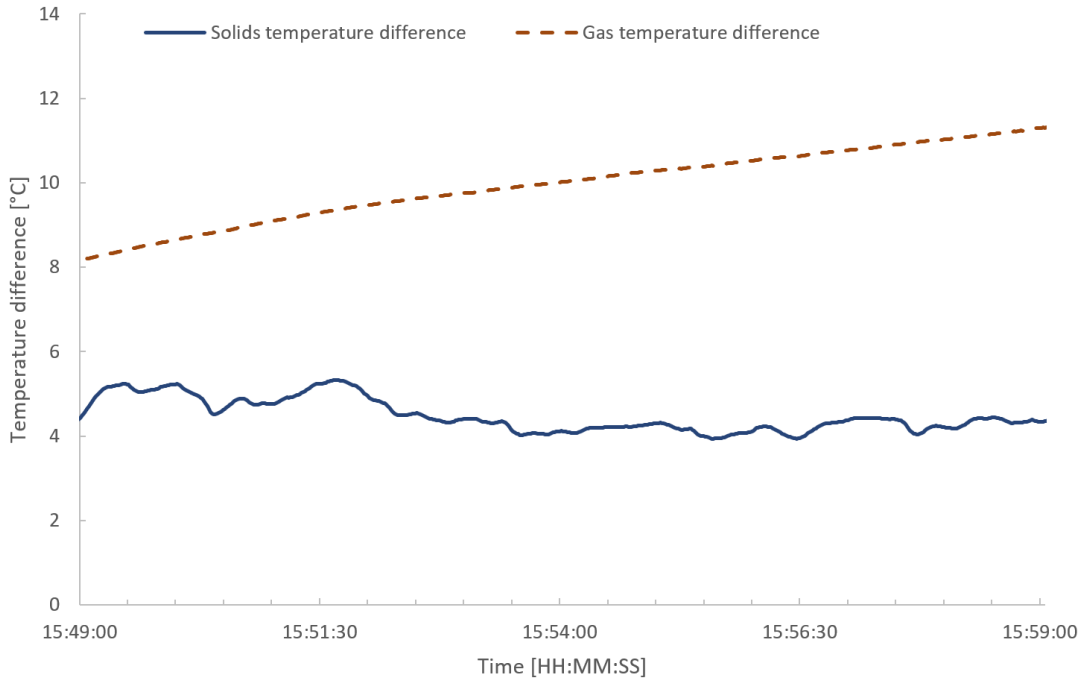

Figure 8. The average differential temperature (out – in) of the solids and the gas throughout a typical test condition.

A study of the impact of gas differential temperature was completed to determine if the increase in gas differential temperature influenced the calculated solid circulation rate. The gas contributed less than 3% - 5% of the overall heat balance, with a maximum of 8% across all conditions tested. For this reason, the changing absolute and differential gas temperatures were not considered an issue since the gas contribution to the energy balance is quite low.

2.2.1 Comparison of two heater configuration

There were two in-bed electric heater configurations that could be used to determine the solid circulation rate. The first option was a heater consisting of three 0.019 m diameter cartridges for a maximum power output of 5400 W. The second option was a heater consisting of seven 0.013 m diameter cartridges for a maximum power output of 7000 W. The two heater configurations are shown in Figure 9. A diagram of

the heater holders for both in bed heaters is used to show the orientation of the heater cartridges in the fuel reactor.

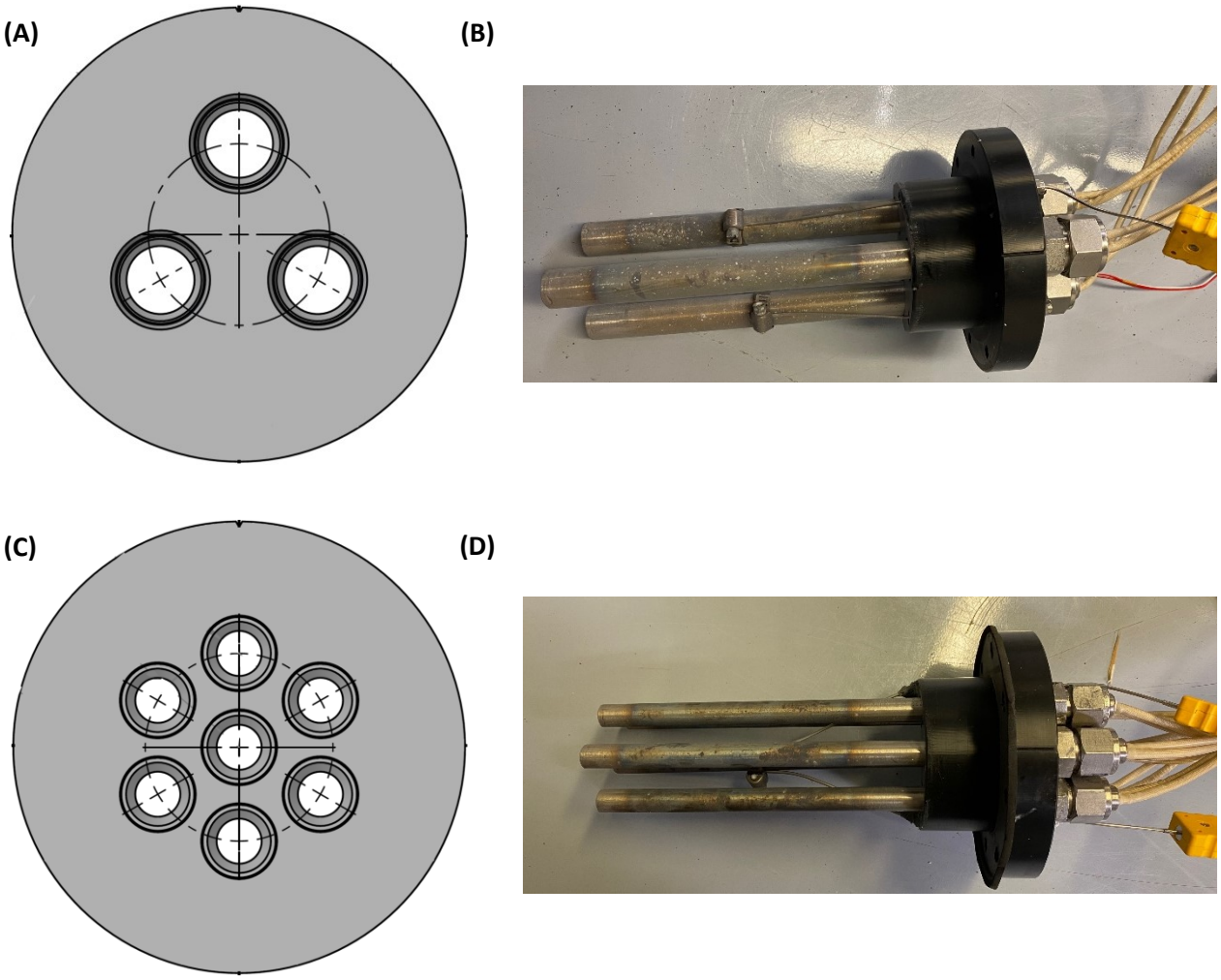

Figure 9. In-bed electric heater configurations, showing the three cartridge heater (A,B) and the seven cartridge heater (C,D). A front view diagram of the three-cartridge heater holder is shown in (A), with a photo of the top-down view in (B). A front view diagram of the seven-cartridge heater holder is shown in (C), with a photo of the top-down view in (D).

The heaters were compared at a similar power output to determine if the configuration had any impact on solid circulation rate. Table 2 shows the solid circulation rate at two conditions for both heater configurations. Note that the conditions chosen used a smaller tuyere pitch of 0.028 m, a larger particle diameter of 367 µm, and a heater power of 2200 W (± 150W). At air flowrates of 2 U/Umf, both heater configurations perform similarly, with only an 8.2% difference in calculated solid circulation rate between the three-cartridge heater and the seven-cartridge heater. Increasing the air flowrates to 3 U/Umf caused the percent difference between configurations to increase to 21.6%, or an absolute difference of 1500 kg/h. The estimated standard deviation for the average solid circulation rate at 3 U/U_{mf} is 2700 kg/h, using

the highest coefficient of variation that was seen across all conditions reported herein. The absolute difference is 2200 kg/h, which is within the estimated standard deviation, so this variability is considered acceptable.

Table 2. Difference in solid circulation rate between heater configurations at a heater power of 2200 W (± 150 W).

Condition	**Solid circulation rate [kg/h]**		**Percent difference [%]**
	Three-cartridge heater	**Seven-cartridge heater**	
2 U/U_{mf}	3700	3400	8.2
3 U/U_{mf}	9100	11300	21.6

The solid circulation rate was calculated using both heaters with similar results, so the heater configuration chosen for subsequent tests was based on operability and ease maintenance. Though the seven-cartridge heater has a higher maximum power output, the heaters cannot be operated above about 3300 W without overheating the bed and risking damaging the plastic walls or plastic heater holder before steady state is reached. Both heaters can achieve this power, so the maximum power output was not a factor when choosing which heater to use. Another operability criteria to look at is the amount of horizontal flow that is blocked by the heaters. The seven-cartridge heater blocked about 2.5 times more horizontal flow than the three-cartridge heater, indicating that using the seven-cartridge heater is a more invasive measurement method. The heaters can also be compared in terms of how easy it is to perform maintenance on the heaters. The heating cartridges may get damaged during operations and need to be replaced. The seven-cartridge heater was harder to maintain as the space between the heating cartridges is much smaller compared to the three-cartridge heater. Since the three-cartridge heater blocked less horizontal flow and was easier to perform maintenance on, the three-cartridge heater was used for all subsequent tests.

2.2.2 Comparison of two temperature measurement configurations

There were two temperature measurement configurations that could be used to determine solid circulation rate. The first configuration consisted of three RTDs placed vertically in the weir opening, with the tip of the RTD approximately halfway into the weir opening. The second configuration consisted of a two-point RTD that was inserted from the side of the column, approximately 0.051 m above the distributor plate. Photos of the two temperature measurement configurations is shown in Figure 10. The three vertical RTD configuration had the benefit of better characterizing any temperature gradients across the weir opening compared to the two-point RTD configuration. The only issue with the three vertical RTDs

was that if one of the RTDs failed, replacing the damaged RTD would be quite difficult. The solid circulation rate using both temperature measurement configurations were compared.

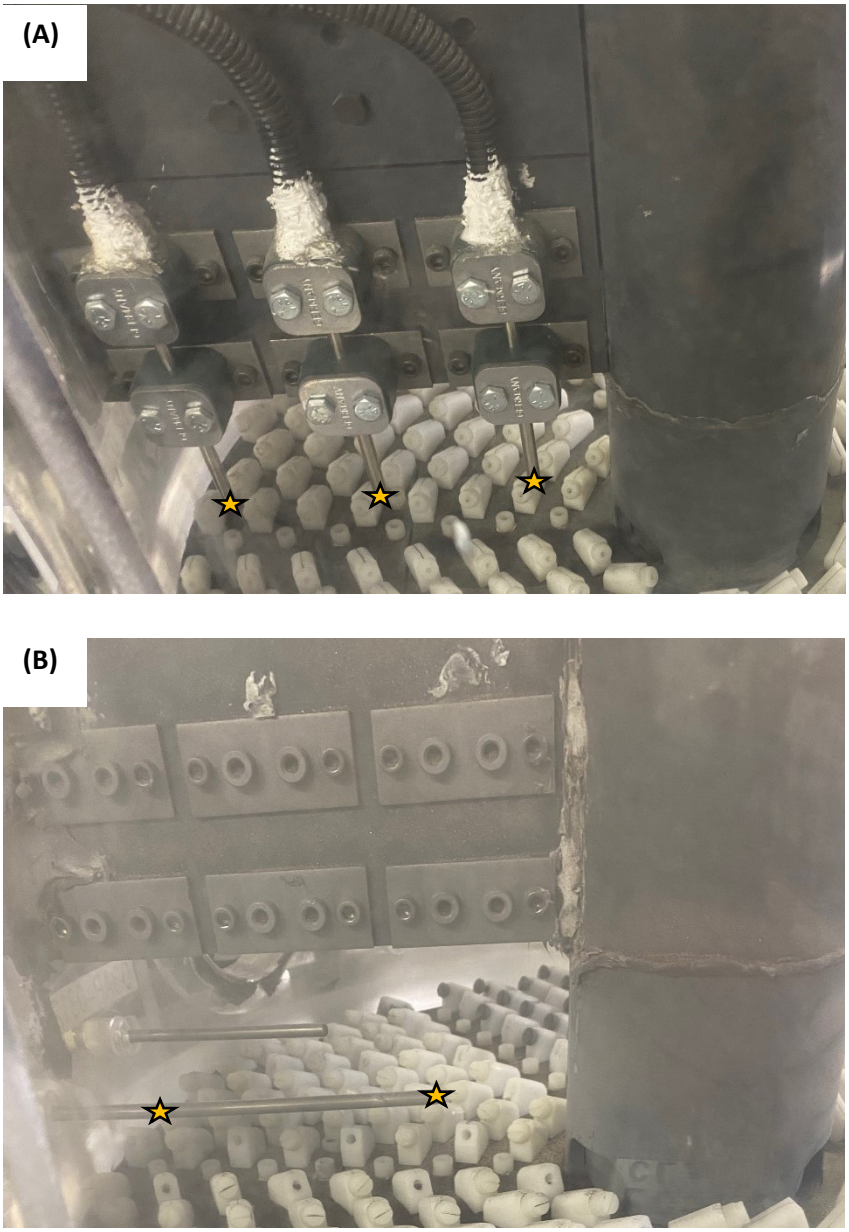

Figure 10. Photos of (A) the three vertical RTDs configuration and (B) the two-point RTD configuration. The approximate solids temperature measurement locations are indicated on the photos by yellow stars.

The solid circulation rate using the two temperature measurement configurations at three air flowrates were compared in Table 3. Note that these solid circulation rates used the same distributor plate and bed material as for the heater configuration test in Table 2, except the in-bed heater was operating at around 2700 W. There is very little difference in solid circulation rate between the two temperature measurement methods. The largest percent difference between the two measurement configurations for a given

condition was 6.4%, which equates to a 500 kg/h absolute difference. This difference is considered negligible, since it is within the estimated standard deviation rate of the solid circulation rate at 3 U/U_{mf} (2000 kg/h), using the highest coefficient of variation that was seen across all conditions reported herein. Either temperature measurement method can be used to calculate solid circulation rate. Since the two-point RTD configuration was easier to replace and less likely to fail, it was chosen as the RTD configuration to use for subsequent tests.

Table 3. Difference in solid circulation rate between temperature measurement at three different air flowrates.

Condition	**Solid circulation rate [kg/h]**		**Percent difference [%]**
	Three vertical RTDs	**Two-point RTD**	
2 U/U_{mf}	3400	3600	5.2
3 U/U_{mf}	7900	7400	6.4
3.5 U/U_{mf}	12800	12900	0.5

2.2.3 Maximum measurement error in key measurements for calculating solid circulation rate

The measurement error of the instrumentation used to calculate solid circulation rate is in Table 4. Mass flow, temperature and heater power were all measured values that have an associated instrument error. All errors have an additional error due to logging accuracy.

Table 4. Measurement error for instrumentation used in solid circulation rate analysis.

Variable	**Description**	**Error**
$\dot{m}_{gas,\ FRin}$	Mass flow of gas entering fuel reactor	0.35% reading + 0.0005 kg/h
$\dot{m}_{gas,\ FRout}$	Mass flow of gas exiting fuel reactor	1% reading + 0.0005 kg/h
$T_{FR,\ in}$	Temperature of gas entering fuel reactor	0.17% reading + 0.21°C
$T_{FR,\ out}$	Temperature of gas exiting fuel reactor	0.17% reading + 0.21°C
$T_{solid,\ AR\rightarrow FR}$	Temperature of solids entering fuel reactor	0.17% reading + 0.21°C
$T_{solid,\ FR\rightarrow AR}$	Temperature of solids exiting fuel reactor	0.17% reading + 0.21°C
P_{heater}	Heater power	0.16% reading + 0.0005 V

2.3 Gas leakage and purge gas fate methodology

Gas leakage tests were performed by injecting a known amount of a helium tracer gas into the fluidizing air for either the fuel reactor section or the air reactor section of the PFIR column at a known

concentration. Helium was chosen as a tracer gas since it is not present in high concentrations in the air, it is detectable at low concentrations (400 ppm), it is non-toxic, and the cylinders are commercially available. All gas flowrates into and out of the PFIR column were measured. Samples of the gas entering and exiting both sections of the PFIR were collected into Cali-5-Bond sample bags. A total of 4 gas bags were taken for a given operating point. The gas samples were analyzed with an Agilent 7890 gas chromatograph to determine the gas composition. A simplified diagram of the experiment is shown in Figure 11, for helium injection into the fuel reactor. Helium was injected into the air reactor in a subsequent test condition to obtain the full complement of gas leakage data.

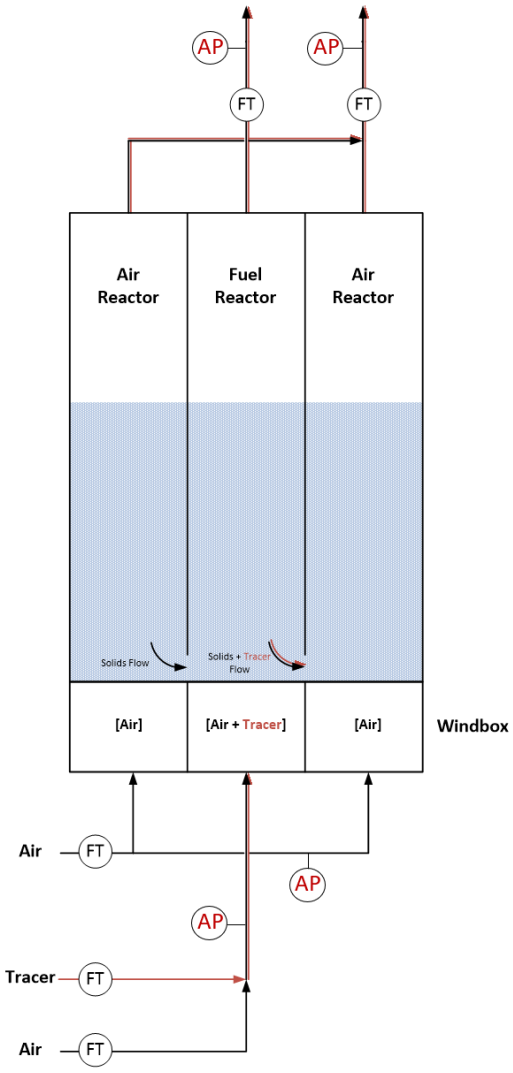

Figure 11. Experimental concept for quantifying gas bypassing for helium injection into the fuel reactor. FT indicates the location of flowmeters and AP indicates the location where the gas bag sample are taken from.

The mass flowrate of air going from the air reactor to the fuel reactor ($m_{AR \rightarrow FR}$) was determined via a helium mass balance in the air reactor (equation (3)), while the fuel reactor to the air reactor ($m_{FR \rightarrow AR}$) was determined via a helium mass balance in the fuel reactor (equation (4)). There were three assumptions: the helium concentration in fresh feed air was low enough to be considered zero; helium did not recirculate into the section it originated from; and the concentration of helium in the gas leakage stream was equal to the concentration of helium entering the air reactor or the fuel reactor.

$$\dot{m}_{AR\ in} x_{He,AR\ in} + \dot{m}_{FR \rightarrow AR} x_{He,FR \rightarrow AR} - \dot{m}_{AR \rightarrow FR} x_{He,AR \rightarrow FR} = \dot{m}_{AR\ out} x_{He,AR\ out} \quad (3)$$

$$\dot{m}_{FR\ in} x_{He,FR\ in} + \dot{m}_{AR \rightarrow FR} x_{He,AR \rightarrow FR} - \dot{m}_{FR \rightarrow AR} x_{He,FR \rightarrow AR} = \dot{m}_{FR\ out} x_{He,FR\ out} \quad (4)$$

The gas bag compositions were determined as mole concentrations, and the amount of argon and oxygen were given as one value as they cannot be differentiated by the gas chromatograph. The first step in the data transformation was to determine the argon, oxygen and nitrogen composition in air. The air composition is taken as the average nitrogen, oxygen and argon concentrations in the inlet gas samples where no helium is injected. The concentration of argon, oxygen and nitrogen in the air was calculated using equations (5)-(7). The concentration of oxygen was then calculated using equation (8) and argon was calculated using equation (9).

$$y_{Ar,air} = \frac{0.934}{(0.934 + 20.946)} y_{(Ar+O_2),air} \quad (5)$$

$$y_{O_2,air} = y_{(Ar+O_2),air} - y_{Ar,air} \quad (6)$$

$$y_{N_2,air} = y_{N_2} \quad (7)$$

$$y_{O_2} = \frac{y_{N_2}}{y_{N_2,air} * y_{O_2,air}} \quad (8)$$

$$y_{Ar} = y_{Ar+O_2} - y_{O_2} \quad (9)$$

The mole concentrations were converted to mass concentrations by multiplying each species by their molecular weight to get the concentrations on a mass per mol basis, which was then divided by the summation of all the species' masses to obtain the mass concentrations.

The next step is to get the mass of helium in the air reactor/ fuel reactor inlet/exhaust. Air flowrates were taken as the average flowrate over a one-minute period when the gas bag was taken. For inlet flowrates where helium was injected, the flowrate was taken as the air flowrate plus the helium flowrate. The helium concentrations (mass fractions) were then multiplied by the relevant flowrate to get the total mass of helium in each stream.

Gas leakage was determined by a helium mass balance around the PFIR column. Gas leakage can either be determined using a helium balance over the air reactor section or over the fuel reactor section. It was determined that the helium balance should be taken over the reactor section in which helium was injected into, as the helium concentrations were the highest. The helium concentrations in the other reactor section were the same order of magnitude as the detection limit of the gas chromatograph, so using these values was avoided to keep errors low. The simplified expressions used to calculate the air reactor to fuel reactor gas leakage is shown in equation (10) and fuel reactor to air reactor gas leakage is shown in equation (11).

$$\dot{m}_{AR\rightarrow FR} = \frac{\dot{m}_{He,AR\ in} - \dot{m}_{He,ARout}}{x_{He,AR\ in}} \tag{10}$$

$$\dot{m}_{FR\rightarrow AR} = \frac{\dot{m}_{He,FRin} - \dot{m}_{He,FRout}}{x_{He,FR\ in}} \tag{11}$$

To prevent gas leakage between reactor sections, one or more rows can have an inert gas flowing through them, acting as purge row(s). It is important to determine the fate of the purge gas, i.e., what percent of the purge gas flows through the air reactor compared to the fuel reactor, to better understand this reactor design. To determine the fate of the purge gas, either the purge row(s) at the air reactor-fuel reactor interface (AR/FR), or the fuel reactor-air reactor interface (FR/AR) have argon flowing through them instead of air. The gas samples taken to determine gas leakage were used to determine the amount of argon that remained in the reactor it was injected into and how much moved to the adjacent reactor.

The fate of the purge gases was determined by comparing the oxygen content in the air reactor or fuel reactor gas stream with the expected concentration of oxygen if the exhaust stream only consisted of air. Equation (12) is used to determine the amount of purge gas that goes into the air reactor and equation (13) is used to determine the amount of purge gas that goes into the fuel reactor. This calculation was repeated for a paired condition where argon was used as the other purge gas to determine the fate of that purge gas, using the same equations.

$$\dot{m}_{purge,AR\ out} = \dot{m}_{AR\ out} * \left(1 - \frac{x_{O_2,AR\ out}}{x_{O_2,air}}\right) \tag{12}$$

$$\dot{m}_{purge,FR\ out} = \dot{m}_{FR\ out} * \left(1 - \frac{x_{O_2,FR\ out}}{x_{O_2,air}}\right) \tag{13}$$

2.3.1 Maximum measurement error in key measurements for calculating gas leakage and purge gas fate

The measurement error of the instrumentation used to calculate gas leakage and purge fate is in Table 5. Mole concentration and mass flowrates were measured values that have an associated instrument error. All errors have an additional error due to logging accuracy.

Table 5. Uncertainties used in gas leakage and purge fate analysis.

Variable	Description	Error
y_X	Mole concentration of all gas species	Larger of: 10% reading or 0.001
$\dot{m}_{gas,\ ARin}$	Mass flow of gas entering air reactor	0.5% reading + 0.0005 kg/h
$\dot{m}_{gas,\ FRin}$	Mass flow of gas entering fuel reactor	0.35% reading + 0.0005 kg/h
$\dot{m}_{gas,AR\text{-}FR\ purge}$	Mass flow of AR-FR purge gas entering PFIR	0.5% reading + 0.0005 kg/h
$\dot{m}_{gas,FR\text{-}AR\ purge}$	Mass flow of FR-AR purge gas entering PFIR	0.5% reading + 0.0005 kg/h
$\dot{m}_{He}$	Measured mass flow of helium entering PFIR	0.5% reading + 0.00109 kg/h

2.4 Timeseries and statistical analysis

The solid circulation rate was taken as an average over a period of about 10-15 minutes. The gas leakage and purge fate were taken as an average over about a 1–2-minute period. Timeseries analysis was done on the calculated values to determine if the system was in control over the period where the averages were taken. The system was considered in control if no points in the entire period fall above or below the upper and lower control limits. Three-sigma control limits (CLs) were chosen and are defined in equation (14). Calculated averages that were out of control were either removed entirely, or the period over which the average was taken was shortened slightly to ensure the average was taken during an in-control period only. In a few circumstances, an outlier point outside of the control limits was simply removed.

$$CL = \mu \pm 3\sigma \tag{14}$$

Figure 12, Figure 13 and Figure 14 show representative graphs of the timeseries for the base case condition for solid circulation rate, gas leakage and purge gas fate respectively. The mean value of the timeseries is shown by the red line, the upper control limit is shown by the green line, and the lower control limit is shown by the purple line. No points fall above the upper control limit or below the control limit, indicating that the system is in control. The graphs for the gas leakage and purge fate have no data in the middle since the gas compositions were taken as gas bags over the course of two one-minute

periods. Generally, the timeseries data for all calculated values were near the mean value. All of the time series graphs can be found in Appendix A: Additional data, tables, and figures in Figure 30 - Figure 162.

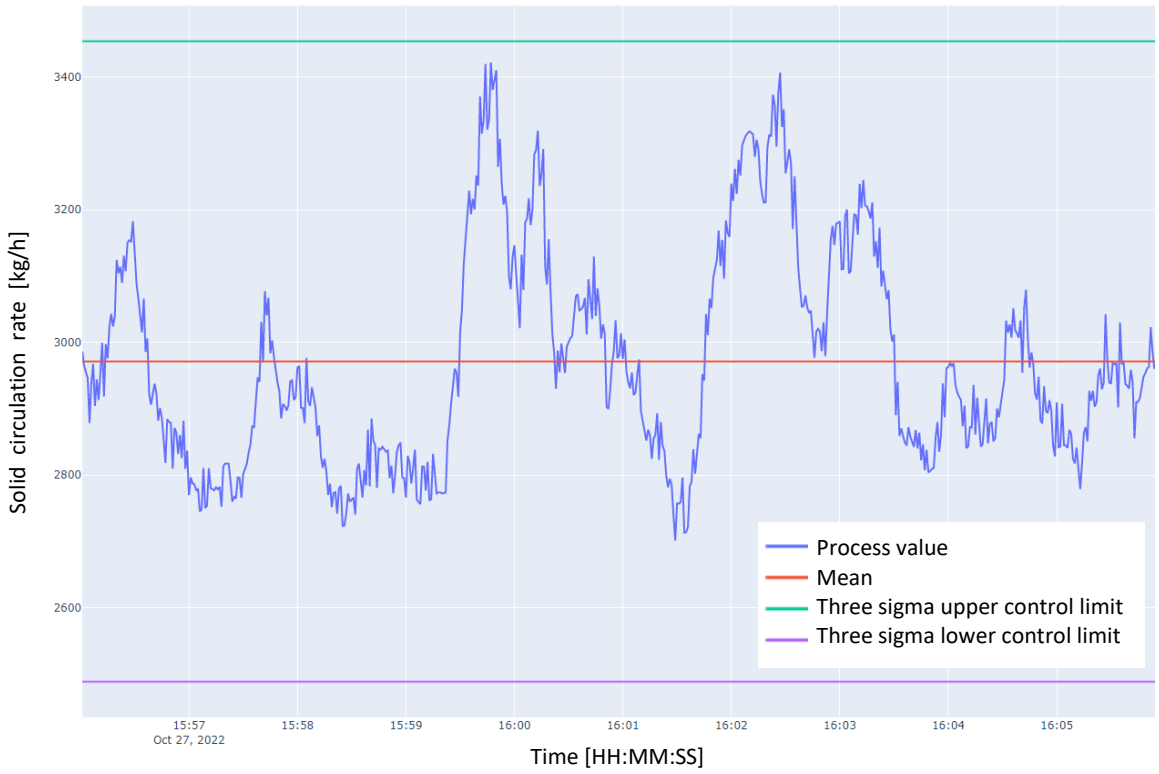

Figure 12. Representative timeseries graphs for solid circulation rate.

Figure 13. Representative timeseries graphs for gas leakage.

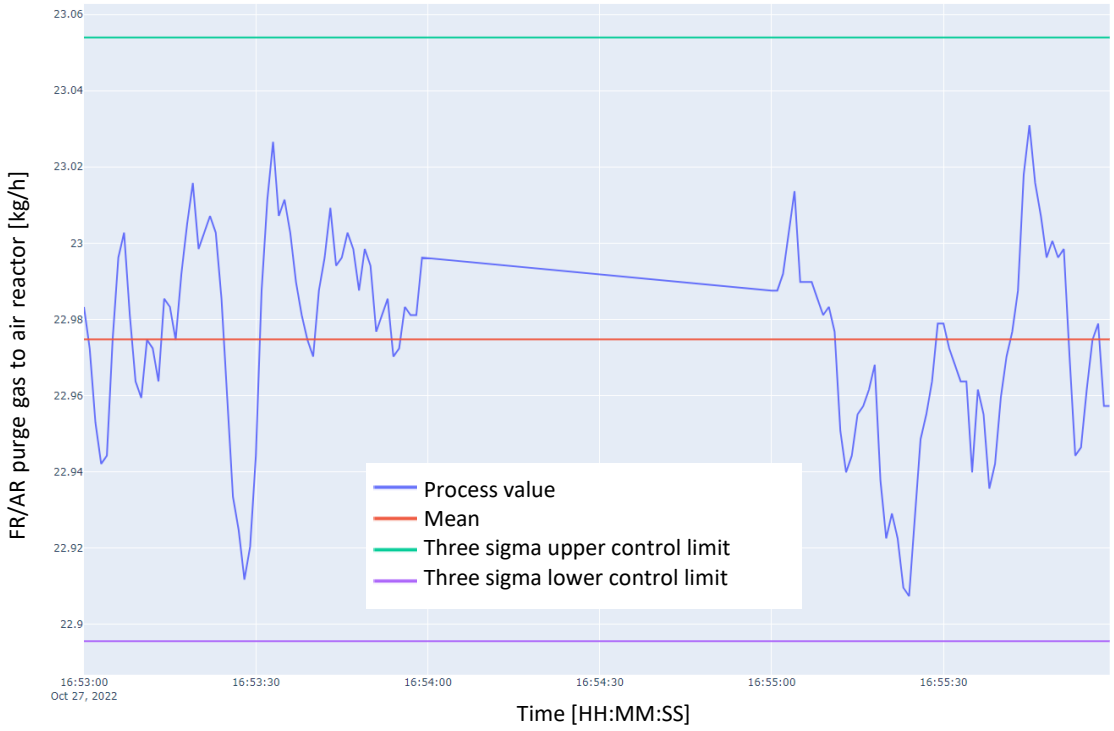

Figure 14. Representative timeseries graphs for purge gas fate.

The estimates of the population standard deviation are shown in Appendix A: Additional data, tables, and figures in Table 16 – Table 22. The population standard deviation (σ) was calculated using the sample standard deviation (s), using a tabulated constant (c_4) based on the sample size, shown in equation (15) [17].

$$\sigma = \frac{s}{c_4} \tag{15}$$

After confirming all the timeseries were in statistical control and removing data that was not in statistical control, statistical analysis was done on all the data. A one-way analysis of variance (ANOVA) was performed using the means of the timeseries data to determine if the solid circulation rate, gas leakage and/or purge fate was statistically different between test conditions. If the ANOVA revealed that at least two of the means were statistically different, Tukey's honest significant difference (HSD) test was performed to determine which conditions have statistically different means. A significance level of 0.05 was used for the ANOVA and Tukey's HSD test. It should be noted that for some test conditions, there were no repeats for gas leakage or purge fate. In this case, the pooled variance is used for the intra-group variance for a given value.

3 Results and discussion

3.1 Solid circulation rate

The effect of static bed height, weir opening height and purge configuration on solid circulation rate was investigated. The solid circulation rate is a key performance indicator of the PFIR reactor for PCL since the circulation must be sufficient to ensure enough oxygen is transferred to the fuel reactor to achieve the desired fuel conversion and to ensure enough heat is transferred to the fuel reactor to ensure reaction rates remain high [8], [14]. Though the reduction reaction of the oxygen carrier that will be initially tested in the PCL pilot plant is slightly exothermic, most other oxygen carriers have exothermic reduction reactions, making the solid circulation rate especially important for the heat balance [7]. The solid circulation rate data can be found in Appendix A: Additional data, tables, and figures, Table 16.

3.1.1 Varying the static bed height

Figure 15 shows the effect of static bed height. A one-way ANOVA showed that there was a statistically significant difference in solid circulation rate between at least two bed heights ($F(3, 7) = [31.87]$, $p = 0.0002$). The results of Tukey's HSD test is shown in Table 6, with further information in Appendix A: Additional data, tables, and figures, Table 23. The solid circulation rate with a 0.15 m bed height (B1) was

4000 kg/h and was statistically different compared to the solid circulation rate at all other bed heights (B2 – B4). The solid circulation rate decreased to around 3100 kg/h with bed heights between 0.25 m – 0.5 m.

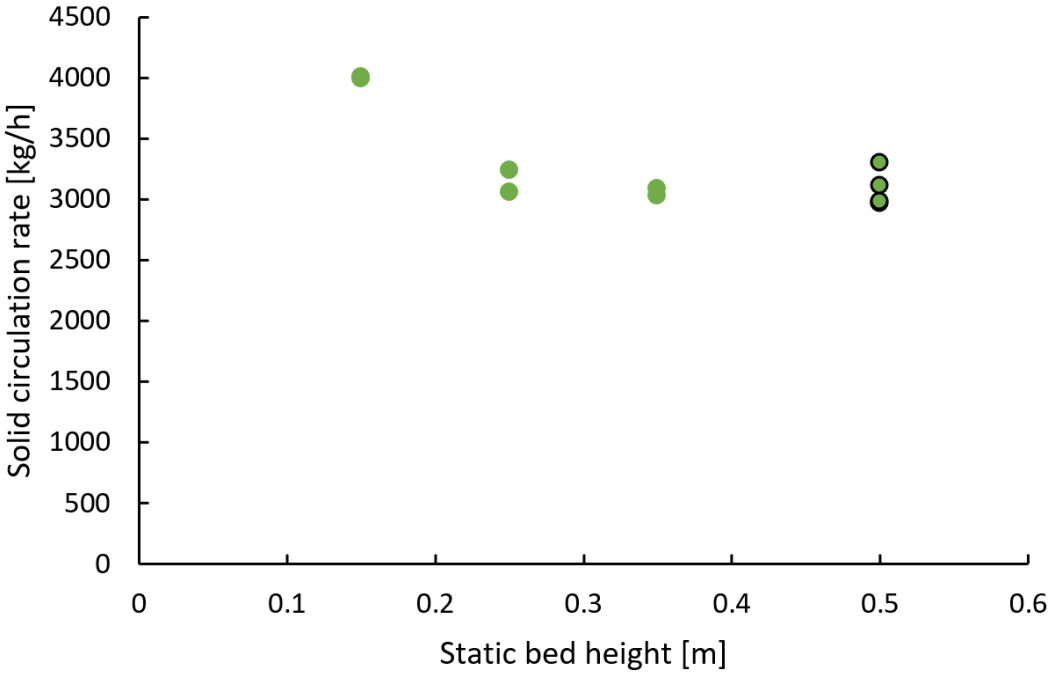

Figure 15. The effect of static bed height on solid circulation rate. The base case is indicated by the data points with a black outline.

Table 6. Results of Tukey's HSD test for the effect of bed height on the mean solid circulation rate.

Comparison	Difference	Statistical difference?
BH1 – BH2	-850	Yes
BH1 – BH3	-946	Yes
BH1 – BH4	-933	Yes
BH2 – BH3	-96	No
BH2 – BH4	-83	No
BH3 – BH4	13	No

Increasing the bed height is expected to decrease the solid circulation rate indirectly. With a constant mass flowrate, an increased bed height will increase the pressure at the distributor plate, which decreases the volumetric flowrate and jet velocity, and thus decreases the gas momentum. This trend was seen between 0.15 m and 0.25 m bed heights, but not for the taller beds that were tested. The changes in bed

height that were investigated are relatively small and the solid circulation rate measurement technique produced a relatively coarse measurement. It is very likely that any changes in solid circulation rate due to the changes in bed height were too small to consistently measure.

3.1.2 Varying the weir opening height

The effect of weir opening height on solid circulation rate is shown in Figure 16. A one-way ANOVA revealed that there was a statistically significant difference between one or more weir opening heights ($F(3, 11) = [86.30]$, $p = 6 \times 10^{-8}$). The results of Tukey's HSD test is shown in Table 7, with further information in Appendix A: Additional data, tables, and figures, Table 24. The solid circulation rate increased from 1800 kg/h to around 3000 kg/h when the weir opening height was increased from 0.05 m (W1) to 0.1 m (W2). Tukey's HSD test indicated that the solid circulation rate at a weir opening height of 0.125 m (W3) and 0.15 m (W4) were different, but this result is unlikely physical as both solid circulation rates were determined to be the same as the solid circulation rate at a weir opening height of 0.1 m (W2).

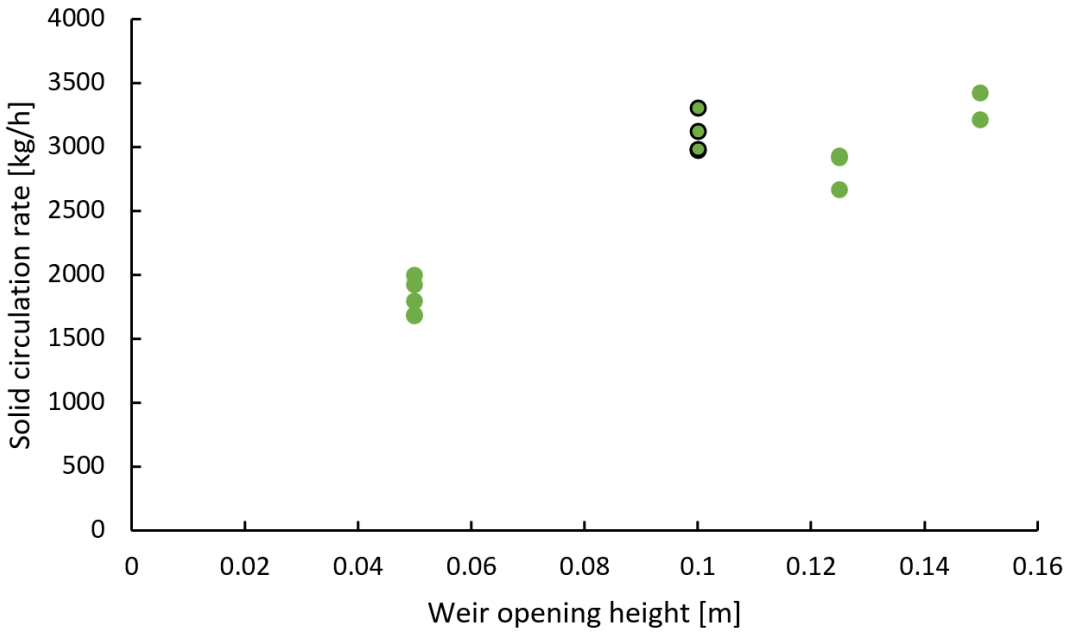

Figure 16. The effect of weir opening height on solid circulation rate. The base case is indicated by the data points with a black outline.

Table 7. Results of Tukey's HSD test for the effect of weir opening height on the mean solid circulation rate.

Comparison	Difference	Statistical difference?
W1 – W2	1255	Yes
W1 – W3	1021	Yes
W1 – W4	1502	Yes
W2 – W3	-234	No
W2 – W4	247	No
W3 – W4	481	Yes

A CPFD study of the PFIR reactor for biomass pyrolysis indicated the presence of a circulation zone at the bottom of the fluidized bed when it was modelled with a 0.35 m weir opening height and a tuyere jet velocity of 80 m/s [18]. The horizontal mass flux was highest about 0.03 m above the distributor, and it decreased above this; at an elevation of about 0.18 m, there is almost no horizontal solids flux. In the cold flow PFIR, the results indicated that the solids circulation zone was within the bottom 0.1 m. Increasing the weir opening height beyond 0.1 m did not increase the solid circulation rate within the range of weir opening heights tested.

3.1.3 Varying the purge configuration

The influence of purge configuration on solid circulation rate is shown in Figure 17. All purge tuyeres had approximately the same jet velocity of 65 m/s. A one-way ANOVA showed that there was a statistically significant difference in purge configuration between at least two of the configurations ($F(4, 15) = [131.53]$, $p = 2 \times 10^{-11}$). The results of Tukey's HSD test is shown in Table 8, with further information in Appendix A: Additional data, tables, and figures, Table 25. The solid circulation rate decreased from 3100 kg/h to 2000 kg/h when going from the one purge configuration (P3) to the no purge (P1) or blank purge configuration (P2). The two AR/FR purge configuration (P4) is considered statistically the same as both the one purge configuration and the no purge configuration. The vertical purge configuration (P5) caused the solid circulation rate to decrease to 0 kg/h.

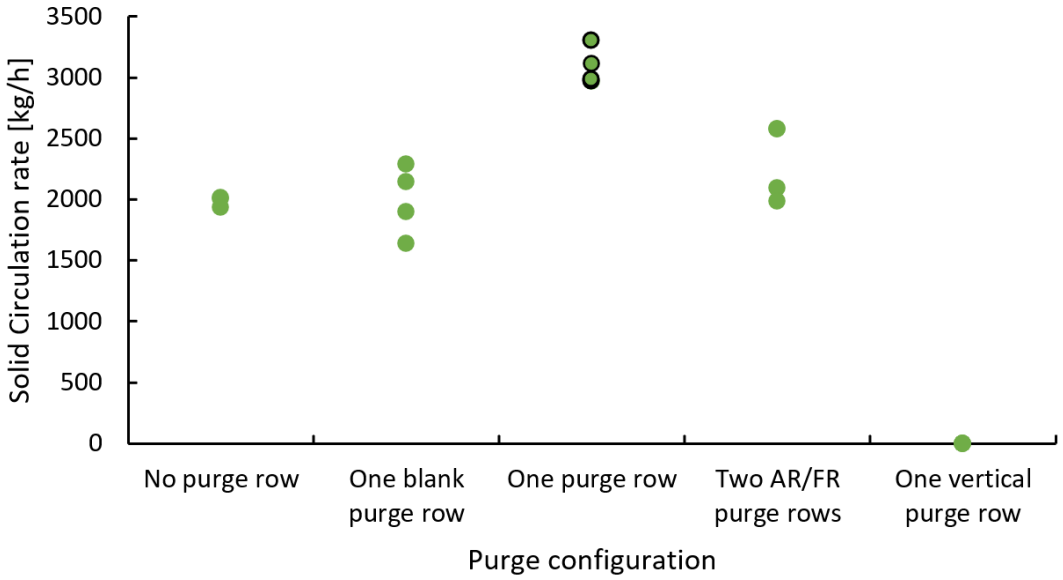

Figure 17. The effect of purge configuration on solid circulation rate. The base case is indicated by the data points with a black outline.

Table 8. Results of Tukey's HSD test for the effect of purge configuration on the mean solid circulation rate.

Comparison	Difference	Statistical difference?
P1 – P2	8	No
P1 – P3	1080	Yes
P1 – P4	321	No
P1 – P5	-1987	Yes
P2 – P3	1072	Yes
P2 – P4	313	No
P2 – P5	-1995	Yes
P3 – P4	-759	Yes
P3 – P5	-3067	Yes
P4 – P5	-2308	Yes

Additional gas was used as the purge gas, so the addition of one purge row introduces 10% more gas into the PFIR column, which caused an increase in solid circulation rate, as seen between the no purge/ blank purge configuration and the one purge configuration. However, adding a second purge row at the at the

air reactor/fuel reactor interface did not have a noticeable impact on solid circulation rate. The increase in the total air flowrate was 5% from the base case, which likely caused a change in solid circulation rate that was too small to adequately measure. It appears that the vertical purge tuyeres acted as a break, preventing circulation around the PFIR, despite the rest of the tuyeres inducing angular momentum. It is possible that there is a purge jet velocity that would allow for solid circulation, but it is not within the scope of this research to determine what that would be.

3.2 Gas leakage

The effect of bed height, weir opening height and purge configuration on gas leakage was investigated. Gas leakage from the air reactor to the fuel reactor is defined as air that enters the air reactor through the distributor plate and circulates into the fuel reactor via the AR/FR weir opening. The fuel reactor to air reactor gas leakage is defined as the air that enters the fuel reactor and circulates into the air reactor via the FR/AR weir opening. The gas leakage data can be found in Appendix A: Additional data, tables, and figures, Table 17 and Table 18.

3.2.1 Varying static bed height

The effect of bed height on gas leakage is shown in Figure 18. A one-way ANOVA confirmed that there was no statistically significant difference in air to fuel reactor gas leakage ($F(3, 1) = [1.70]$, $p = 0.501$), or fuel to air reactor gas leakage ($F(3, 2) = [0.16]$, $p = 0.917$) with static bed height over the range investigated. At the base case conditions, the air to fuel reactor gas leakage was about 27.3 kg/h, or 10.1% of the total air reactor fluidizing gas flowrate. The fuel reactor to air reactor gas leakage was lower at 12.9 kg/h, or 31.1% of the total fuel reactor gas flow rate.

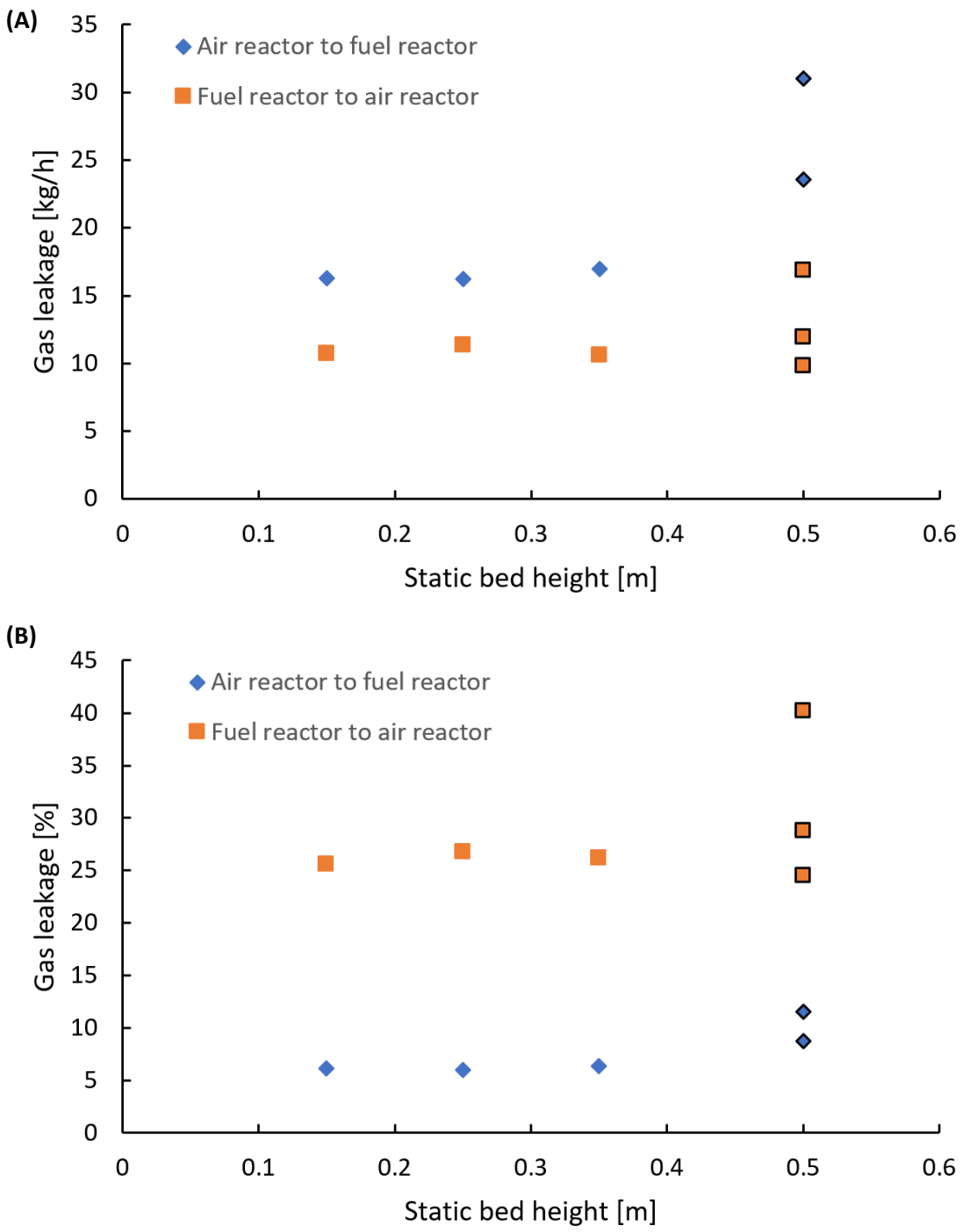

Figure 18. The effect of static bed height on gas leakage between reactor sections as a function of (A) gas flow rate and (B) percent of the gas entering the reactor section in the air reactor or fuel reactor. The base case is indicated by the data points with a black outline.

A decrease in gas leakage was expected with increasing bed heights. An increased bed height will increase the pressure at the distributor, which will decrease jet velocity with a constant mass flowrate. The

pressure at the distributor increased by approximately 6.2 kPa between the 0.15 m static bed height and the 0.5 m bed height. This pressure increase equates to a 5.7% decrease in gas momentum. It is reasonable that there was no apparent change in gas leakage across the bed heights tested, since the change in gas momentum was small. If taller beds were tested, it was expected that eventually the bed height will have an effect on gas momentum, and thus gas leakage, as seen in the CPFD study of the PFIR reactor by McIntyre [15].

A higher percentage of fuel reactor fluidizing gas leaked into the air reactor in comparison to the air reactor fluidizing gas leaking into the fuel reactor. This result was due to the big difference in air flowrates through the fuel reactor and air reactor respectively. The fuel reactor was fluidized with 41.5 kg/h of fluidizing gas, while the air reactor was fluidized with 265.3 kg/h of fluidizing gas, which was a bit more than a six-fold increase in air flowrate. When looking at the absolute gas leakage rate, the amount of gas leaking from the air reactor to fuel reactor was higher than the amount leaking from the fuel reactor to air reactor.

3.2.2 Varying the weir opening height

Figure 19 shows the influence of weir opening height on gas leakage. One-way ANOVAs showed that there was a statistically significant difference in air reactor to fuel reactor gas leakage between at least two weir opening heights ($F(3, 4) = [9.34]$, $p = 0.028$), but no statistical significant difference in fuel reactor to air reactor gas leakage ($F(3, 4) = [2.54]$, $p = 0.195$). The fuel reactor to air reactor gas leakage was on average 12.3 kg/h (29.7%). The results of Tukey's HSD test for air to fuel reactor gas leakage is shown in Table 9, with further information in Appendix A: Additional data, tables, and figures, Table 26. The air reactor to fuel reactor gas leakage increased from 11.6 kg/h (4.4%) to 27.3 kg/h (10.1%) when the weir opening was increased from 0.05 m (W1) to 0.1 m (W2). It then decreased to 14.1 kg/h (5.3%) when the weir opening was increased further to 0.125 m (W3). Tukey's HSD test determined that the air reactor to fuel reactor gas leakage at weir openings of 0.1 m and 0.15 m (W4) were statistically the same. This result does not make sense physically as it also determined that the air reactor to fuel reactor gas leakage at a weir opening height of 0.15 m was the same as the gas leakage at 0.05 m and 0.125 m. The results of Tukey's HSD test for air to fuel reactor gas leakage comparing 0.1 m to 0.15 m weir opening height showed that it is within a 90% confidence interval of being statistically different ($p = 0.07$). These values will be considered statistically different to ensure that the results are consistent statistically and physically. The air reactor to fuel reactor gas leakage at a 0.15 m weir opening height was 15.3 kg/h (5.7%).

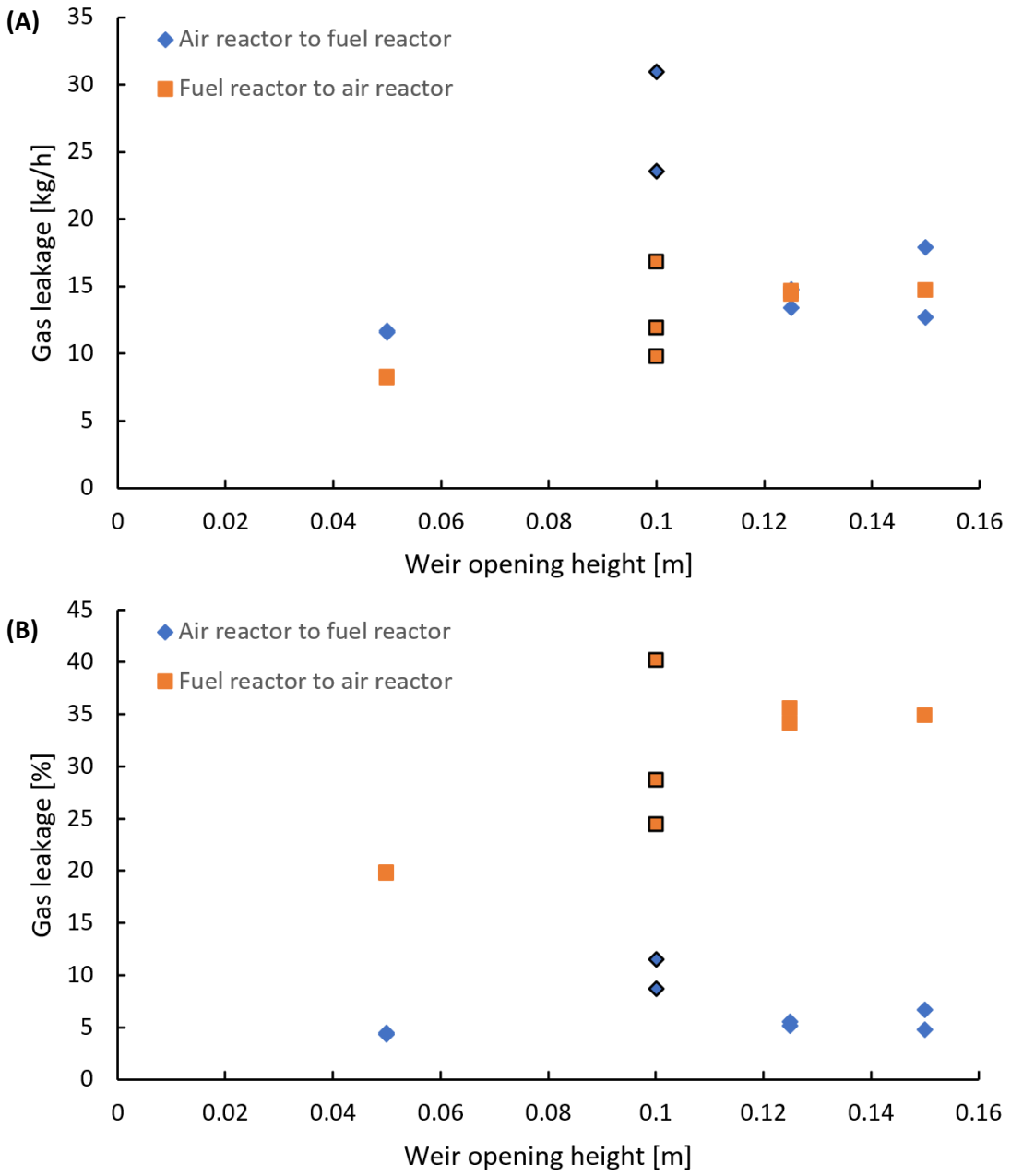

Figure 19. The effect of weir opening height on gas leakage between reactor sections as a function of (A) gas flow rate and (B) percent of the gas entering the reactor section in the air reactor or fuel reactor. The base case is indicated by the data points with a black outline.

Table 9. Results of Tukey's HSD test for the effect of weir opening height on the air reactor to fuel reactor gas leakage.

Comparison	Difference	Statistical difference?
W1 – W2	15.7	Yes
W1 – W3	2.5	No
W1 – W4	3.7	No
W2 – W3	-13.2	Yes
W2 – W4	-12.0	No
W3 – W4	1.2	No

There was no difference in air reactor to fuel reactor gas leakage across the weir opening heights tested, except at a weir opening height of 0.1 m. This difference was unexpected, as the air reactor to fuel reactor gas leakage was expected to either increase across the range of weir openings tested, since the area where gas leakage occurs was also increasing, or to increase from a weir opening of 0.05 m to a weir opening of 0.1 m, plateauing at 0.1 m, mimicking what was seen with the solid circulation rate in in Figure 16, assuming much of the gas that leaks is a part of the gas-solid emulsion. The reason for this unexpected behaviour could be due to solid circulation patterns near the weirs. Once the CPFD model of the PFIR reactor is validated, it should be used to investigate/ confirm these patterns.

The fuel reactor to air reactor gas leakage also did not follow the expected trend. As discussed for the air reactor to fuel reactor gas leakage, it was expected that the gas leakage from a weir opening height of 0.05 m would be lower than the gas leakage at the other weir opening heights tested. This was not observed based on the ANOVA, but it does appear that there might be an increase in gas leakage. The change in gas leakage that occurred is likely too small to detect.

3.2.3 Varying the purge configuration

The effect of purge configuration on gas leakage is shown in Figure 20. A one-way ANOVA determined that there was no significant difference between air reactor to fuel reactor gas leakage across any of the purge configurations tested ($F(4, 5) = [4.63]$, $p = 0.062$). The air reactor to fuel reactor averaged about 24.3 kg/h (9.2%) across all purge conditions. A second one-way ANOVA revealed that there was a significant difference in fuel reactor to air reactor gas leakage between at least two purge configurations ($F(4, 6) = [15.89]$, $p = 0.002$). The results of Tukey's HSD test for fuel to air reactor gas leakage is shown in Table 10, with further information in in Appendix A: Additional data, tables, and figures, Table 27. The blank purge configuration (P2) had the lowest fuel reactor to air reactor gas leakage at 1.1 kg/h (2.6%).

The no purge (P1) and one purge (P3) configurations increased the gas leakage to on average 12.3 kg/h (29.8%). Tukey's HSD test determined that the two AR/FR purge (P4) configuration was the same as all other configurations, except the vertical purge configuration (P5). This result does not make sense physically, as this configuration was effectively the same at the FR/AR weir opening and should yield similar results as the one purge configuration. Tukey's HSD test indicated that the two AR/FR purge configuration was statistically different from the blanked purge configuration within a 90% confidence interval ($p = 0.066$), which makes more sense physically. The vertical purge configuration increased the fuel reactor to air reactor gas leakage the furthest to 18.7 kg/h (44.6%).

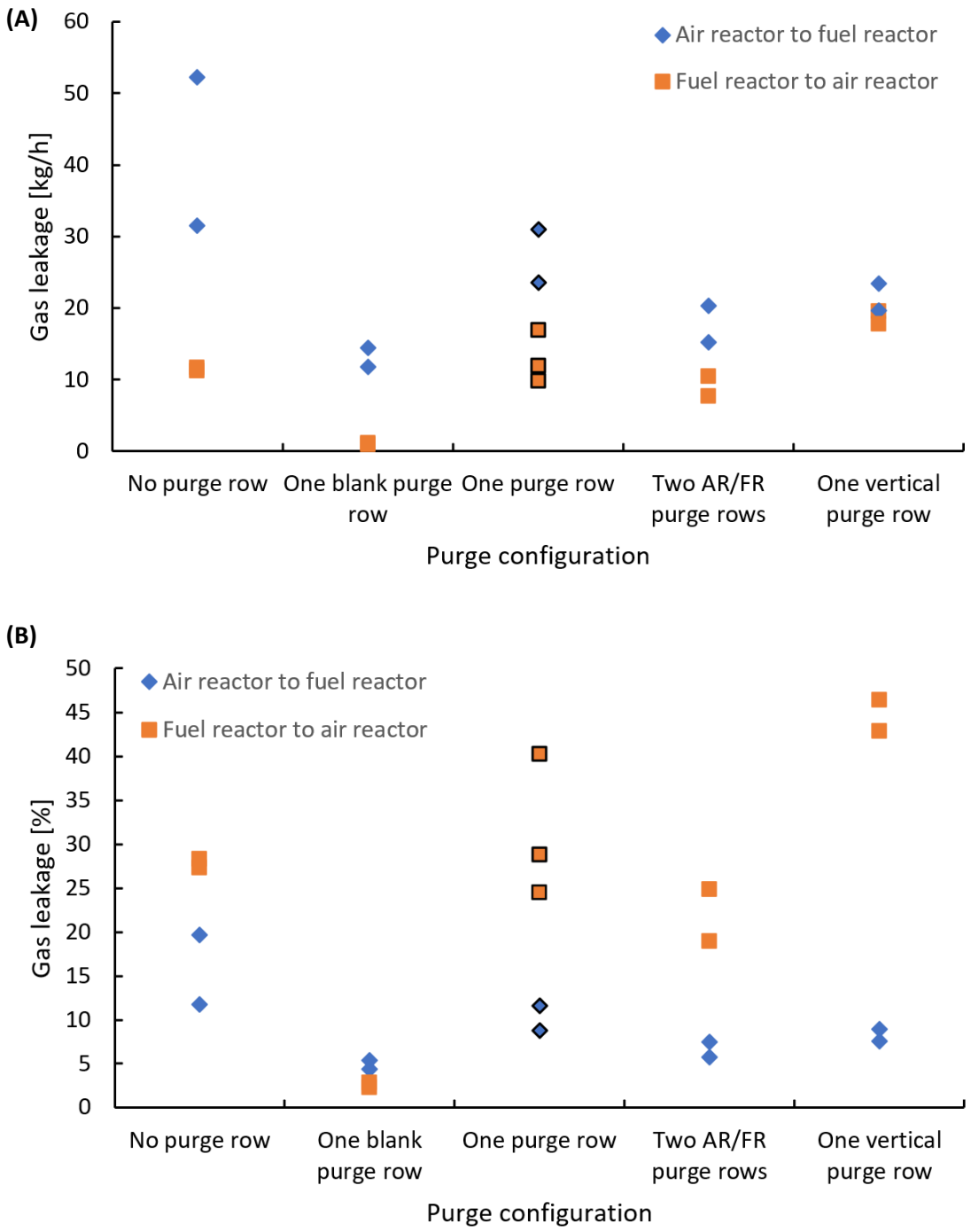

Figure 20. The effect of purge configuration on gas leakage between reactor sections as a function of (A) gas flow rate and (B) percent of the gas entering the reactor section in the air reactor or fuel reactor. The base case is indicated by the data points with a black outline.

Table 10. Results of Tukey's HSD test for the effect of purge configuration on the fuel reactor to air reactor gas leakage.

Comparison	Difference	Statistical difference?
P1 – P2	-10.4	Yes
P1 – P3	1.4	No
P1 – P4	-2.4	No
P1 – P5	7.2	No
P2 – P3	11.8	Yes
P2 – P4	8.0	No
P2 – P5	17.6	Yes
P3 – P4	-3.8	No
P3 – P5	5.8	No
P4 – P5	9.6	Yes

The air reactor to fuel reactor gas leakage results were unexpected, since it was expected that the purge configuration would have an influence on gas leakage in either direction. It was likely that the change in air reactor to fuel reactor gas leakage was too small to determine any effects. Though the purge configuration influenced fuel reactor to air reactor gas leakage, some of the results were unexpected. Using a purge configuration with one purge row had no benefit compared to having no purge rows. However, there was a benefit to having a blanked purge row. The blanked purge configuration decreased gas leakage by approximately 90% from the no purge/one purge configuration. It was expected that some purge gas would be required to sweep away fluidizing gas, but these results show that it is not the case. This result indicates that the dominant mechanism of gas leakage is likely through bubble movement, rather than through the movement of the gas-solid emulsion phase.

3.3 Purge gas fate

The effect of static bed height, weir opening height and purge configuration on the fate of the purge gas was investigated. The AR/FR purge tuyeres were located at the edge of the air reactor, while the FR/AR purge tuyeres were located at the edge of the fuel reactor. The fate of the purge gases is presented as the percent that stayed in the reactor it originated from compared to the amount that moved to the adjacent reactor. Only conditions that include purge rows are presented. The purge fate data can be found in Appendix A: Additional data, tables, and figures, Table 19 – Table 22.

3.3.1 Varying the static bed height

Figure 21 shows the influence of bed height on purge fate. At base case conditions, 66.5% of the AR/FR purge gas moved to the fuel reactor. With increasing bed height, increasing amounts of AR/FR purge gas moved to the fuel reactor, rather than staying in the air reactor. At a bed height of 0.15 m, only 36.8% of the AR/FR purge gas moved into the fuel reactor. This increased to 67.9% at a bed height of 0.35 m, where the AR/FR purge gas fate plateaued and did not increase further with increasing bed height. This increase in AR/FR purge gas that moved into the fuel reactor is unexpected as the purge jet penetration length is expected to decrease with increased bed height/ pressure. The exact reasoning for this difference is not known. This phenomenon needs to be further investigated.

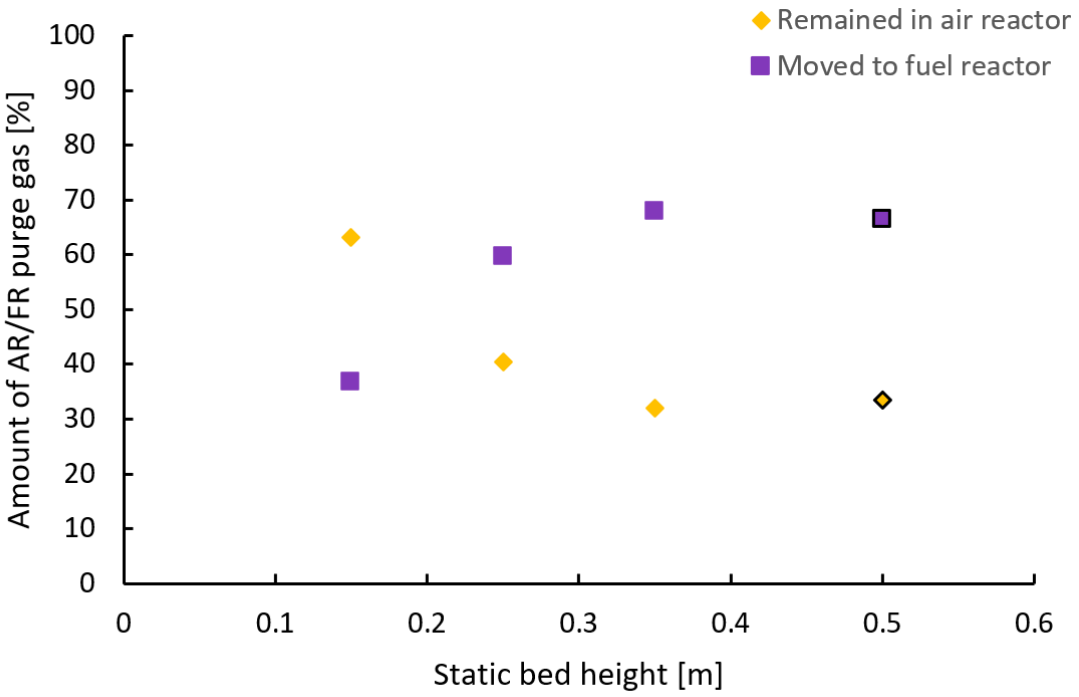

Figure 21. The effect of static bed height on AR/FR purge gas fate. The base case is indicated by the data points with a black outline.

Comparatively, the FR/AR purge gas fate had less variation across the bed heights, shown in Figure 22. A one-way ANOVA revealed that there was no change in the percent of FR/AR purge gas that moved to the fuel reactor over the range of bed heights tested ((F(3, 2) = [2.28], p = 0.319). At base case conditions, 81.1% of the FR/AR purge gas moved to the air reactor. A constant percent of FR/AR purge gas that moved to the air reactor was expected, as the pressure at the distributor plate only changes by 6.2 kPa across all bed heights tested, so the change in purge gas movement was likely too small to detect.

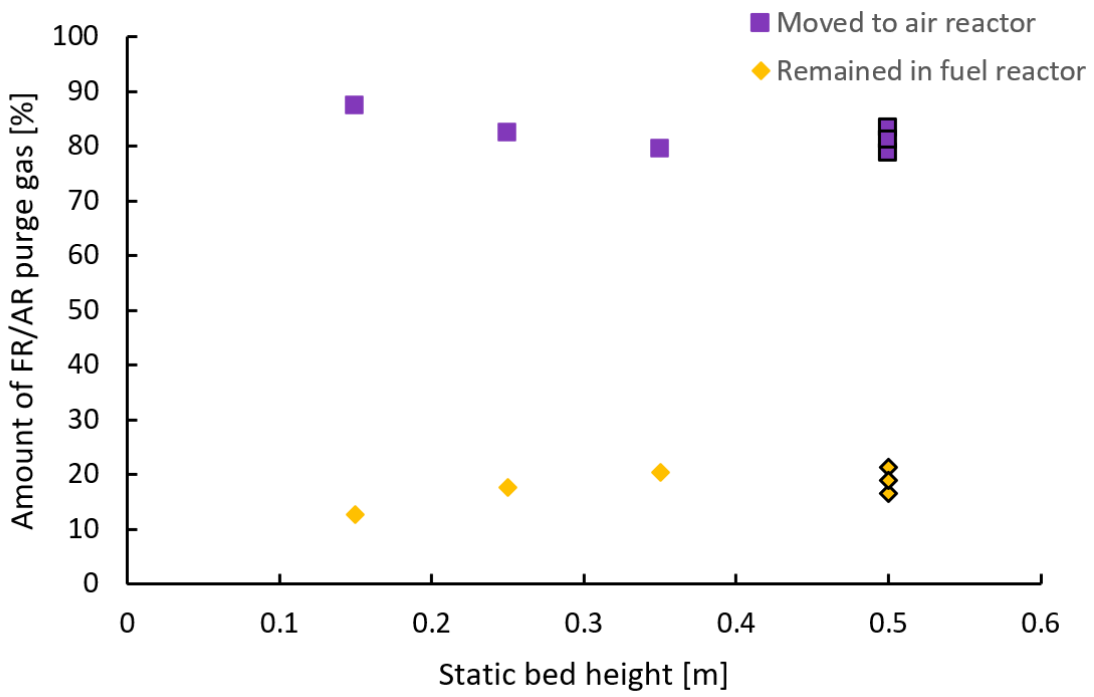

Figure 22. The effect of static bed height on FR/AR purge gas fate. The base case is indicated by the data points with a black outline.

3.3.2 Varying the weir opening height

Figure 23 shows the effect of weir opening height on AR/FR purge fate. A one-way ANOVA determined that there was a statistically significant difference in AR/FR purge fate with weir opening height ((F(3, 3) = [9.90], p = 0.046). The results of Tukey's HSD test for the percent of AR/FR purge gas that moved to the fuel reactor is shown in Table 11, with further information in Appendix A: Additional data, tables, and figures Table 28. The percent of AR/FR purge gas that moved to the fuel reactor decreased from 74.0% to 54.1% when increasing the weir opening height from 0.05 m (W1) to 0.15 m (W4). This was opposite of the expected trend, as a larger weir opening should allow for more AR/FR purge gas to move to the fuel reactor, since the transfer area increases. The cause of this trend is unknown, and this phenomenon needs to be further investigated.

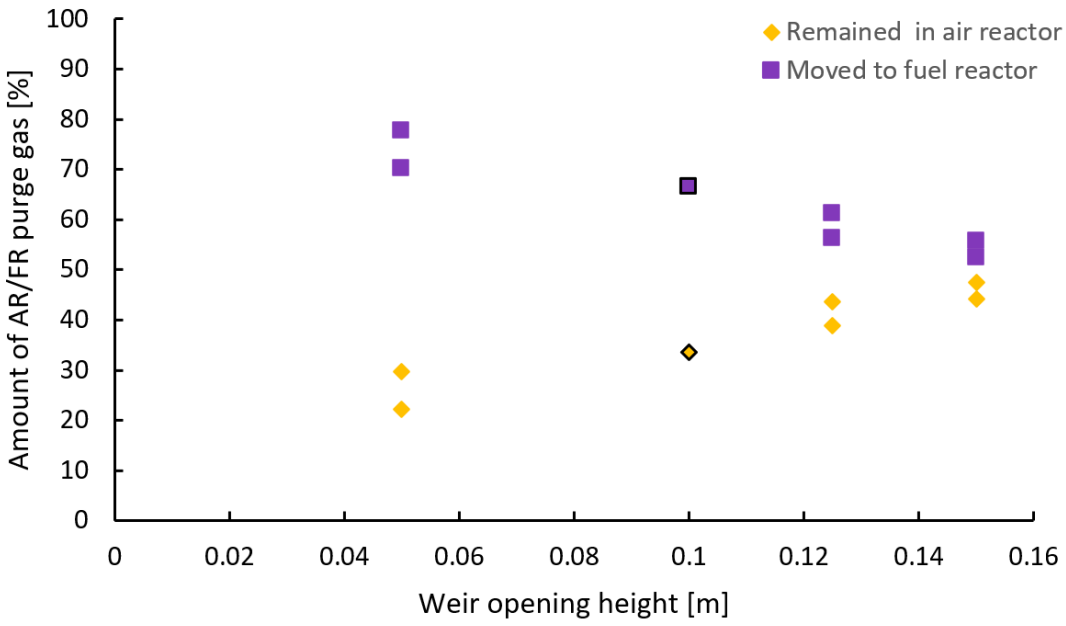

Figure 23. The effect of weir opening height on AR/FR purge gas fate. The base case is indicated by the data points with a black outline.

Table 11. Results of Tukey's HSD test for the effect of weir opening height on the percent of AR/FR purge gas that moved into the fuel reactor.

Comparison	Difference	Statistical difference?
W1 – W2	-7.5	No
W1 – W3	-15.3	No
W1 – W4	-19.9	Yes
W2 – W3	-7.8	No
W2 – W4	-12.4	No
W3 – W4	-4.6	No

Figure 24 shows the effect of weir opening height on FR/AR purge fate. A one-way ANOVA determined that there was a statistically significant difference in FR/AR purge fate with weir opening height ((F(3, 4) = [6.92], p = 0.046). The results of Tukey's HSD test for the percent of FR/AR purge gas that moved to the air reactor is shown in Table 12, with further information in Appendix A: Additional data, tables, and figures Table 29. Tukey's HSD test revealed that the percent of FR/AR purge gas that moved into the air reactor with a weir opening height of 0.1 m (W2) was significantly different from the percent with a weir opening height of 0.125 m (W3), while all other combinations were the same. This result does not make

sense physically, so it will be disregarded and the percent of FR/AR purge gas that moved to the air reactor will be considered constant across the weir opening heights tested, at on average 77.6%. This result is unexpected as more purge gas is expected to move to the air reactor as the weir opening height increases due to an increased opening area. These results indicate that the purge gas mostly stays within the first 0.05 m above the distributor plate before it reaches the weir opening, which would explain why the amount remains unchanged across all weir opening heights. This phenomenon needs to be further investigated.

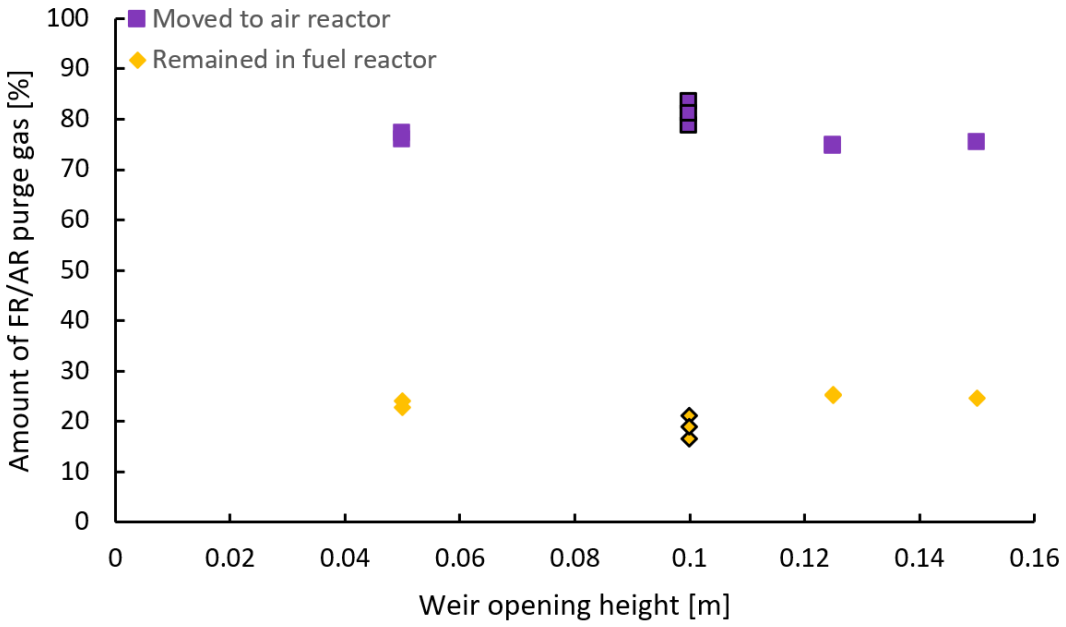

Figure 24. The effect of weir opening height on FR/AR purge gas fate. The base case is indicated by the data points with a black outline.

Table 12. Results of Tukey's HSD test for the effect of weir opening height on the percent of AR/FR purge gas that moved into the fuel reactor.

Comparison	Difference	Statistical difference?
W1 – W2	4.5	No
W1 – W3	-1.8	No
W1 – W4	-1.2	No
W2 – W3	-6.3	Yes
W2 – W4	-5.7	No
W3 – W4	0.6	No

3.3.3 Varying the purge configuration

Figure 25 shows the effect of purge configuration on AR/FR purge gas fate. The no purge (P1) and blanked purge (P2) configurations were not included since these conditions do not have purge tuyeres with gas flowing through them. A one-way ANOVA determined that there was a statistically significant difference in AR/FR purge fate with purge configuration ((F(2, 2) = [142.50], p = 0.007). The results of Tukey's HSD test for the percent of AR/FR purge gas that moved to the fuel reactor is shown in Table 13, with further information in Appendix A: Additional data, tables, and figures Table 30. As expected, adding a second purge row (P4) decreased the percent of AR/FR purge gas that moved in the fuel reactor to about 37.0% compared to only having one purge row (P3). The absolute value of AR/FR purge gas that moved to the fuel reactor increased from 14.4 kg/h to 18.9 kg/h when adding a second AR/FR purge row. As expected, a vertical purge row (P5) ensured that most of the purge gas did not circulate into the fuel reactor.

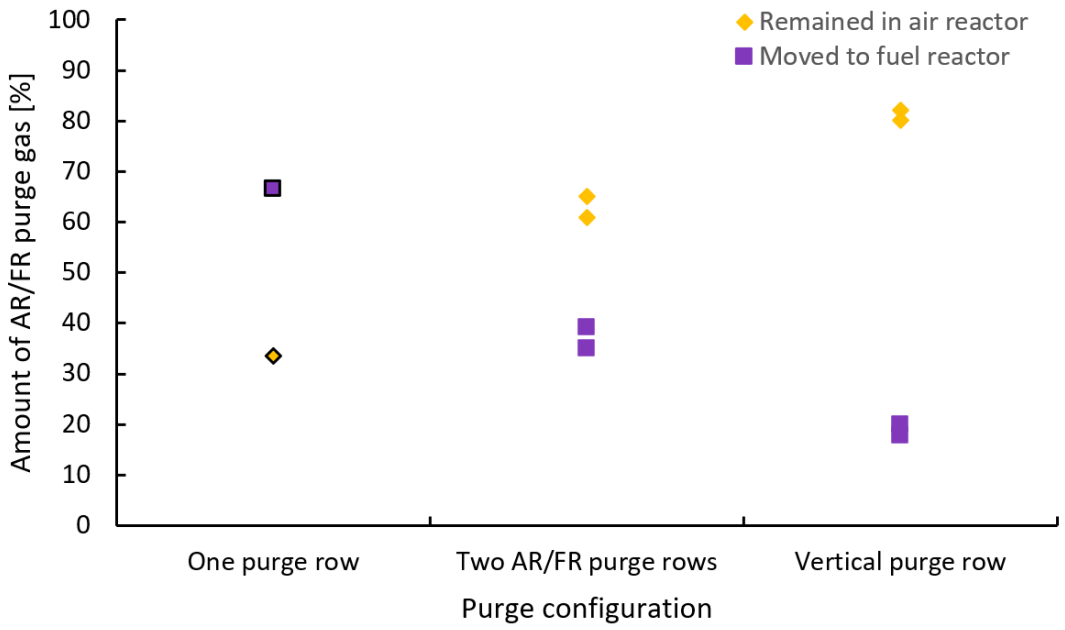

Figure 25. The effect of purge configuration on AR/FR purge gas fate. The base case is indicated by the data points with a black outline.

Table 13. Results of Tukey's HSD test for the effect of purge configuration on the air reactor to fuel reactor gas leakage.

Comparison	Difference	Statistical difference?
P3 – P4	-29.5	Yes
P3 – P5	-47.7	Yes
P4 – P5	-18.1	Yes

Figure 26 shows the effect of purge configuration on FR/AR purge gas fate. A one-way ANOVA determined that there was a statistically significant difference in FR/AR purge fate with purge configuration ((F(2, 4) = [255.14], p = 0.00006). The results of Tukey's HSD test for the percent of FR/AR purge gas that moved to the air reactor is shown in Table 14, with further information in Appendix A: Additional data, tables, and figures Table 31. Tukey's HSD test indicated that there was a slight decrease in the amount of FR/AR purge gas that moved into the air reactor at the two AR/FR purge condition (P4) compared to the one purge row condition (P3). This difference should be negligible as the FR/AR purge is the same for both conditions. This result indicated that there might be more variability in the system between tests than what is seen in the repeats. As expected, the vertical purge row (P5) decreased the amount of FR/AR purge gas that moves into the air reactor to 32.8%, since the purge row is in the fuel reactor.

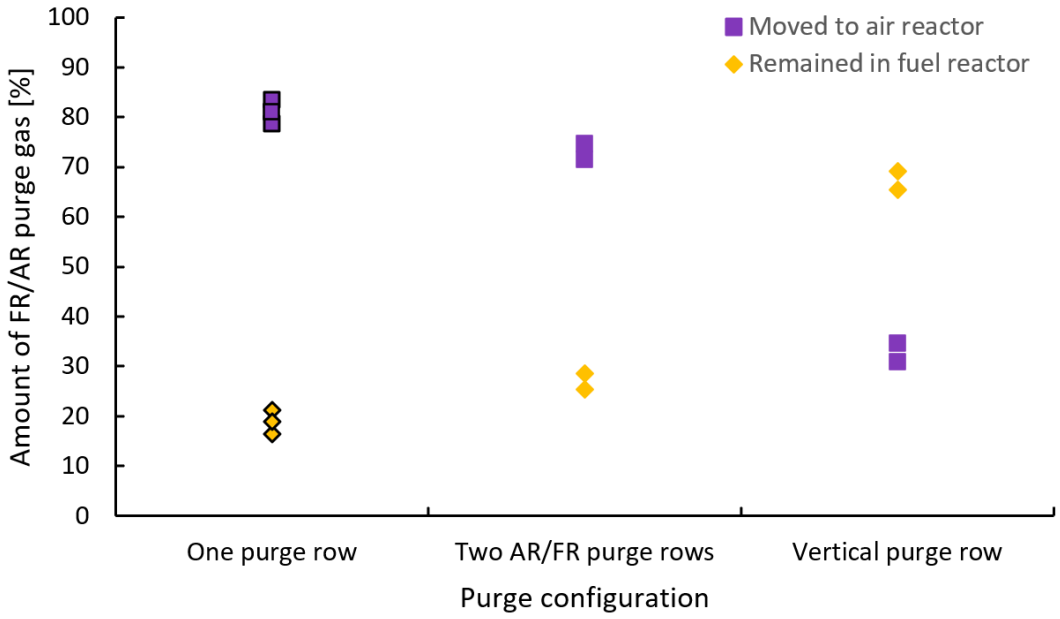

Figure 26. The effect of purge configuration on FR/AR purge gas fate. The base case is indicated by the data points with a black outline.

Table 14. Results of Tukey's HSD test for the effect of purge configuration on the fuel reactor to air reactor gas leakage.

Comparison	Difference	Statistical difference?
P3 – P4	-8.1	Yes
P3 – P5	-48.3	Yes
P4 – P5	-40.2	Yes

3.4 Relationship between solid circulation rate, gas leakage and purge fate

Bed and weir opening height affected solid circulation rate and gas leakage similarly. With the range of bed heights tested, there was no significant change in solid circulation rate and gas leakage in either direction. The trend seen with weir opening height was similar. Both gas leakage and solid circulation rate were lower at a weir opening height of 0.05 m and were generally constant from 0.1 m to 0.15 m. With this configuration of the PFIR column, a bed height between 0.15 m – 0.5 m can be used without greatly affecting the solid circulation rate or gas leakage. A weir opening height above 0.1 m provided no benefit to increasing the solid circulation rate and did not affect the gas leakage in either direction.

Changing the purge configuration did not affect the solid circulation rate and gas leakage in the same way. Additional purge rows help prevent gas leakage, but can also increase solid circulation rate by increasing the amount of gas entering the PFIR. The optimal purge configuration for this system is either one purge row, or to provide a row of blank tuyeres in lieu of a purge row. Two purge rows did not provide much benefit by preventing gas leakage, nor did it affect solid circulation rate. One vertical purge row had no benefit at the conditions tested herein, as it prevented solid circulation and did not improve gas leakage compared to the base case.

It has been noted previously that the rate of gas leakage can be related to solid circulation rate in the PFIR reactor [15]. Figure 27 shows the solid circulation rate as a function of gas leakage for the base case and all bed height and weir height conditions. There is no clear trend between solid circulation rate and gas leakage in either direction. An estimate of the amount of gas leaking with the gas-solid emulsion at a given solid circulation rate was completed. The amount of gas leaking with the gas-solid emulsion was calculated assuming the solids holdup in the gas-solid emulsion was constant and equal to the solids holdup at minimum fluidization. Taking the solid circulation rate as the amount of solids in the gas-solids emulsion moving to the adjacent reactor section, the amount of gas moving to the adjacent reactor as a part of the emulsion was calculated using the solids holdup at minimum fluidization. The solids holdup at minimum fluidization was calculated to be 0.47. Across the base case, bed height and weir opening conditions, the percent of gas leaking as part of the emulsion was 1.1 to 4.2% of the total amount of gas leaking. These results suggest that the gas leakage is not dominated by the amount of gas that moves into an adjacent reactor with the emulsion, but is likely dominated by bubbles. A sensitivity analysis on the solids holdup at minimum fluidization was done and determined that it has a negligible impact on the percent of gas leaking as part of the emulsion. With a solids holdup of 0.35, the percent of gas leaking as part of the

emulsion decreased to 1.0 to 3.9%. With a solids holdup of 0.55, the percent of gas leaking as part of the emulsion remained at 1.1 to 4.2%.

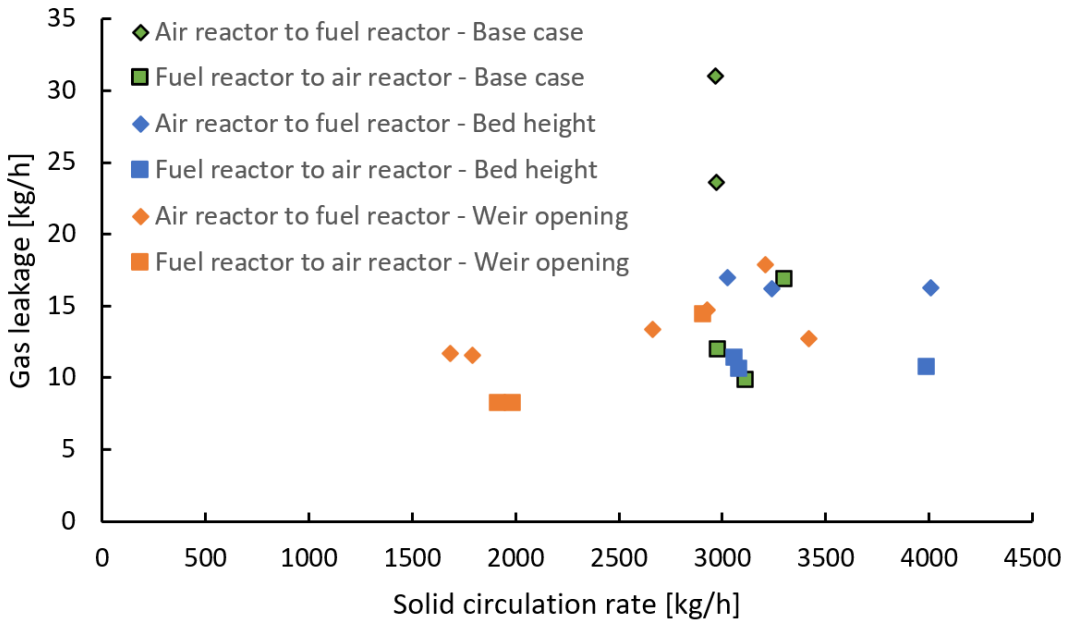

Figure 27. Relationship between solid circulation rate and gas leakage across the base case and all bed height and weir height conditions.

Figure 28 shows the relationship between solid circulation rate and the amount of purge gas that moved into the adjacent reactor for the base case and all bed height and weir height conditions. There appeared to be an increasing amount of FR/AR purge gas that moves into the adjacent reactor with increasing solid circulation rate. There did appear to be a sight downward trend between the AR/FR purge gas fate and the solid circulation rate. An increased movement of purge gas to the adjacent reactor with solid circulation rate was expected since some gas was expected to move between the reactors as a part of the solid-gas emulsion. This result is further evidence that the primary mode of gas movement between reactor sections is not via the emulsion, but via bubbles and/or jetting.

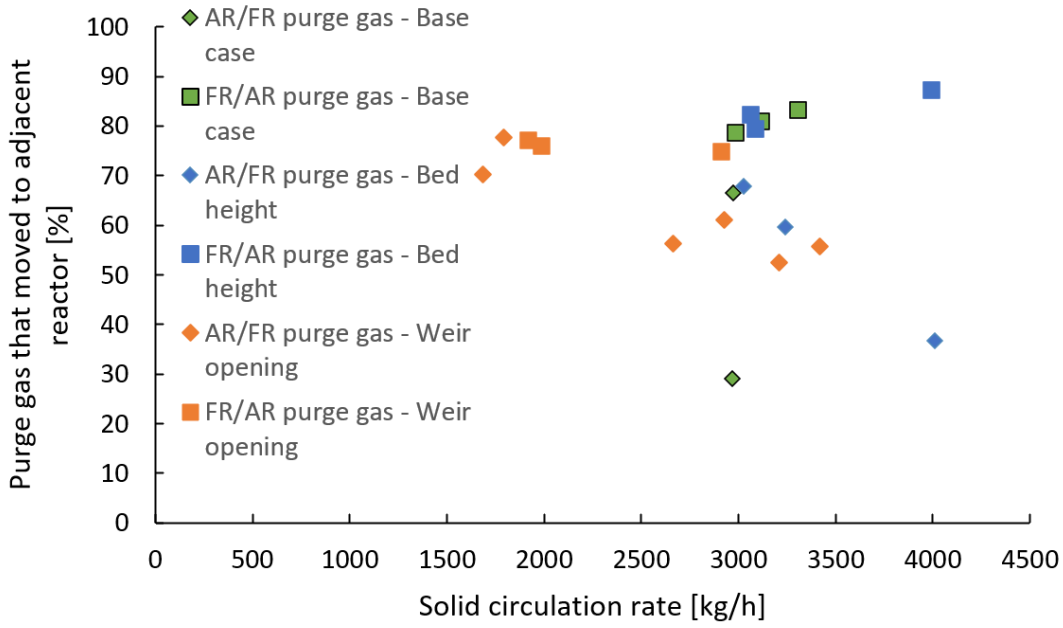

Figure 28. Relationship between solid circulation rate and the amount of purge gas that moved to adjacent reactor across the base case and all bed height and weir height conditions.

The relationship between the amount of purge gas that moved to the adjacent reactor and the gas leakage for the base case and all bed height and weir height conditions is shown in Figure 29. The air reactor to fuel reactor gas leakage was compared to the AR/FR purge gas fate, while the fuel reactor to air reactor gas leakage was compared to the FR/AR purge gas fate. In general, the amount of gas leakage decreased as the amount of purge gas that moved to the adjacent reactor increases. This trend makes sense, since the purge gas was moving to the adjacent reactor, rather than the fluidizing gas leaking into the adjacent reactor.

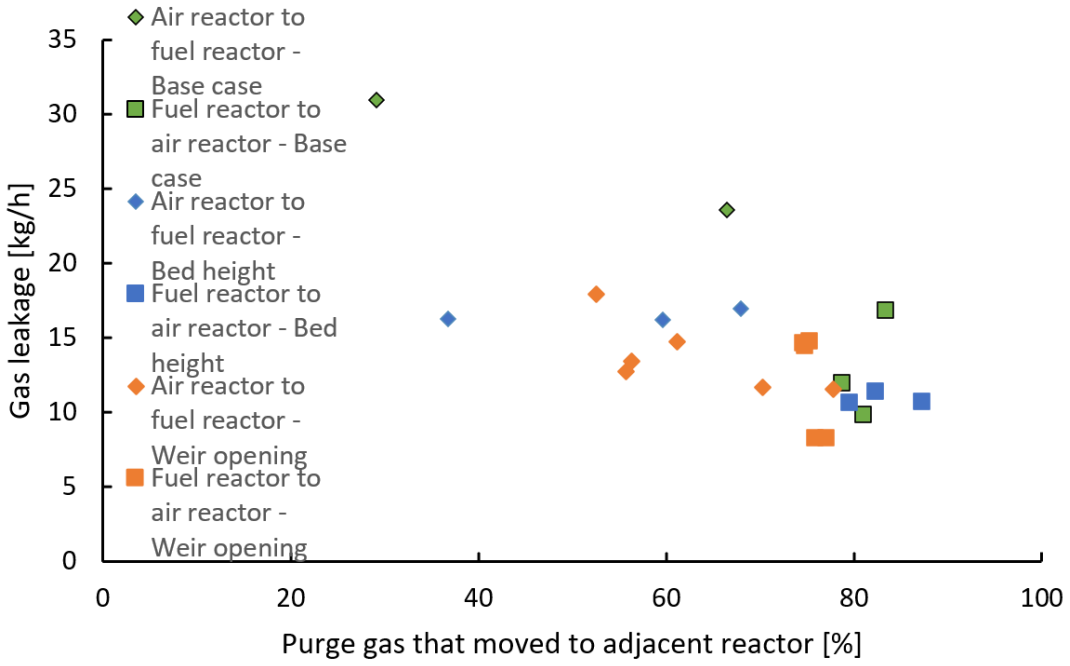

Figure 29. Relationship between the amount of purge gas that moved to adjacent reactor and gas leakage across the base case and all bed height and weir height conditions.

The highest coefficient of variation of the timeseries for all key parameters is shown in Table 15. Of all the parameters tested, the solid circulation rate had the highest coefficient of variation of the timeseries data, followed by the fuel reactor to air reactor gas leakage and then the air reactor to fuel reactor gas leakage. The purge fate time series data had much lower coefficients of variations. The highest coefficient of variation for the solid circulation rate times series was 0.2665, for fuel reactor to air gas leakage was 0.1576 and for air reactor to fuel reactor gas leakage was 0.0837. The highest coefficient of variation for all purge gas fate timeseries was over an order of magnitude less than highest coefficient of variation for the air reactor to fuel reactor gas leakage. The coefficient of variation of the timeseries data gives an indication of how much a given parameter may vary with time in the hot-flow PCL pilot plant. At the pilot scale and beyond, large fluctuations in solid circulation rate with time may influence the extent of reduction and oxidation of oxygen carrier. This fluctuation may affect fuel conversion and cause the fuel reactor effluent stream to have varying purity as it exits the reactor. Having a higher variability in gas leakage between reactors may also contribute to varying concentrations in the fuel reactor effluent and air reactor exhaust streams. The extent of this effect will be investigated during hot flow pilot testing of the PFIR.

Table 15. Highest coefficient of variation seen in timeseries for all key parameters.

Parameter	Highest coefficient of variation of timeseries
Solid circulation rate	0.2665
Air reactor to fuel reactor gas leakage	0.0837
Fuel reactor to air reactor gas leakage	0.1576
AR/FR purge gas remained in air reactor	0.0017
AR/FR purge gas moved to fuel reactor	0.0039
FR/AR purge gas moved to air reactor	0.0020
FR/AR purge gas remained in fuel reactor	0.0041

4 Conclusions and recommendations

This work examined the effect of bed height, weir opening height and purge configuration on solid circulation rate, gas leakage and purge gas fate. The results of this work will be used to better understand the PFIR reactor and to validate a CPFD model of the PFIR reactor to help inform the design and operation of the PCL pilot plant. It appeared that the primary method of gas movement between reactor sections was via bubbles and/or jets, with gas moving with the gas-solid emulsion contributing only a small percent of the gas movement. This is likely due to the fluidization ratio (U/U_{mf}) being around 3 and considering that most gas in excess of the minimum fluidization velocity flow through the bed in the form of gas voids/bubbles.

The solid circulation rate decreased with bed height between heights of 0.15 m and 0.25 m, due to an increased pressure at the distributor plate. Between 0.25 m and 0.5 m bed heights, the solid circulation rate remained unchanged, as the pressure at the distributor only increased by about 6.2 kPa. Solid circulation rate increased from 1800 kg/h to 3000 kg/h when the weir opening height was increased from 0.05 m to 0.1 m, indicating that the mostly solids circulate within the bottom 0.1 m of the bed. The number of purge rows had a small effect on solid circulation rate. Having no purge, a blank purge row and two purge rows had approximately equal solid circulation rate. The one purge row configuration led to a slightly higher solid circulation rate, due to the addition of purge gas. Finally, the vertical purge row configuration caused solid circulation to stop completely, by acting as a break.

Gas leakage between reactor sections was unaffected by bed height within the range of bed heights tested. The air reactor to fuel reactor gas leakage appeared to have a slight increase in gas leakage, while

the fuel reactor to air reactor gas leakage did not change significantly across the weir openings tested. Air reactor to fuel reactor gas leakage was relatively unchanged across all purge configurations. Adding a second AR/FR purge row appeared keep fuel reactor to air reactor gas leakage at a similar level compared to the one purge row configuration. A blanked purge row decreased the fuel reactor to air reactor gas leakage significantly compared to all other configurations. Finally, the vertical purge row caused an increase in fuel reactor to air reactor gas leakage.

The AR/FR purge gas increasingly moved into the fuel reactor with increasing bed heights and plateaued at 66.5%. The FR/AR purge gas fate remained constant across all bed heights tested. Increasing the weir opening height decreased the percent of AR/FR purge gas that moved to the fuel reactor, but did not effect the percent of FR/AR purge gas that moved to the air reactor. Adding a second AR/FR purge row decreased the percent of AR/FR purge gas that moved to the fuel reactor compared to the one purge configuration. Finally, the vertical purge row configuration had the lowest percent of purge gas that moved to the adjacent reactor compared to all other purge configurations.

Interpretation of the data herein had some challenges as the experiments were operating at the limit of the instrumentation. For example, more accurate temperature measurements could help increase the solid circulation rate accuracy, but there are no more accurate RTDs readily available, and the heater power input was already at maximum considering temperature limits of vessel materials. Furthermore, small concentrations of helium tracer were used to avoid impacting gas physical properties for gas leakage tests. The resulting concentrations at the outlet of the PFIR reactor were relatively close (~one order of magnitude) to the detection limit of the gas chromatograph. Increasing helium concentrations and performing more repeats could help with respectively increasing accuracy and precision, but data were deemed of sufficient quality for CPFD model validation and to interpret most of the trends. Finally, the parametric ranges used herein were limited by the constraints imposed on the system, such as pressure in the windbox and the physical constraints of the reactor and measurement methods.

There are a couple areas of future work that can be pursued. Most importantly, the data presented herein can be used to validate the CPFD model of the PFIR reactor. Once validated, the model can be used to help design the PFIR reactor for the PCL pilot plant to determine the viability of PCL as a decarbonization solution for small- and medium-scale emitters. The second area of future work would be completing additional test work in the cold flow PFIR system. This test work could include more repeats of certain conditions, using different superficial gas velocities in the air reactor compared to the fuel reactor, or other targeted tests. Performing additional tests with the vertical purge tuyeres could help determine if

the vertical purge configuration performs better at lower jet velocities (i.e. allows for solid circulation, while preventing gas leakage). The validated CPFD model and additional tests can be used to further investigate the unexpected purge fate results and further investigate gas leakage via bubble movement and jetting.

5 References

[1] X. Lan, P. Tans, and K. W. Thoning, "Trends in globally-averaged CO2 determined from NOAA Global Monitoring Laboratory measurements. Version 2023-04." doi: 10.15138/9N0H-ZH07.

[2] Intergovernmental Panel on Climate Change, "Global warming of 1.5°C," 2018. Accessed: Apr. 09, 2021. [Online]. Available: http://www.ipcc.ch/report/sr15/

[3] United Nations Framework Convention on Climate Change, "The Paris Agreement," *United Nations Framework Convention on Climate Change*. https://unfccc.int/process-and-meetings/the-paris-agreement/ (accessed Apr. 19, 2023).

[4] Environment and Climate Change Canada, "A Clean Electricity Standard in support of a net-zero electricity sector," Environment and Climate Change Canada, Discussion paper, 2022. Accessed: Apr. 19, 2023. [Online]. Available: https://www.canada.ca/en/environment-climate-change/services/canadian-environmental-protection-act-registry/achieving-net-zero-emissions-electricity-generation-discussion-paper.html

[5] IEA, "Carbon capture, utilisation and storage," International Energy Agency, Paris, 2022. Accessed: Apr. 19, 2023. [Online]. Available: https://www.iea.org/reports/carbon-capture-utilisation-and-storage-2

[6] N. S. Sifat and Y. Haseli, "A Critical Review of CO2 Capture Technologies and Prospects for Clean Power Generation," *Energies*, vol. 12, no. 21, Art. no. 21, Jan. 2019, doi: 10.3390/en12214143.

[7] A. Lyngfelt, "Oxygen carriers for chemical-looping combustion," in *Calcium and Chemical Looping Technology for Power Generation and Carbon Dioxide (CO2) Capture*, Elsevier, 2015, pp. 221–254. doi: 10.1016/B978-0-85709-243-4.00011-2.

[8] T. Pröll, "Fundamentals of chemical looping combustion and introduction to CLC reactor design," in *Calcium and Chemical Looping Technology for Power Generation and Carbon Dioxide (CO2) Capture*, Elsevier, 2015, pp. 197–219. doi: 10.1016/B978-0-85709-243-4.00010-0.

[9] R. T. Symonds, R. W. Hughes, D. Y. Lu, P. Navarri, and O. Ashrafi, "Systems analysis of pressurized chemical looping combustion for SAGD applications," *Int. J. Greenh. Gas Control*, vol. 73, pp. 111–123, Jun. 2018, doi: 10.1016/j.ijggc.2018.03.008.

[10] A. Cabello *et al.*, "Economic analysis of pressurized chemical looping combustion for steam assisted gravity drainage applications," *Int. J. Greenh. Gas Control*, vol. 90, p. 102786, Nov. 2019, doi: 10.1016/j.ijggc.2019.102786.

[11] R. Symonds, R. Hughes, N. Bond, S. Champagne, and E. Luka, "Pressurized Chemical Looping – Steam Methane Reforming: Process Modelling and Performance Assessments," 2022.

[12] K. Adham, C. T. HARRIS, and A. KOKOURINE, "Plug flow reactor with internal recirculation fluidized bed," CA2951724C, Jun. 20, 2017 Accessed: Apr. 18, 2023. [Online]. Available: https://patents.google.com/patent/CA2951724C/en

[13] A. Alain *et al.*, "Impact of gas distributor on hydrodynamics in a cold flow annular dual fluidized bed for pressurized chemical looping," in *Proceedings of the Fluidized Bed Conversion Conference 2022*, Gothenburg, Sweden, 2022, p. 9.

[14] B. Kronberger, E. Johansson, G. Löffler, T. Mattisson, A. Lyngfelt, and H. Hofbauer, “A Two-Compartment Fluidized Bed Reactor for CO2 Capture by Chemical-Looping Combustion,” *Chem. Eng. Technol.*, vol. 27, no. 12, pp. 1318–1326, 2004, doi: 10.1002/ceat.200402137.
[15] C. McIntyre, “CPFD Modeling of a Novel Internally Circulating Bubbling Fluidized Bed for Chemical Looping Combustion,” Université d’Ottawa / University of Ottawa, 2021. Accessed: Sep. 20, 2021. [Online]. Available: http://ruor.uottawa.ca.proxy.bib.uottawa.ca/handle/10393/42054
[16] Environment and Climate Change Canada, “Greenhouse Gas Reporting Program (GHGRP) - Facility Greenhouse Gas (GHG) Data.” Government of Canada, 2018. Accessed: Apr. 19, 2023. [Online]. Available: https://open.canada.ca/data/en/dataset/a8ba14b7-7f23-462a-bdbb-83b0ef629823
[17] D. C. Montgomery, *Introduction to Statistical Quality Control*, 4th ed. New York, NY: John Wiley & Sons, Inc., 2001.
[18] K. Adham, C. Harris, and A. Kokourine, “Modeling and Process Features of Plug Flow Reactor with Internal Recirculation for Biomass Pyrolysis,” *J. Chem. Eng. Process Technol.*, vol. 08, no. 04, 2017, doi: 10.4172/2157-7048.1000353.
[19] T. Fitzgerald, N. Catipovic, and G. Jovanovic, “Solid tracer studies in a tube-filled fluidized bed,” in *Proceedings of the 5th International Conference on Fluidised Bed Combustion*, 1966, pp. 135–154.
[20] R. R. Cranfield, “A probe for bubble detection and measurement in large particle fluidised beds,” *Chem. Eng. Sci.*, vol. 27, no. 2, pp. 239–245, Feb. 1972, doi: 10.1016/0009-2509(72)85061-9.
[21] A. Avidan and J. Yerushalmi, “Solids mixing in an expanded top fluid bed,” *AIChE J.*, vol. 31, no. 5, pp. 835–841, May 1985, doi: 10.1002/aic.690310520.
[22] R. Turton, T. J. Fitzgerald, and O. Levenspiel, “An experimental method to determine the heat transfer coefficient between fine fluidized particles and air via changes in magnetic properties,” *Int. J. Heat Mass Transf.*, vol. 32, no. 2, pp. 289–296, 1989, doi: 10.1016/0017-9310(89)90176-2.
[23] D. C. Guío-Pérez, T. Pröll, J. Wassermann, and H. Hofbauer, “Design of an Inductance Measurement System for Determination of Particle Residence Time in a Dual Circulating Fluidized Bed Cold Flow Model,” *Ind. Eng. Chem. Res.*, vol. 52, pp. 10732–10740, Jul. 2013.
[24] A. Alain, “IMT Results and Lessons Learned,” Natural Resources Canada, CanmetENERGY-Ottawa, Internal Report, Jan. 2021.
[25] E. Sette, D. Pallarès, F. Johnsson, F. Ahrentorp, A. Ericsson, and C. Johansson, “Magnetic tracer-particle tracking in a fluid dynamically down-scaled bubbling fluidized bed,” *Fuel Process. Technol.*, vol. 138, pp. 368–377, Oct. 2015, doi: 10.1016/j.fuproc.2015.06.016.
[26] A. Köhler, D. Pallarès, and F. Johnsson, “Magnetic tracking of a fuel particle in a fluid-dynamically down-scaled fluidised bed,” *Fuel Process. Technol.*, vol. 162, pp. 147–156, Jul. 2017, doi: 10.1016/j.fuproc.2017.03.018.
[27] K. A. Buist, P. Jayaprakash, J. A. M. Kuipers, N. G. Deen, and J. T. Padding, “Magnetic particle tracking for nonspherical particles in a cylindrical fluidized bed,” *AIChE J.*, vol. 63, no. 12, pp. 5335–5342, Dec. 2017, doi: 10.1002/aic.15854.
[28] F. Ahrentorp and C. Johansson, “Report on signal resolution regarding magnet volumes and sensor/magnet distances in RISE magnet tracking system,” RISE Research Institutes of Sweden, Internal Report, Sep. 2021.
[29] S. Roy, “Radiotracer and particle tracking methods, modeling and scale-up,” *AIChE J.*, vol. 63, no. 1, pp. 314–326, 2017, doi: 10.1002/aic.15559.
[30] J. S. Lin, M. M. Chen, and B. T. Chao, “A novel radioactive particle tracking facility for measurement of solids motion in gas fluidized beds,” *AIChE J.*, vol. 31, no. 3, pp. 465–473, 1985, doi: 10.1002/aic.690310314.
[31] G. A. Lindner and S. Mišković, “Feasibility of RPT Application for Flow Mapping of Pilot-Scale PFIR Reactor,” The University of British Colombia, Internal Report, Mar. 2022.

Appendix A: Additional data, tables, and figures

Timeseries graphs for all data points

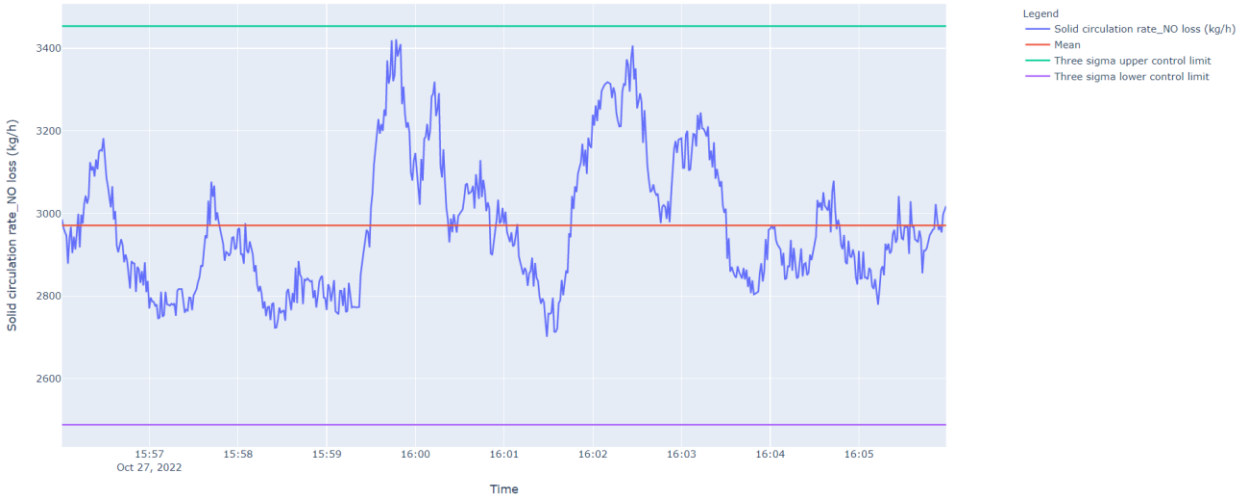

Figure 30. Timeseries graphs for solid circulation rate at the base case condition (first repeat).

Figure 31. Timeseries graphs for solid circulation rate at the base case condition (second repeat).

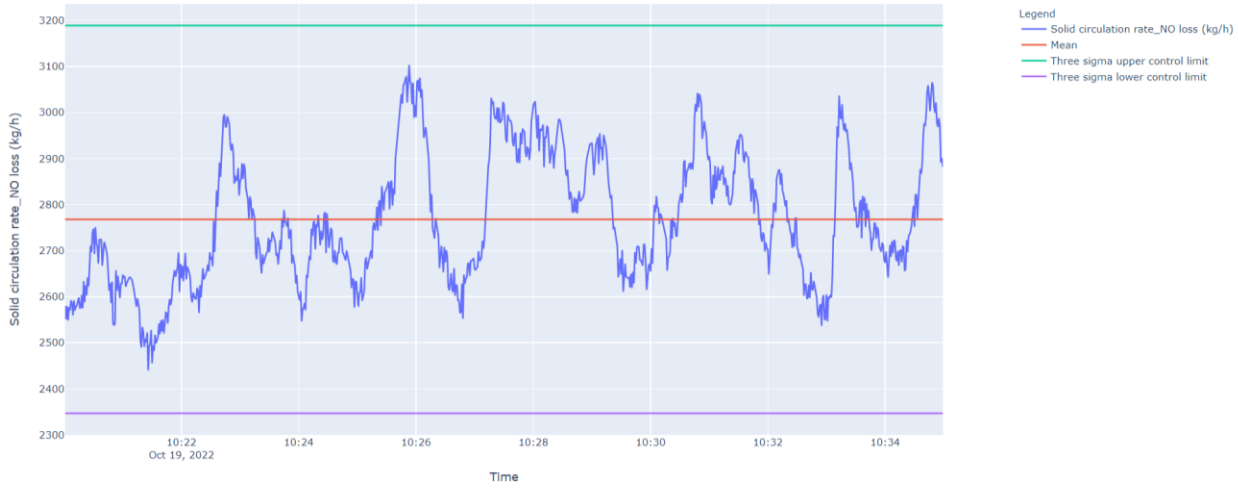

Figure 32. Timeseries graphs for solid circulation rate at the base case condition (third repeat).

Figure 33. Timeseries graphs for solid circulation rate at the base case condition (forth repeat).

Figure 34. Timeseries graphs for solid circulation rate at the base case condition (fifth repeat).

Figure 35. Timeseries graphs for air reactor to fuel reactor gas leakage at the base case condition (first repeat).

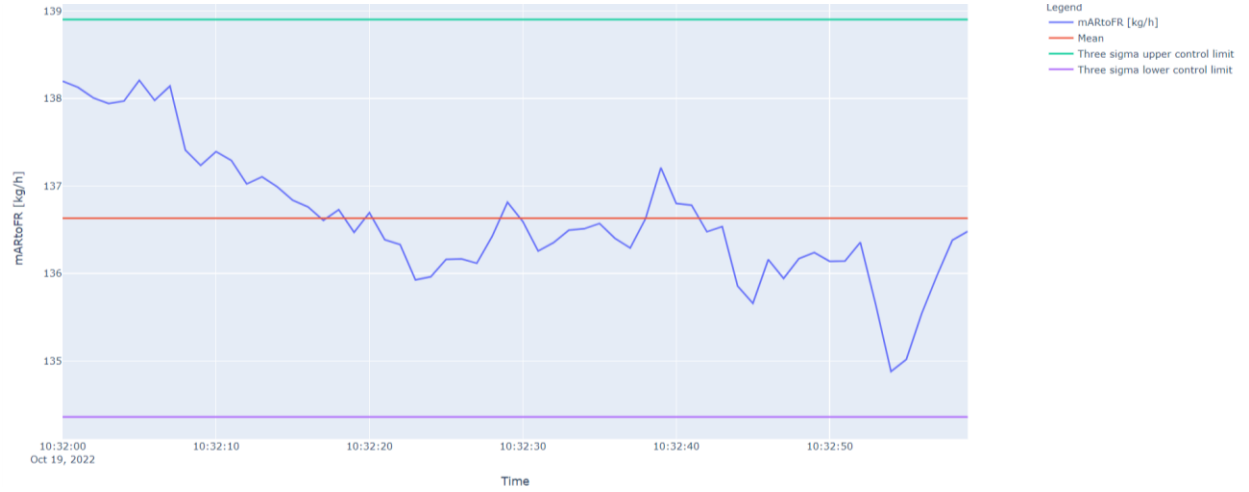

Figure 36. Timeseries graphs for air reactor to fuel reactor gas leakage at the base case condition (second repeat).

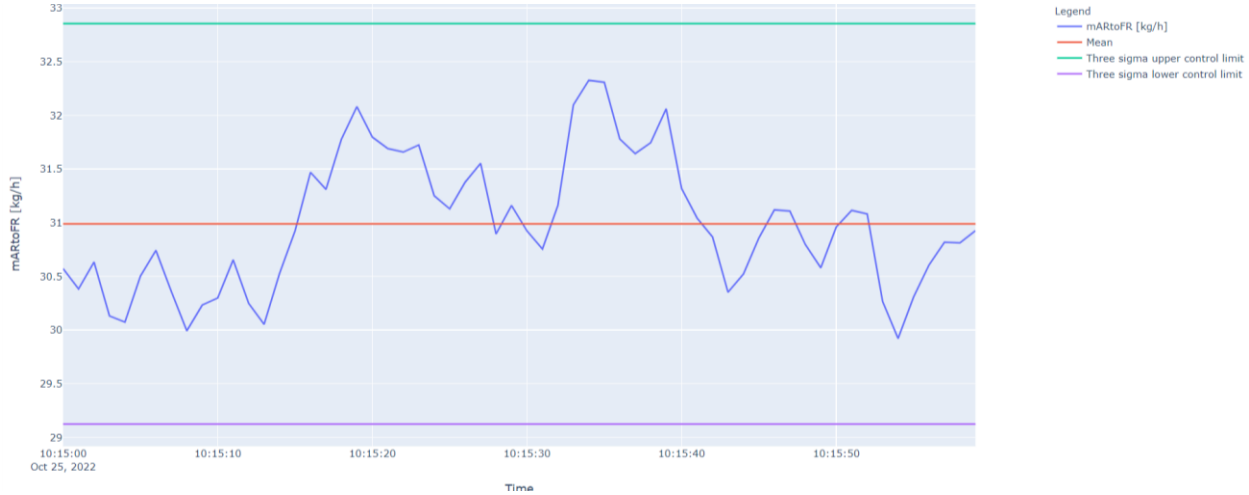

Figure 37. Timeseries graphs for air reactor to fuel reactor gas leakage at the base case condition (third repeat).

Figure 38. Timeseries graphs for fuel reactor to air reactor gas leakage at the base case condition (first repeat).

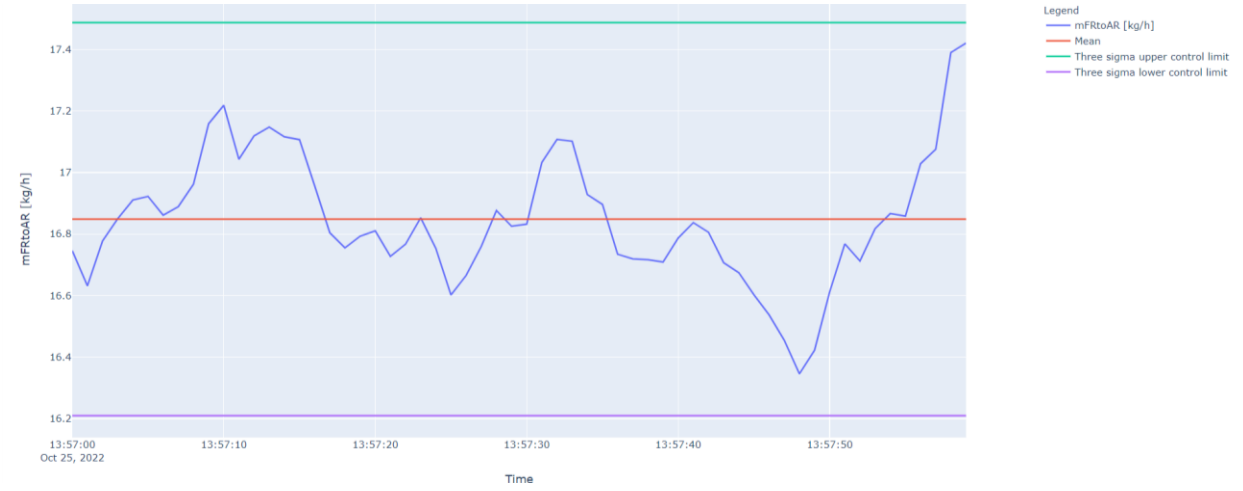

Figure 39. Timeseries graphs for fuel reactor to air reactor gas leakage at the base case condition (second repeat).

Figure 40. Timeseries graphs fate of the amount of AR/FR purge gas that remained in the air reactor at the base case condition (first repeat).

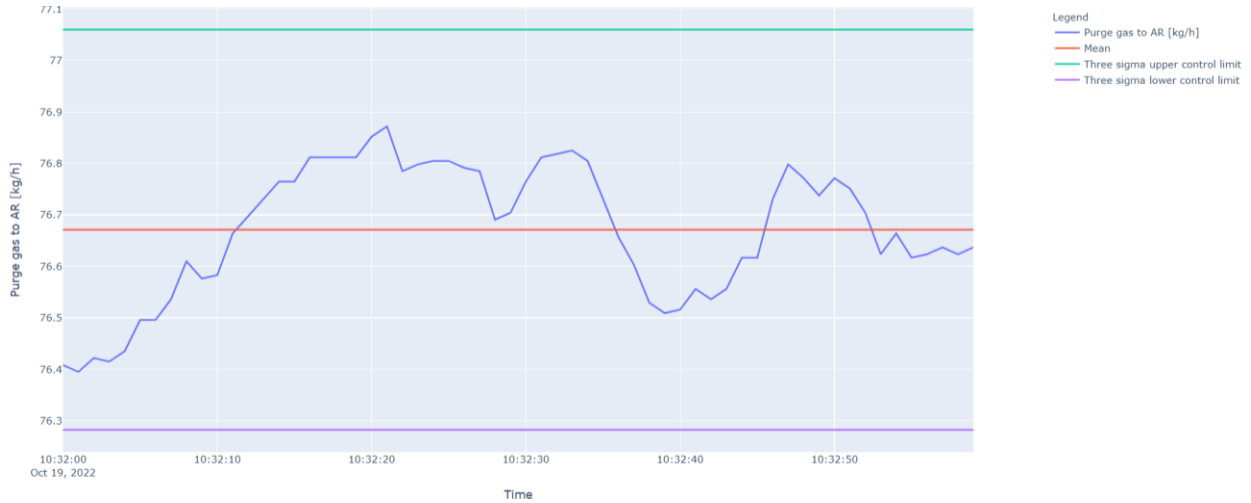

Figure 41. Timeseries graphs fate of the amount of AR/FR purge gas that remained in the air reactor at the base case condition (second repeat).

Figure 42. Timeseries graphs fate of the amount of AR/FR purge gas that remained in the air reactor at the base case condition (third repeat).

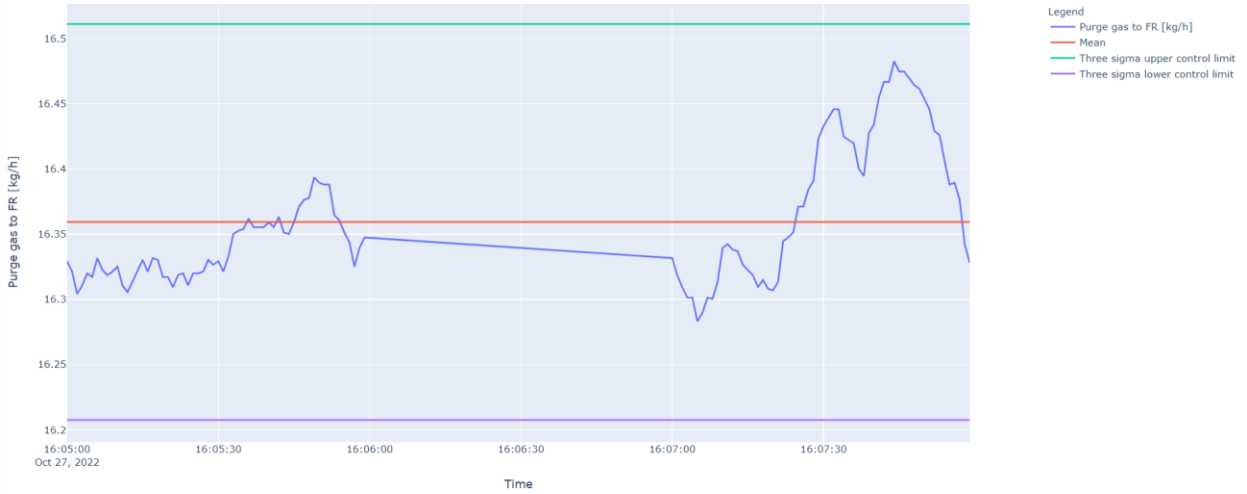

Figure 43. Timeseries graphs fate of the amount of AR/FR purge gas that moved to the fuel reactor at the base case condition (first repeat).

Figure 44. Timeseries graphs fate of the amount of AR/FR purge gas that moved to the fuel reactor at the base case condition (second repeat).

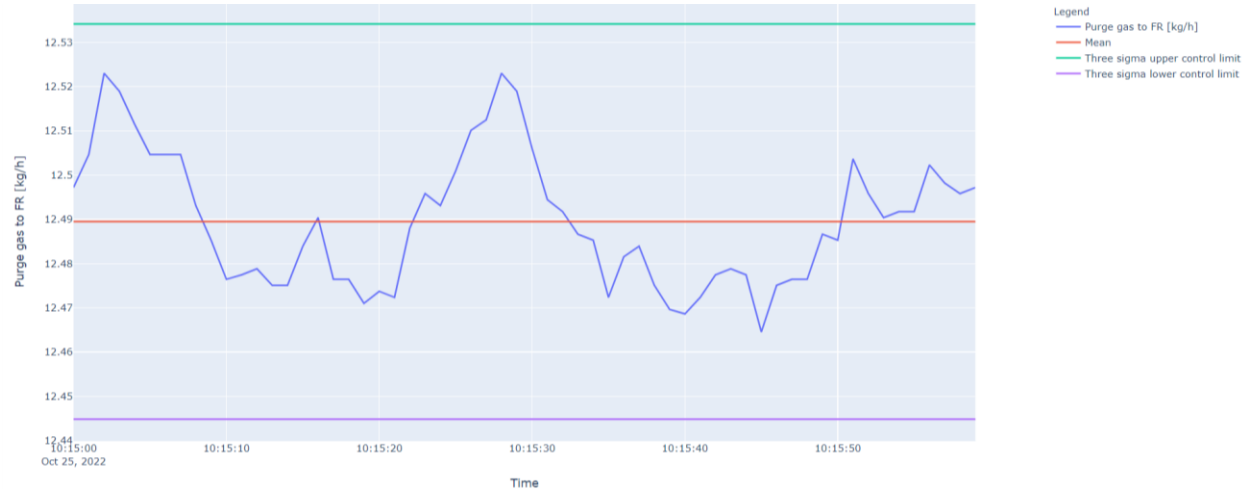

Figure 45. Timeseries graphs fate of the amount of AR/FR purge gas that moved to the fuel reactor at the base case condition (third repeat).

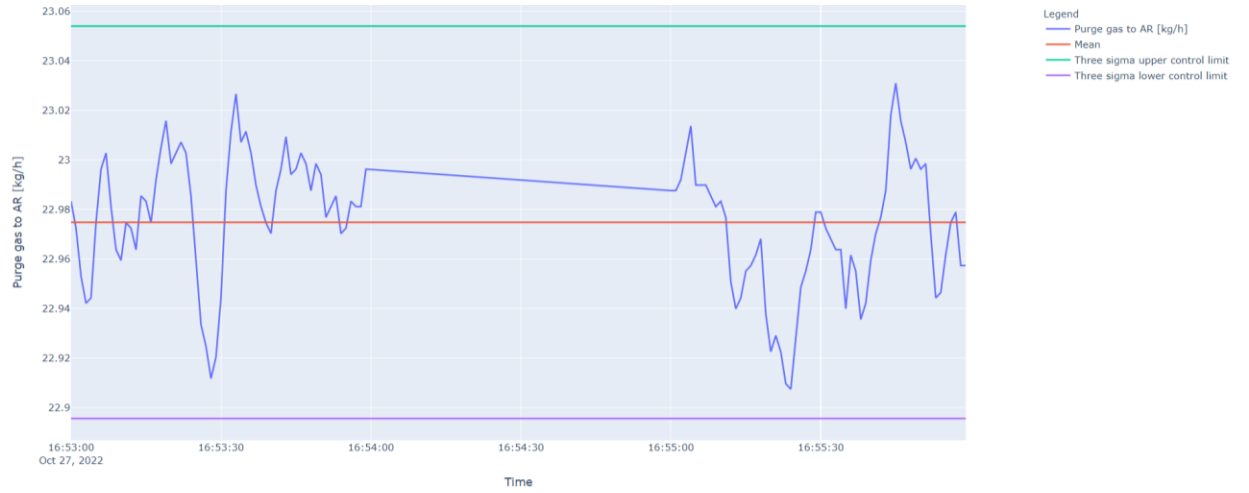

Figure 46. Timeseries graphs fate of the amount of FR/AR purge gas that moved to air reactor at the base case condition (first repeat).

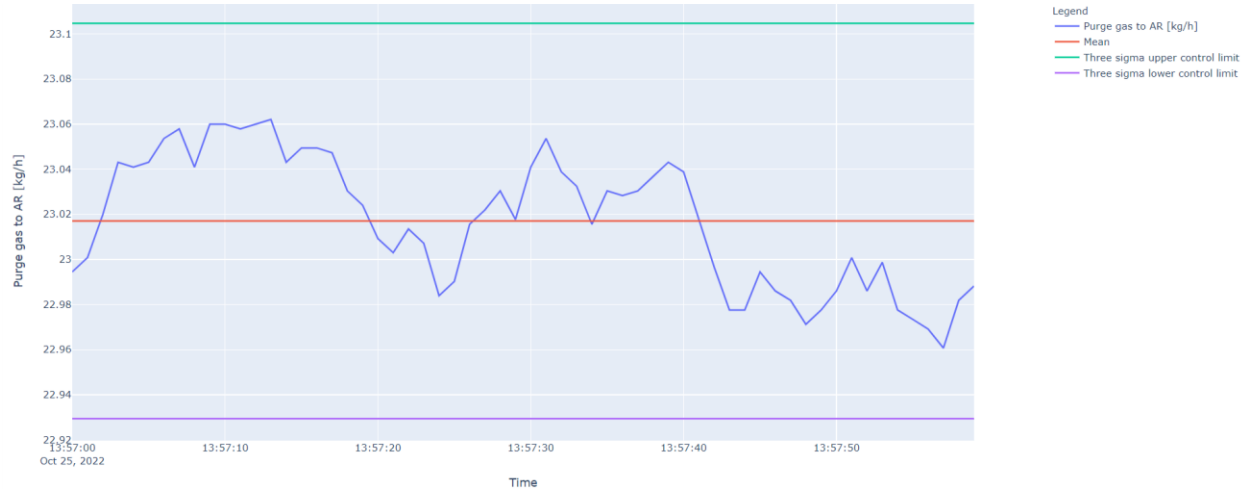

Figure 47. Timeseries graphs fate of the amount of FR/AR purge gas that moved to air reactor at the base case condition (second repeat).

Figure 48. Timeseries graphs fate of the amount of FR/AR purge gas that remained in the fuel reactor at the base case condition (first repeat).

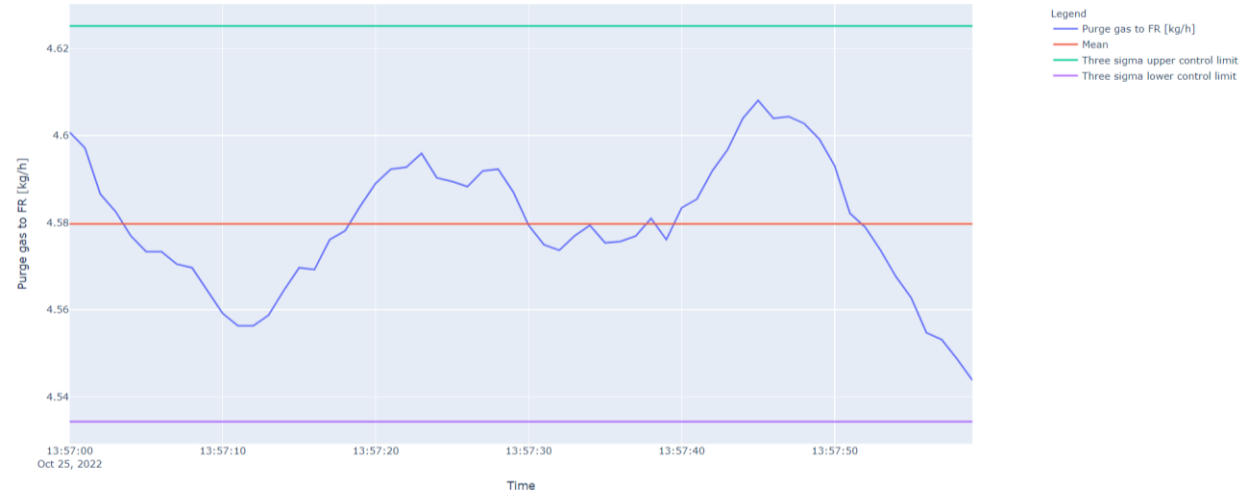

Figure 49. Timeseries graphs fate of the amount of FR/AR purge gas that remained in the fuel reactor at the base case condition (second repeat).

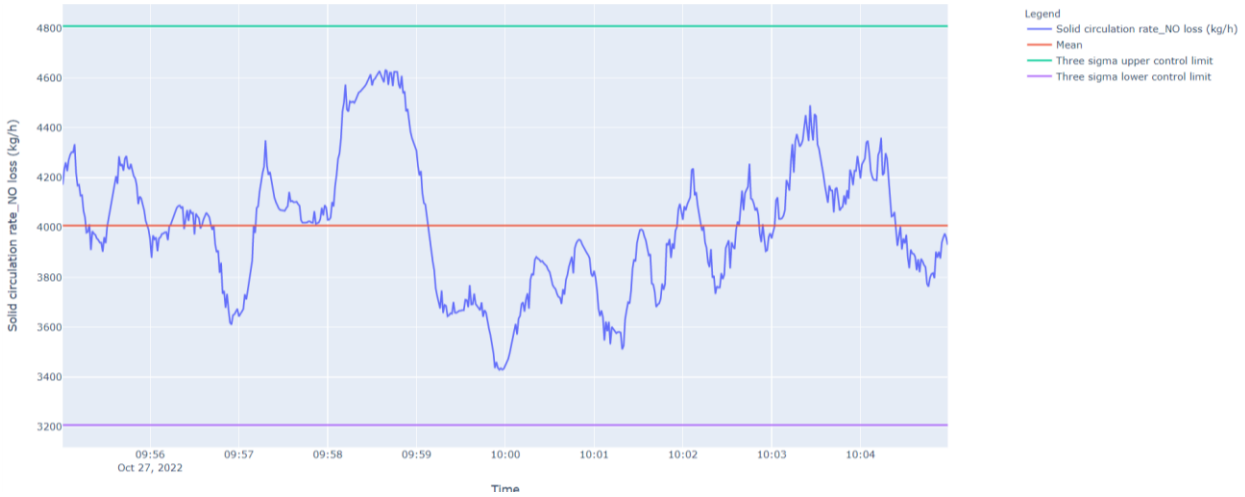

Figure 50. Timeseries graphs for solid circulation rate at the 0.15 m bed height condition (first repeat).

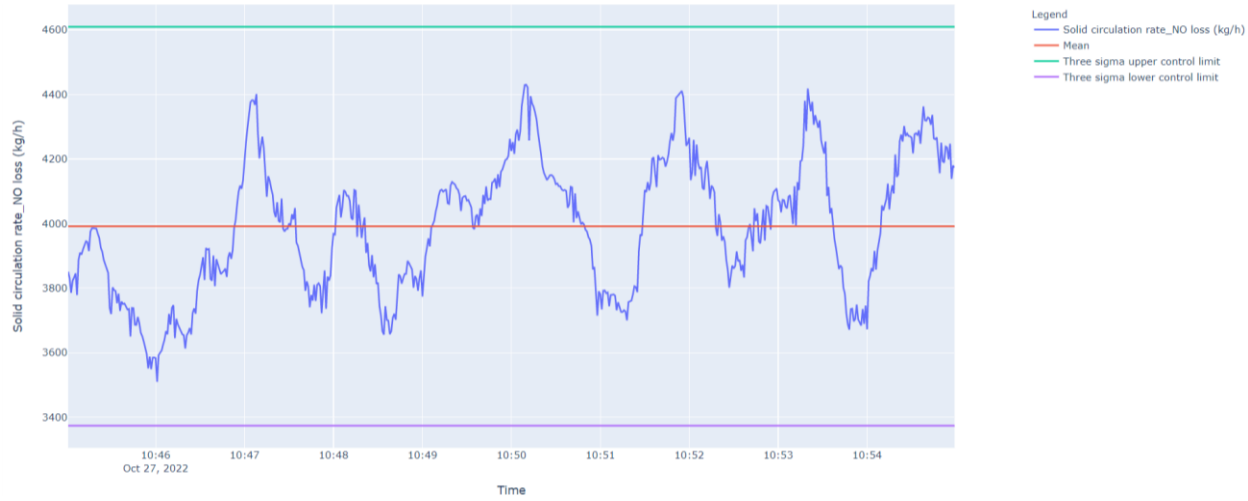

Figure 51. Timeseries graphs for solid circulation rate at the 0.15 m bed height condition (second repeat).

Figure 52. Timeseries graphs for air reactor to fuel reactor gas leakage at the 0.15 m bed height condition.

Figure 53. Timeseries graphs for fuel reactor to air reactor gas leakage at the 0.15 m bed height condition.

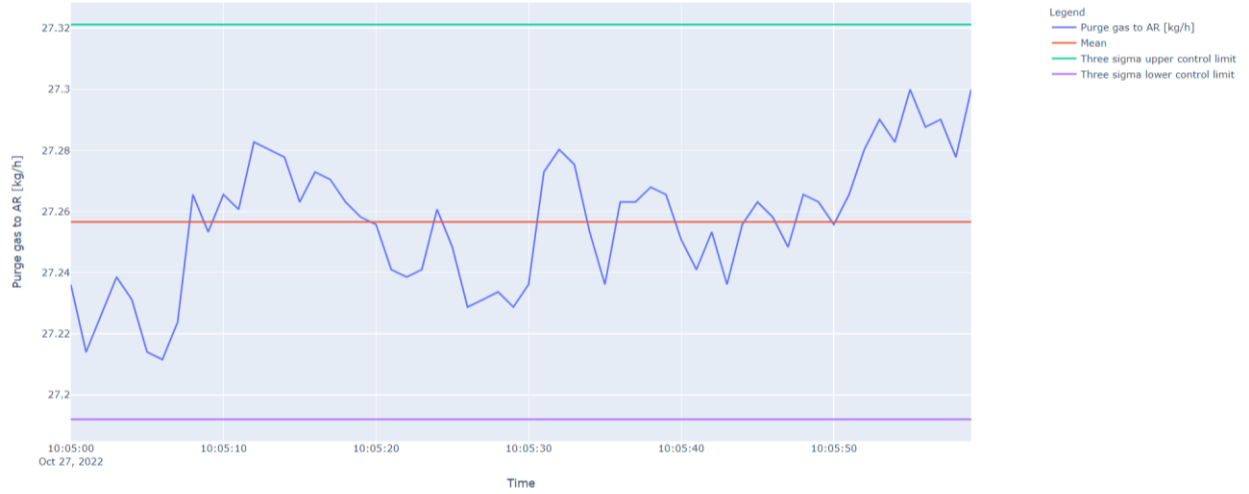

Figure 54. Timeseries graphs fate of the amount of AR/FR purge gas that remained in the air reactor at the 0.15 m bed height condition.

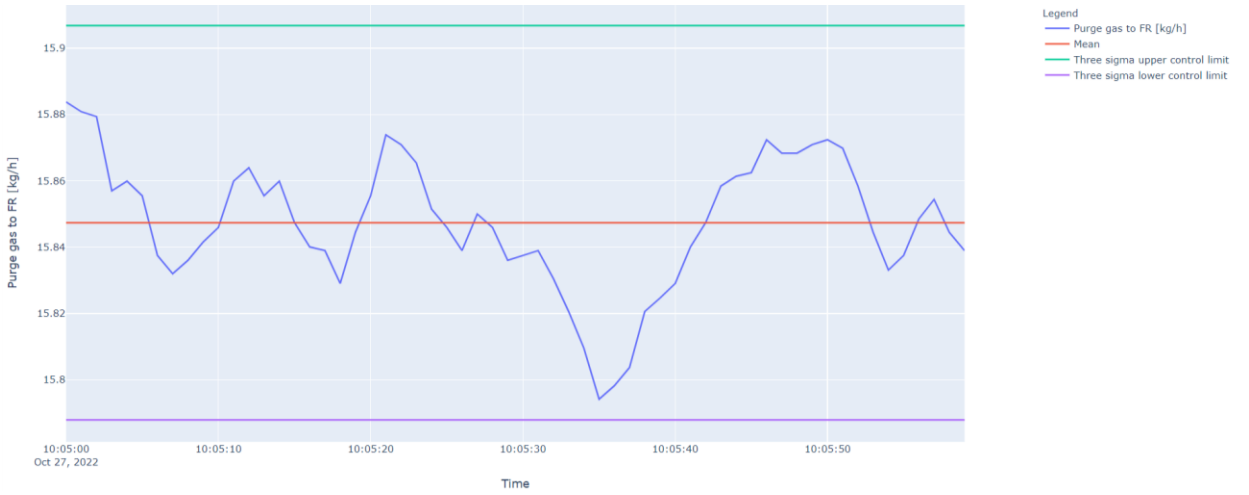

Figure 55. Timeseries graphs fate of the amount of AR/FR purge gas that moved to the fuel reactor at the 0.15 m bed height condition.

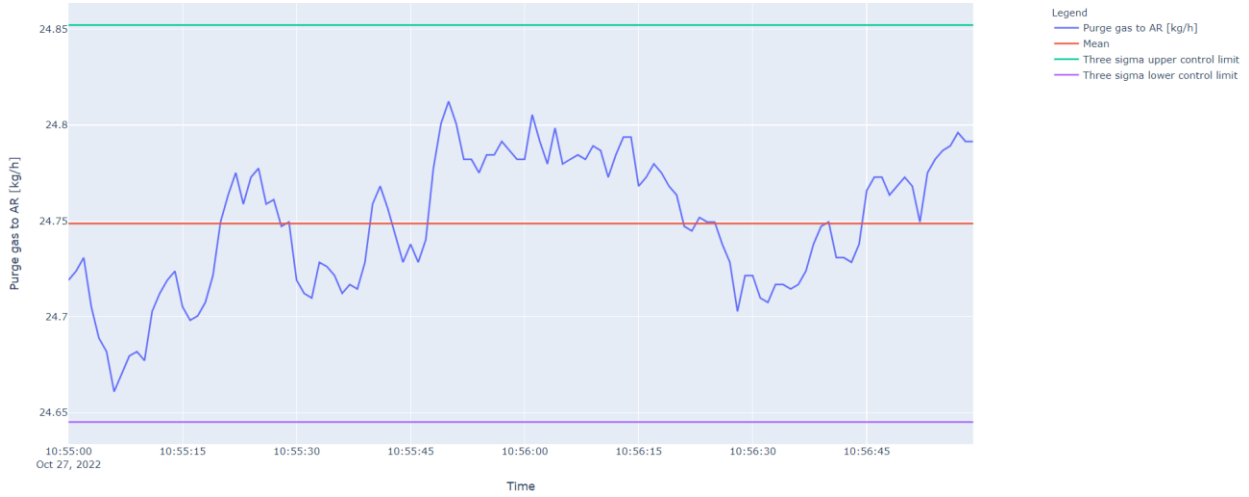

Figure 56. Timeseries graphs fate of the amount of FR/AR purge gas that moved to the air reactor at the 0.15 m bed height condition.

Figure 57. Timeseries graphs fate of the amount of FR/AR purge gas that remained in the fuel reactor at the 0.15 m bed height condition.

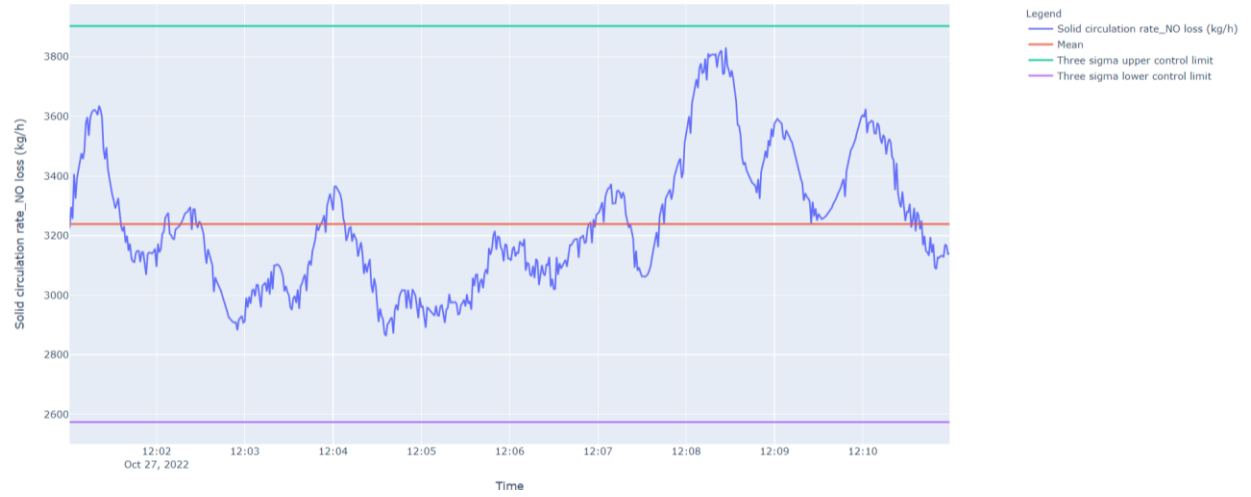

Figure 58. Timeseries graphs for solid circulation rate at the 0.25 m bed height condition (first repeat).

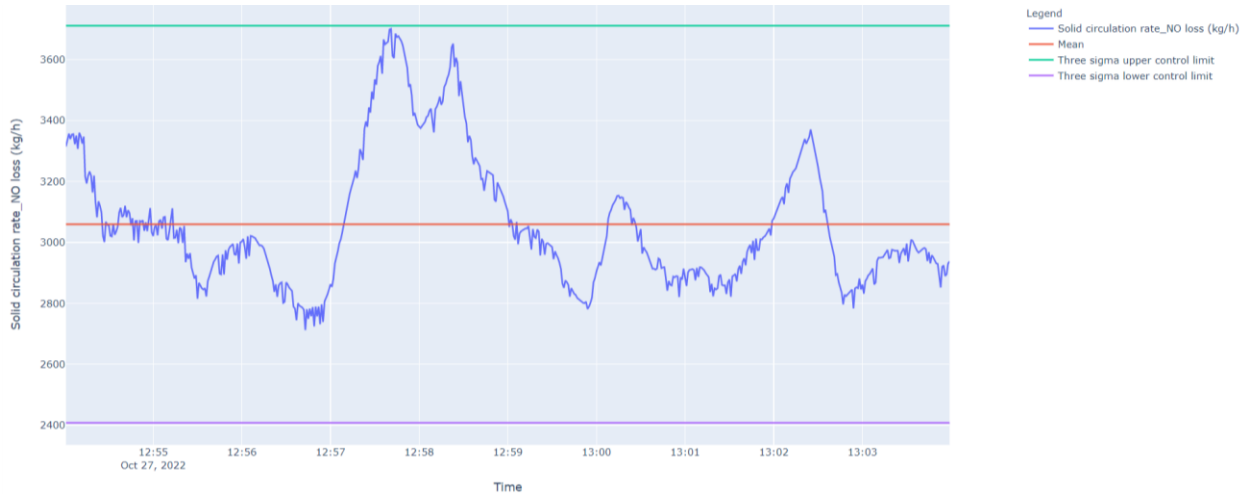

Figure 59. Timeseries graphs for solid circulation rate at the 0.25 m bed height condition (second repeat).

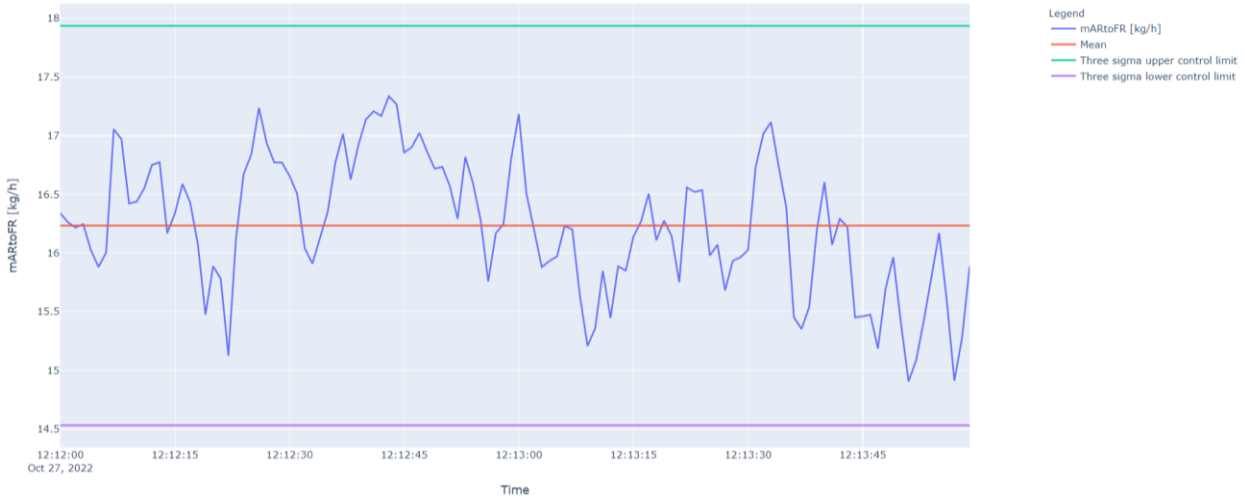

Figure 60. Timeseries graphs for air reactor to fuel reactor gas leakage at the 0.25 m bed height condition.

Figure 61. Timeseries graphs for fuel reactor to air reactor gas leakage at the 0.25 m bed height condition.

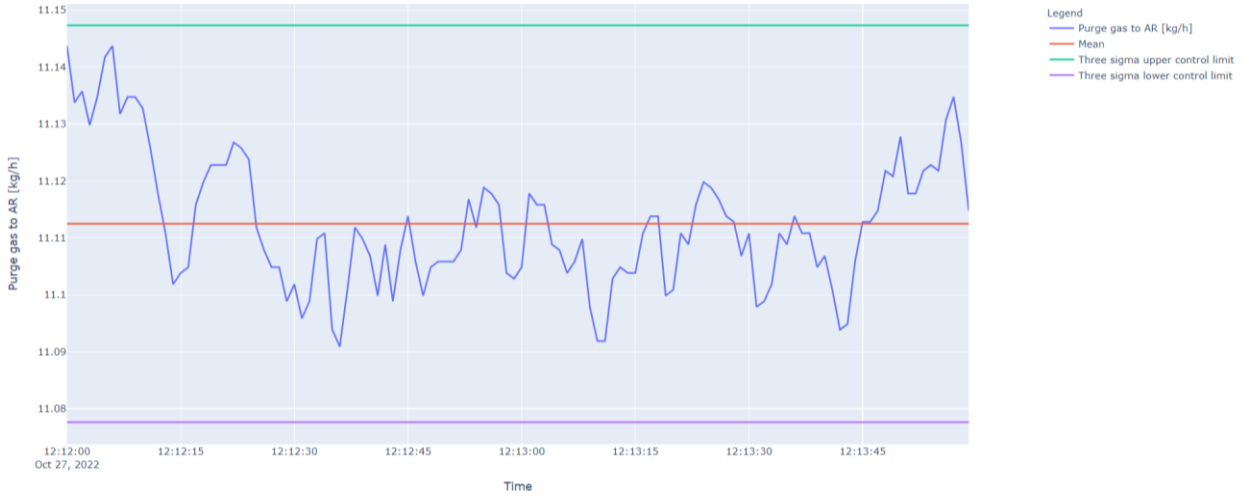

Figure 62. Timeseries graphs fate of the amount of AR/FR purge gas that remained in the air reactor at the 0.25 m bed height condition.

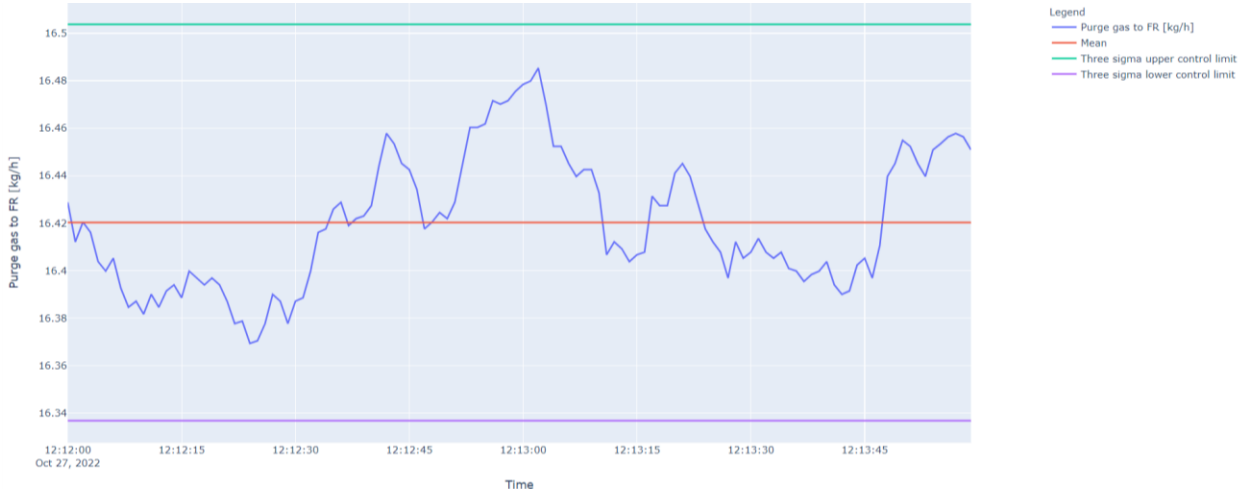

Figure 63. Timeseries graphs fate of the amount of AR/FR purge gas that moved to the fuel reactor at the 0.25 m bed height condition.

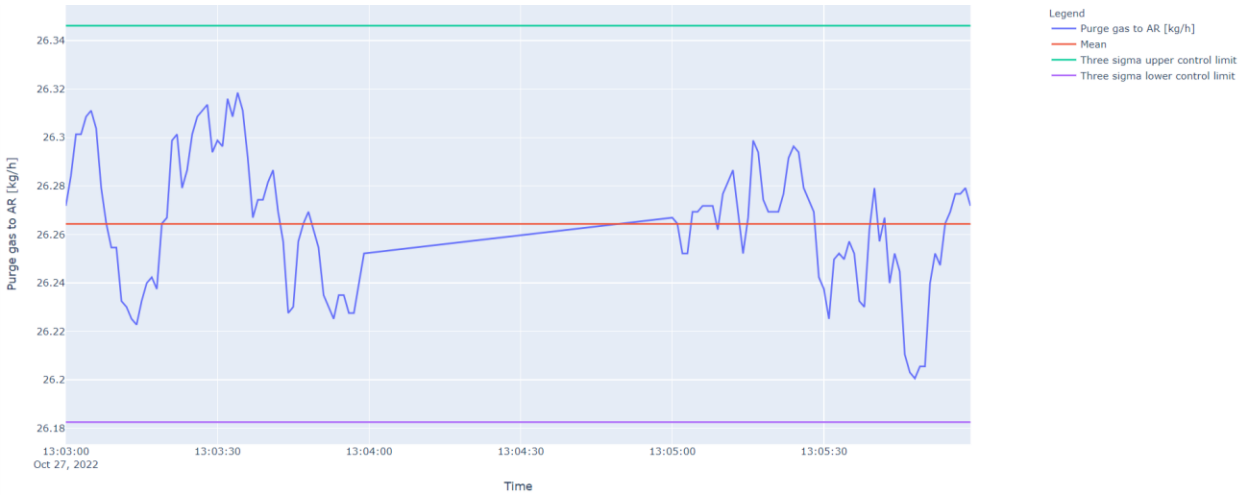

Figure 64. Timeseries graphs fate of the amount of FR/AR purge gas that moved to the air reactor at the 0.25 m bed height condition.

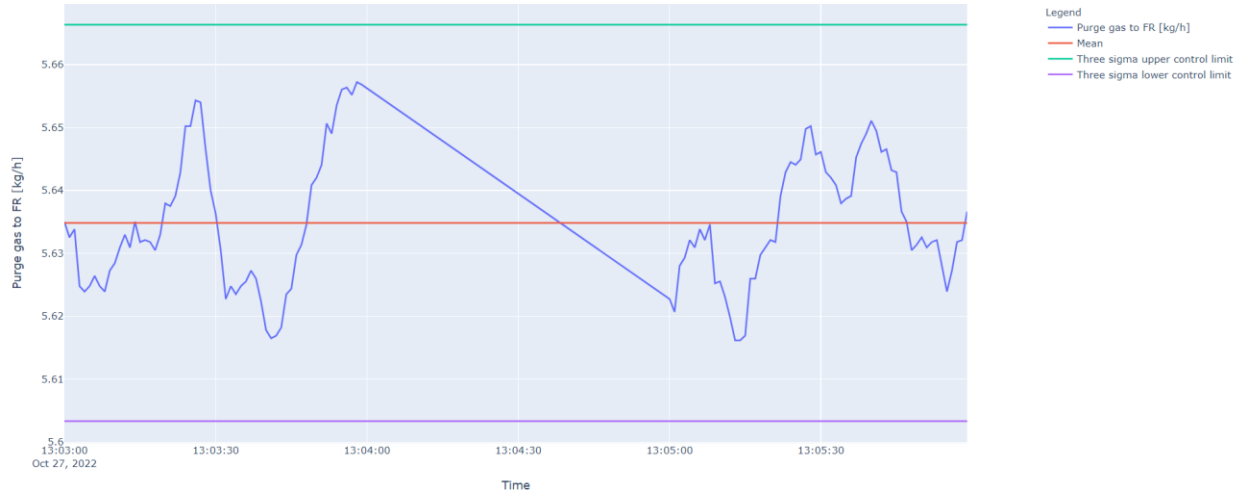

Figure 65. Timeseries graphs fate of the amount of FR/AR purge gas that remained in the fuel reactor at the 0.25 m bed height condition.

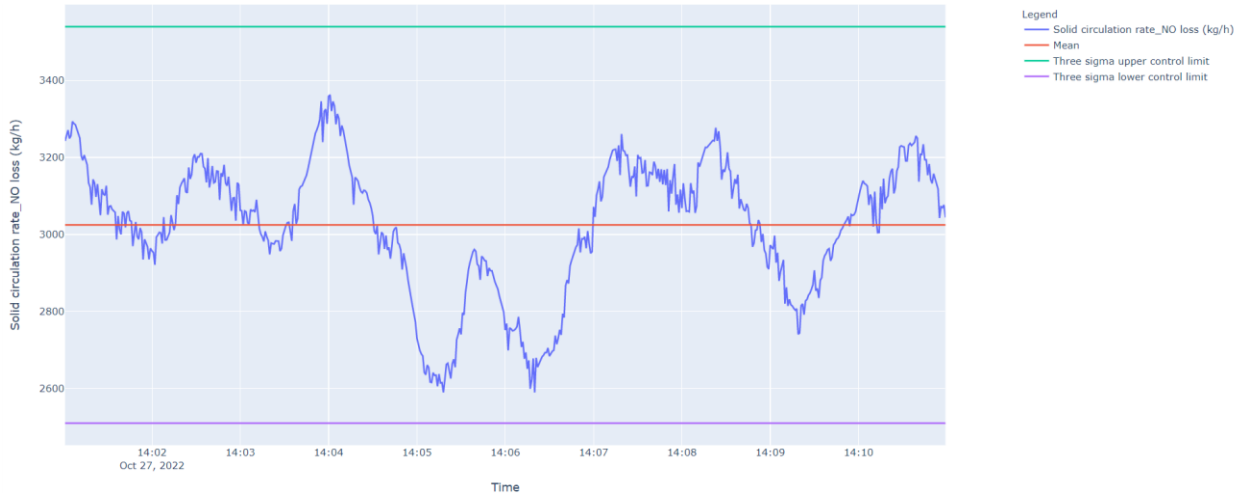

Figure 66. Timeseries graphs for solid circulation rate at the 0.35 m bed height condition (first repeat).

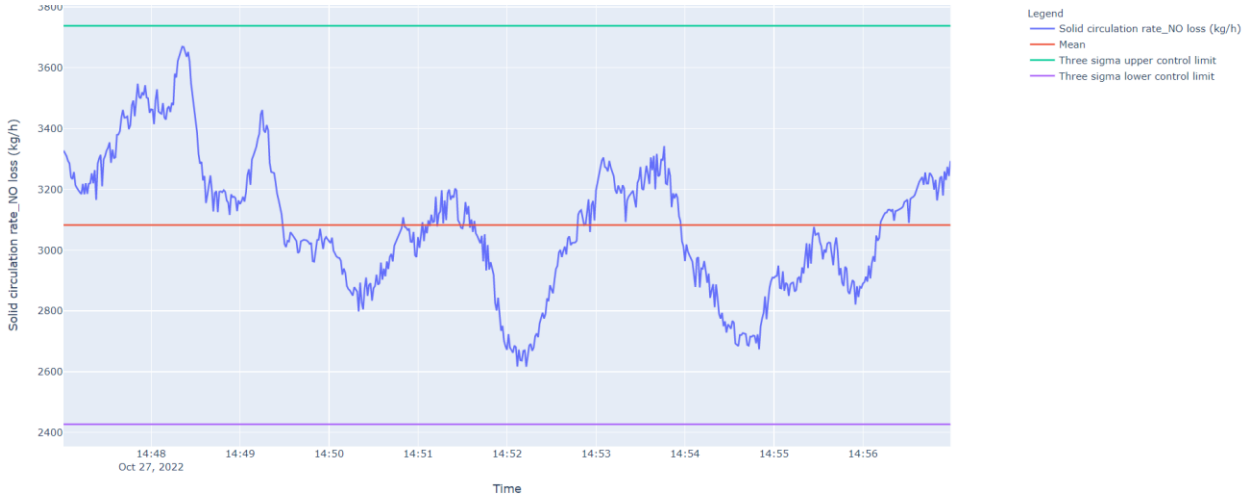

Figure 67. Timeseries graphs for solid circulation rate at the 0.35 m bed height condition (second repeat).

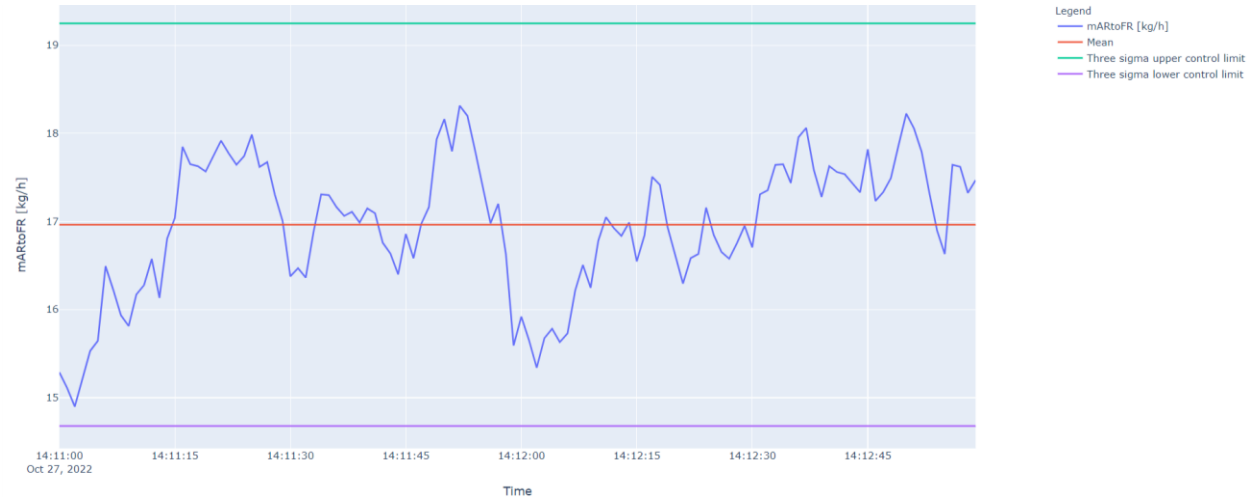

Figure 68. Timeseries graphs for air reactor to fuel reactor gas leakage at the 0.35 m bed height condition.

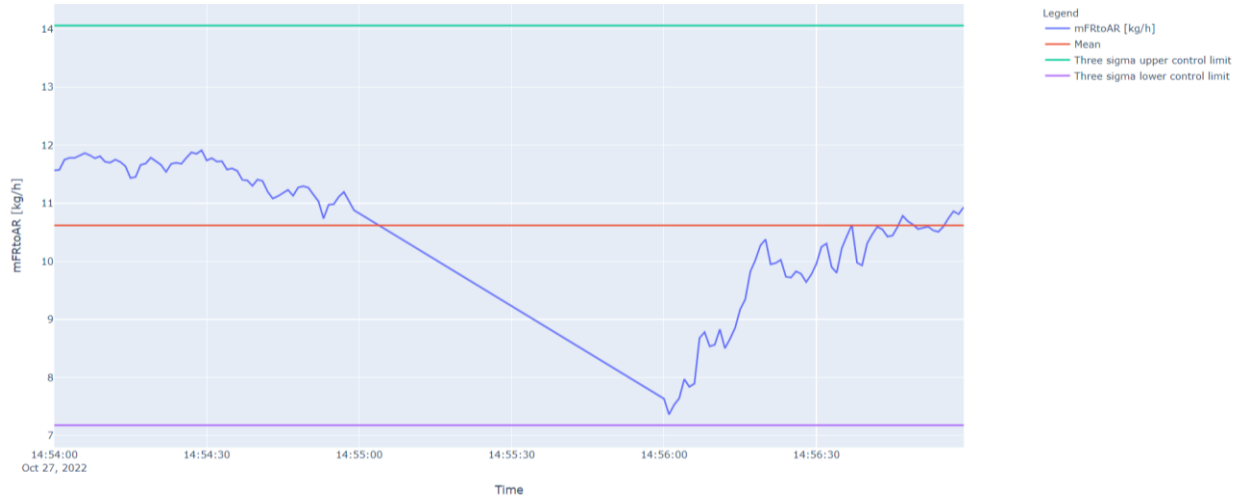

Figure 69. Timeseries graphs for fuel reactor to air reactor gas leakage at the 0.35 m bed height condition.

Figure 70. Timeseries graphs fate of the amount of AR/FR purge gas that remained in the air reactor at the 0.35 m bed height condition.

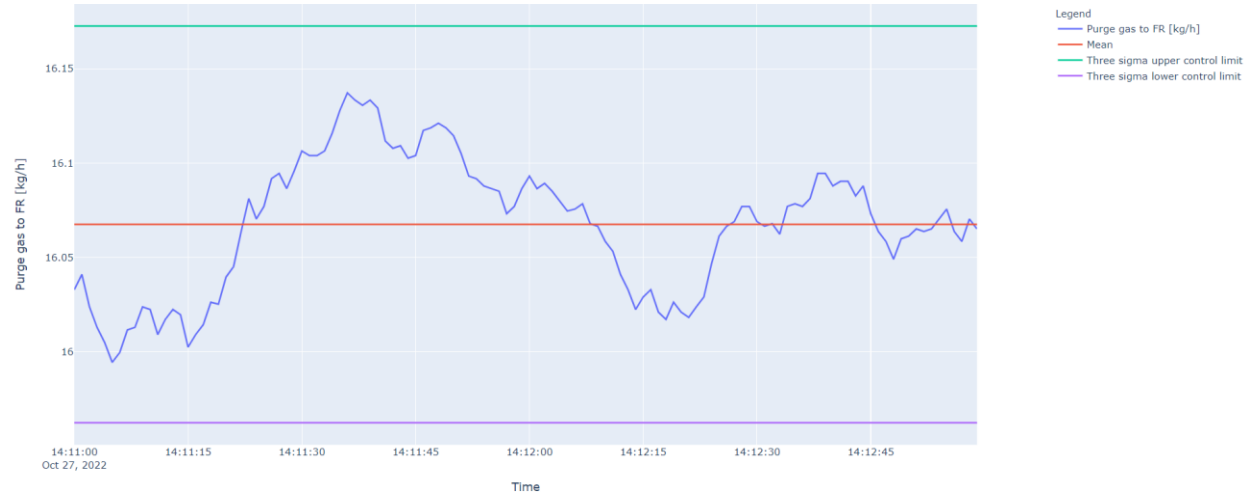

Figure 71. Timeseries graphs fate of the amount of AR/FR purge gas that moved to the fuel reactor at the 0.35 m bed height condition.

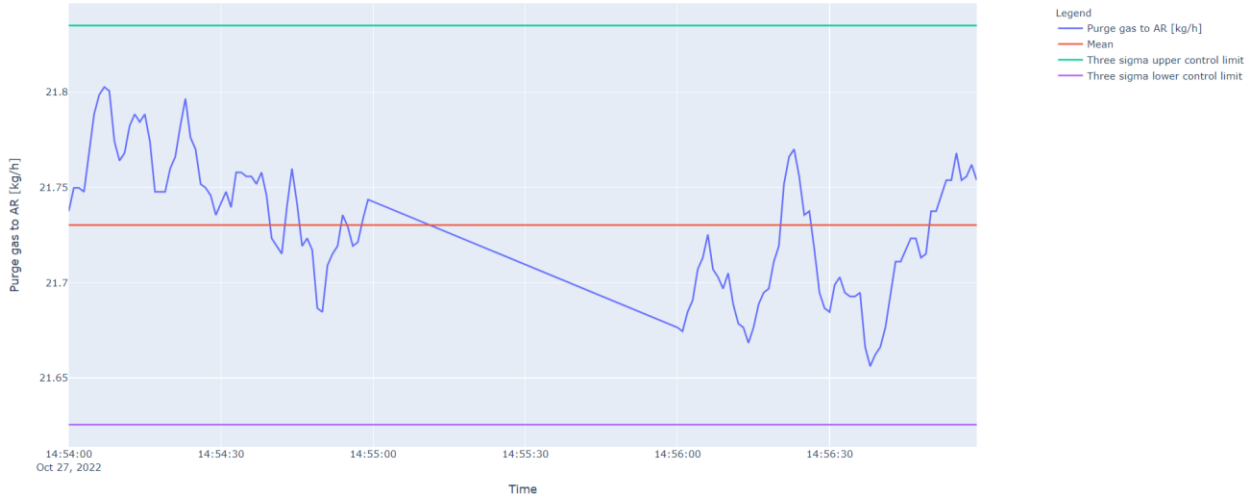

Figure 72. Timeseries graphs fate of the amount of FR/AR purge gas that moved to the air reactor at the 0.35 m bed height condition.

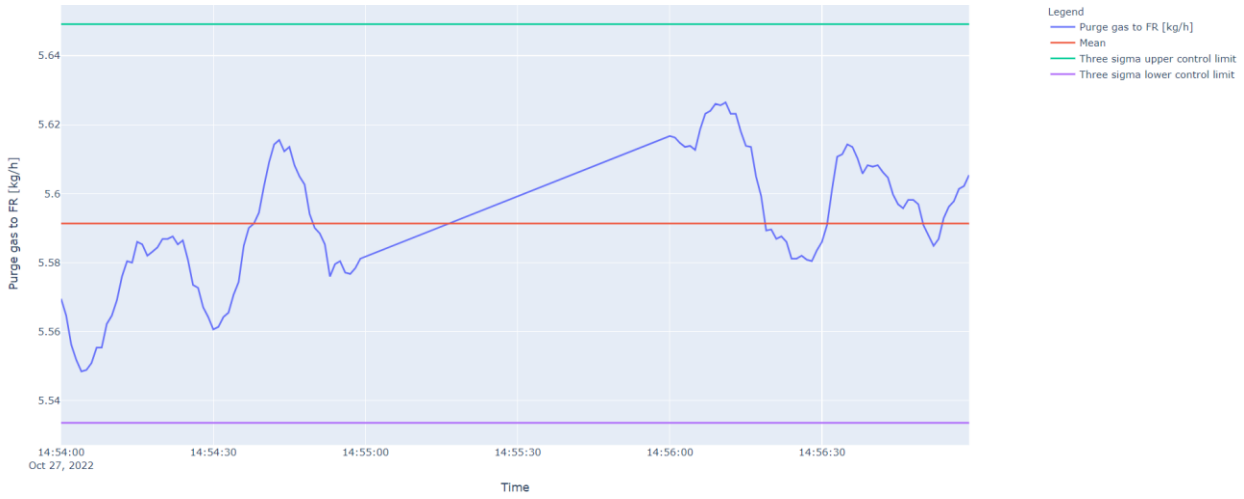

Figure 73. Timeseries graphs fate of the amount of FR/AR purge gas that remained in the fuel reactor at the 0.35 m bed height condition.

Figure 74. Timeseries graphs for solid circulation rate at the 0.05 m weir opening height condition (first repeat).

Figure 75. Timeseries graphs for solid circulation rate at the 0.05 m weir opening height condition (second repeat).

Figure 76. Timeseries graphs for solid circulation rate at the 0.05 m weir opening height condition (third repeat).

Figure 77. Timeseries graphs for solid circulation rate at the 0.05 m weir opening height condition (forth repeat).

Figure 78. Timeseries graphs for air reactor to fuel reactor gas leakage at the 0.05 m weir opening height condition (first repeat).

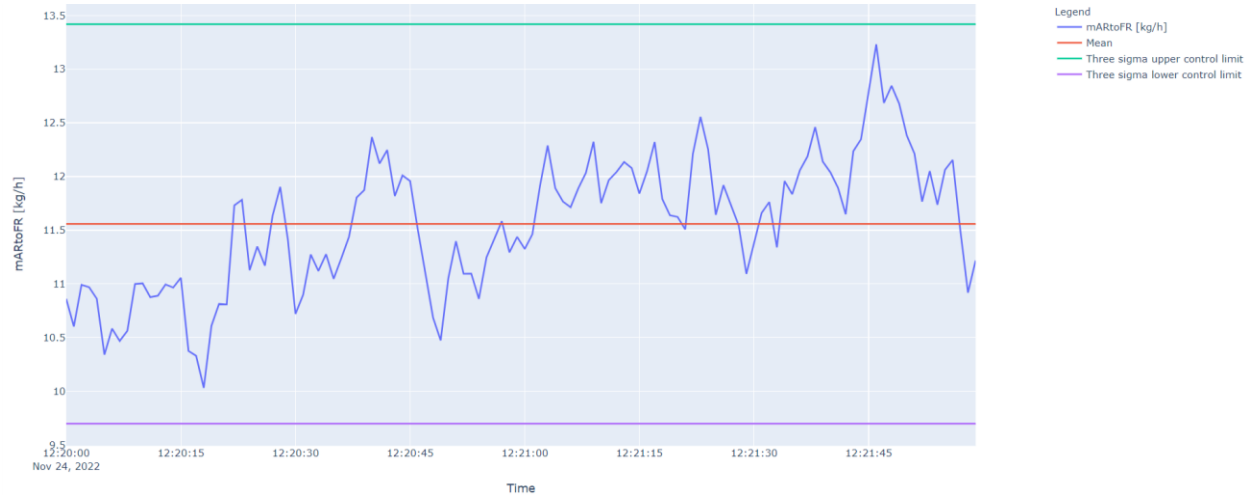

Figure 79. Timeseries graphs for air reactor to fuel reactor gas leakage at the 0.05 m weir opening height condition (second repeat).

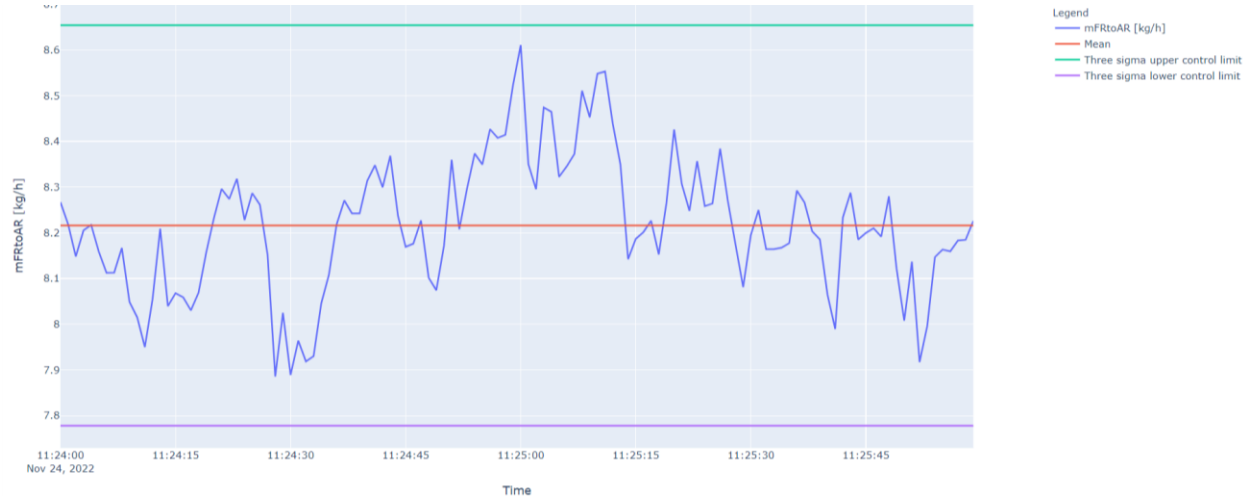

Figure 80. Timeseries graphs for fuel reactor to air reactor gas leakage at the 0.05 m weir opening height condition (first repeat).

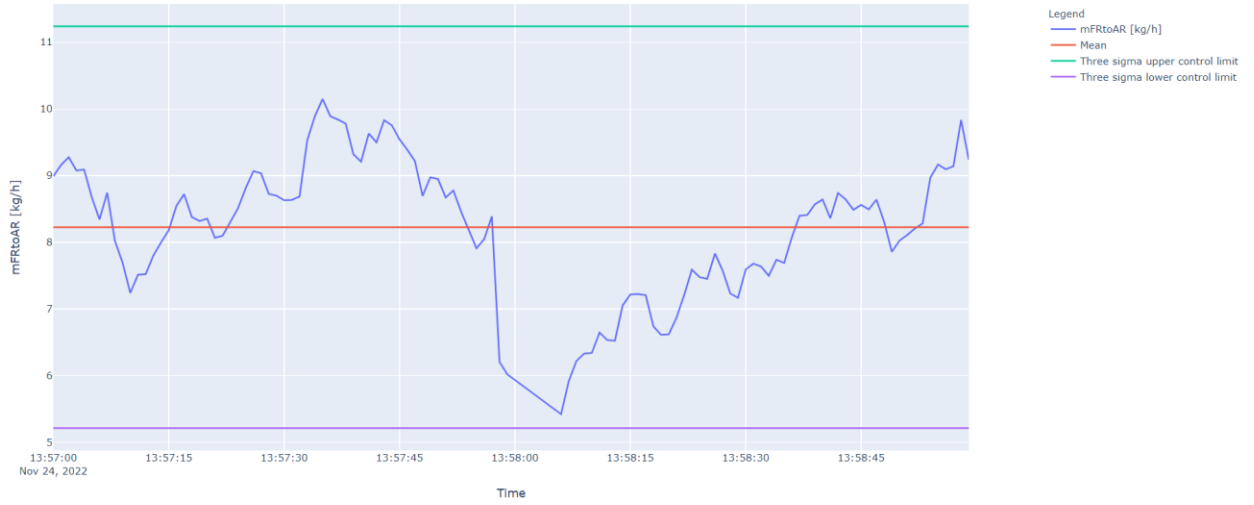

Figure 81. Timeseries graphs for fuel reactor to air reactor gas leakage at the 0.05 m weir opening height condition (second repeat).

Figure 82. Timeseries graphs fate of the amount of AR/FR purge gas that remained in the air reactor at the 0.05 m weir opening height condition (first repeat).

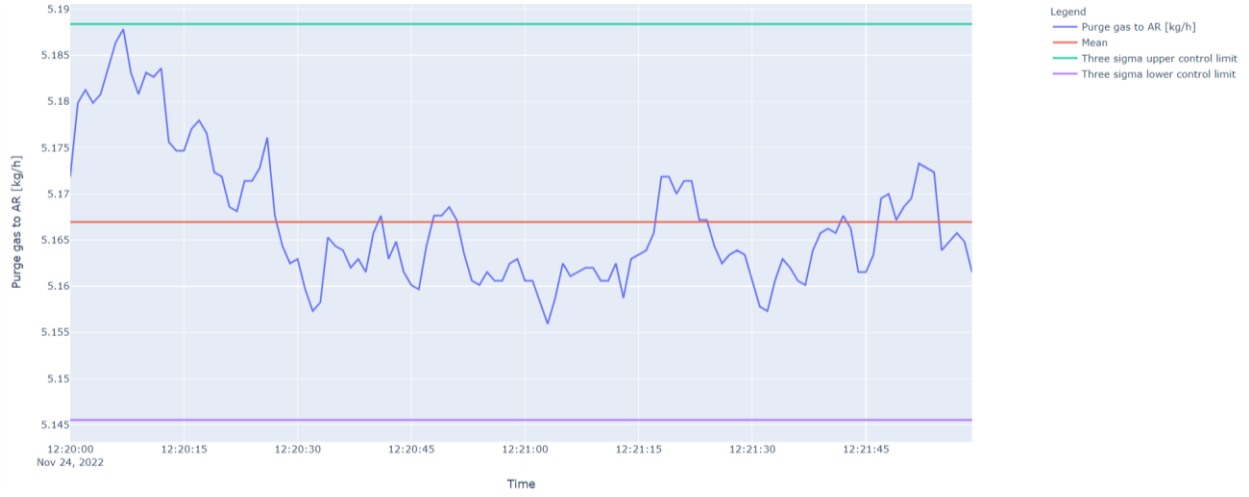

Figure 83. Timeseries graphs fate of the amount of AR/FR purge gas that remained in the air reactor at the 0.05 m weir opening height condition (second repeat).

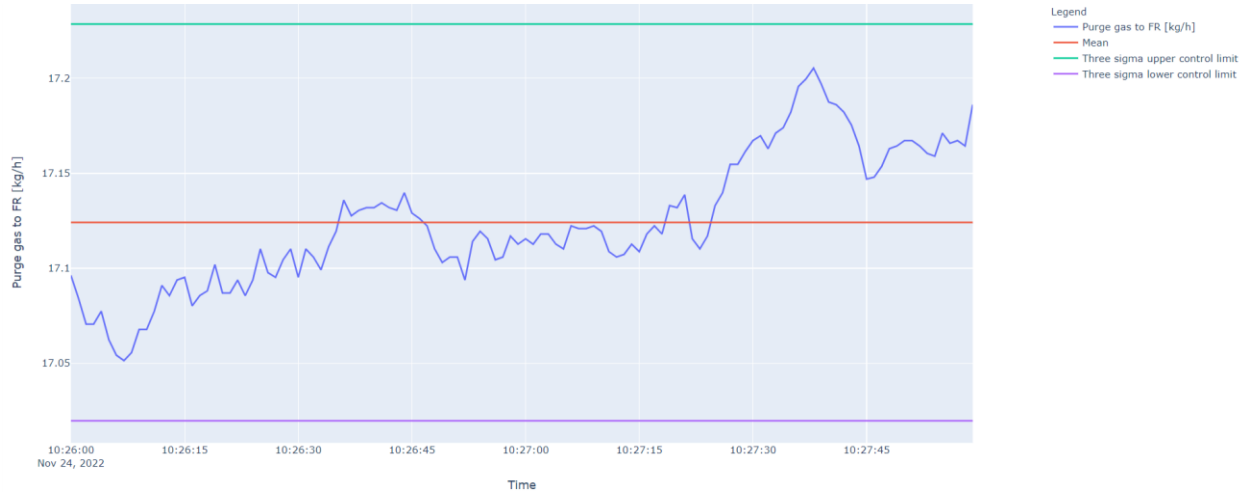

Figure 84. Timeseries graphs fate of the amount of AR/FR purge gas that moved to the fuel reactor at the 0.05 m weir opening height condition (first repeat).

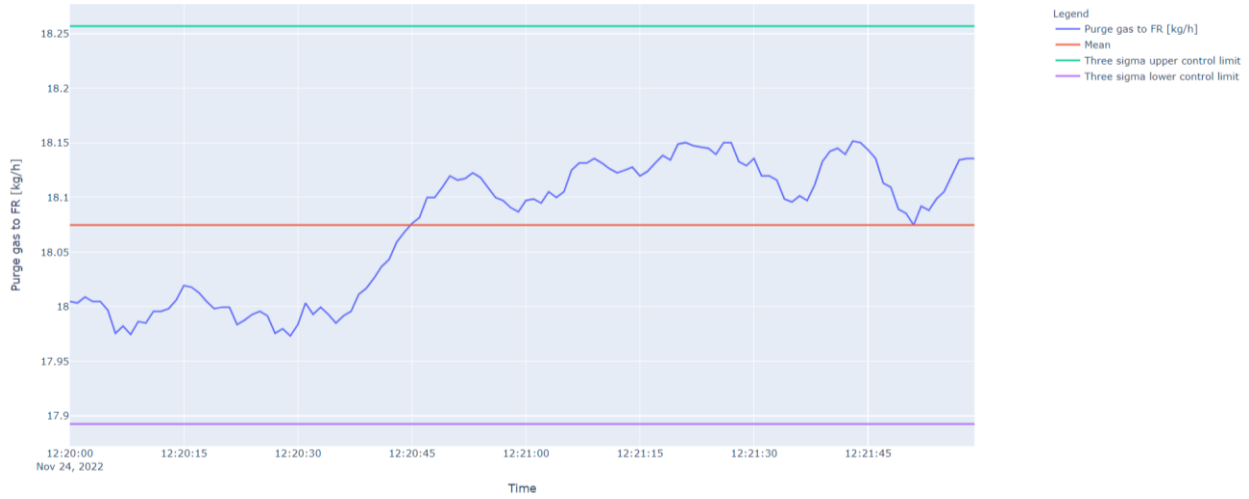

Figure 85. Timeseries graphs fate of the amount of AR/FR purge gas that moved to the fuel reactor at the 0.05 m weir opening height condition (second repeat).

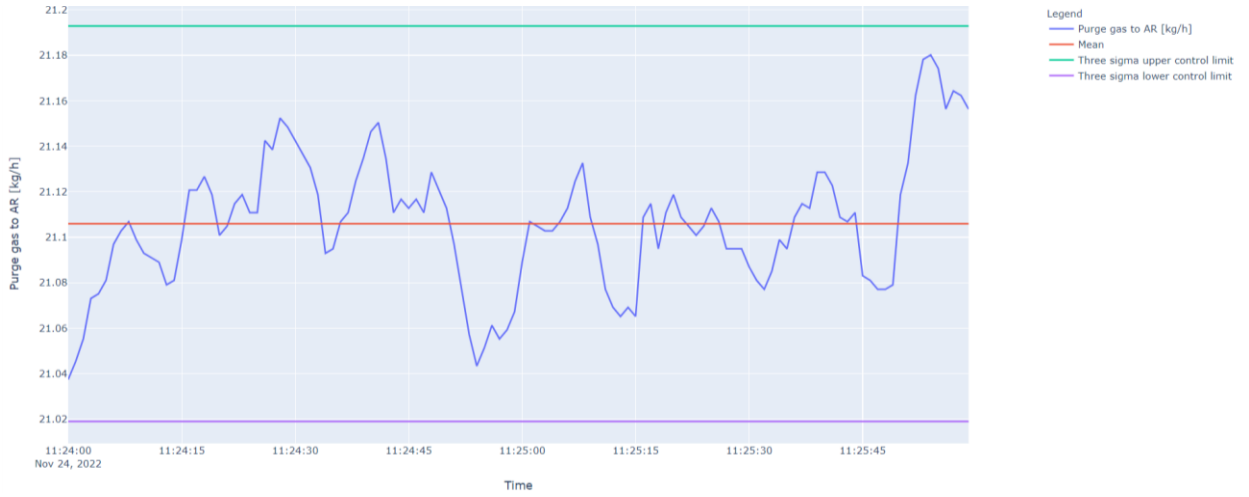

Figure 86. Timeseries graphs fate of the amount of FR/AR purge gas that moved to the air reactor at the 0.05 m weir opening height condition (first repeat).

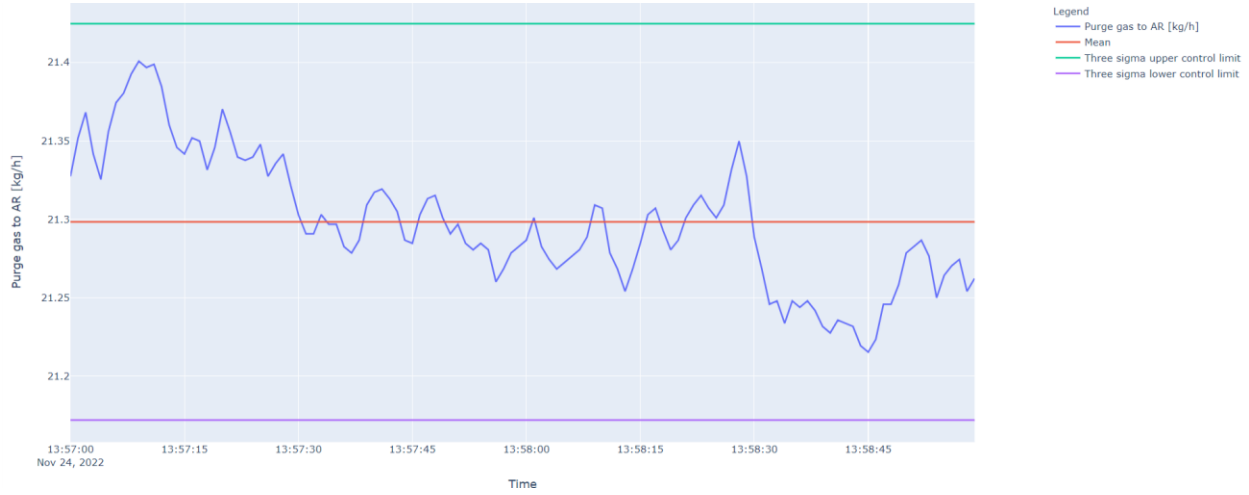

Figure 87. Timeseries graphs fate of the amount of FR/AR purge gas that moved to the air reactor at the 0.05 m weir opening height condition (second repeat).

Figure 88. Timeseries graphs fate of the amount of FR/AR purge gas that remained in the fuel reactor at the 0.05 m weir opening height condition (first repeat).

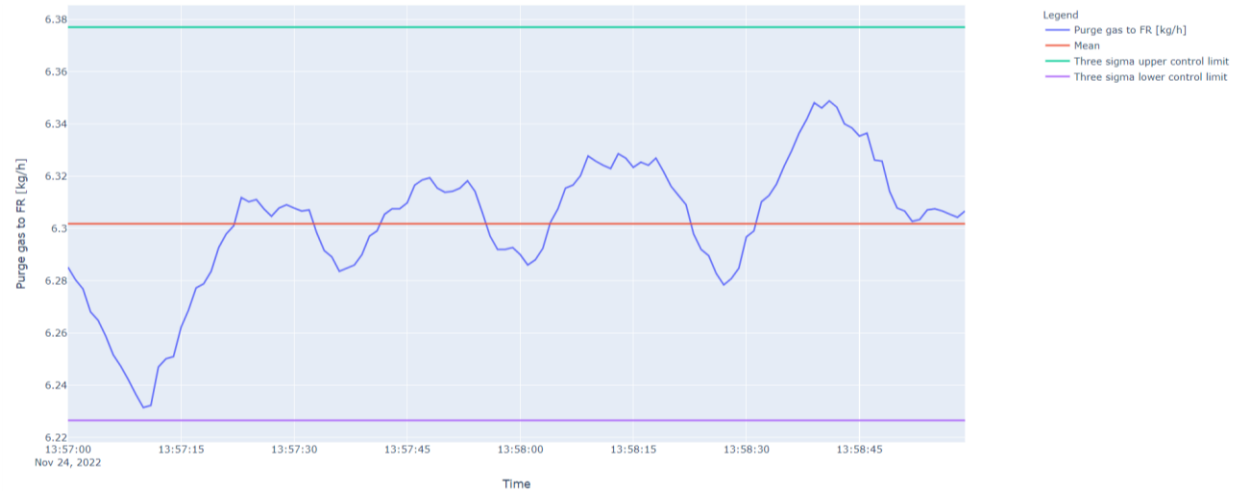

Figure 89. Timeseries graphs fate of the amount of FR/AR purge gas that remained in the fuel reactor at the 0.05 m weir opening height condition (second repeat).

Figure 90. Timeseries graphs for solid circulation rate at the 0.125 m weir opening height condition (first repeat).

Figure 91. Timeseries graphs for solid circulation rate at the 0.125 m weir opening height condition (second repeat).

Figure 92. Timeseries graphs for solid circulation rate at the 0.125 m weir opening height condition (third repeat).

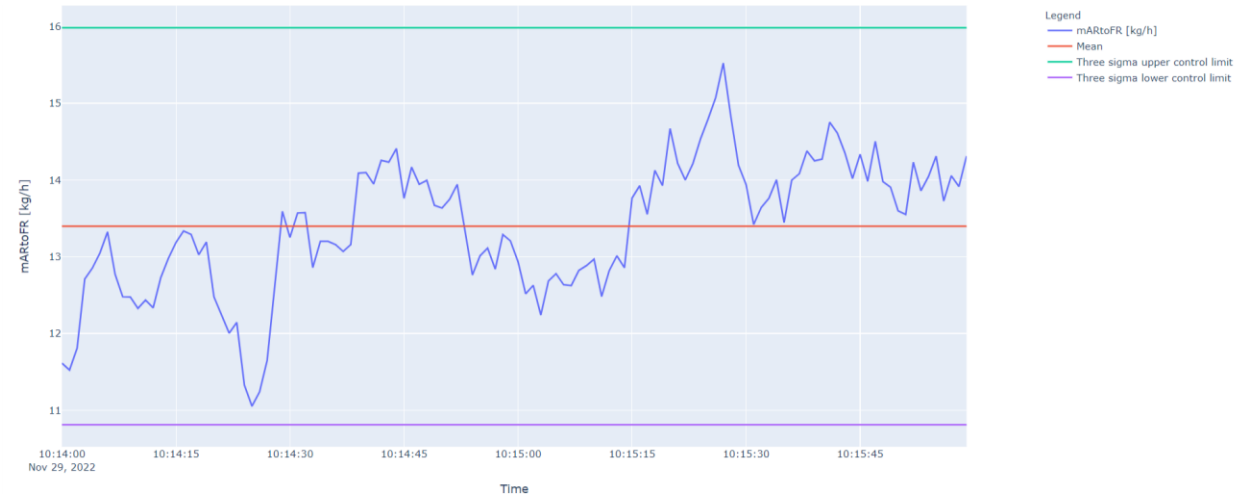

Figure 93. Timeseries graphs for air reactor to fuel reactor gas leakage at the 0.125 m weir opening height condition (first repeat).

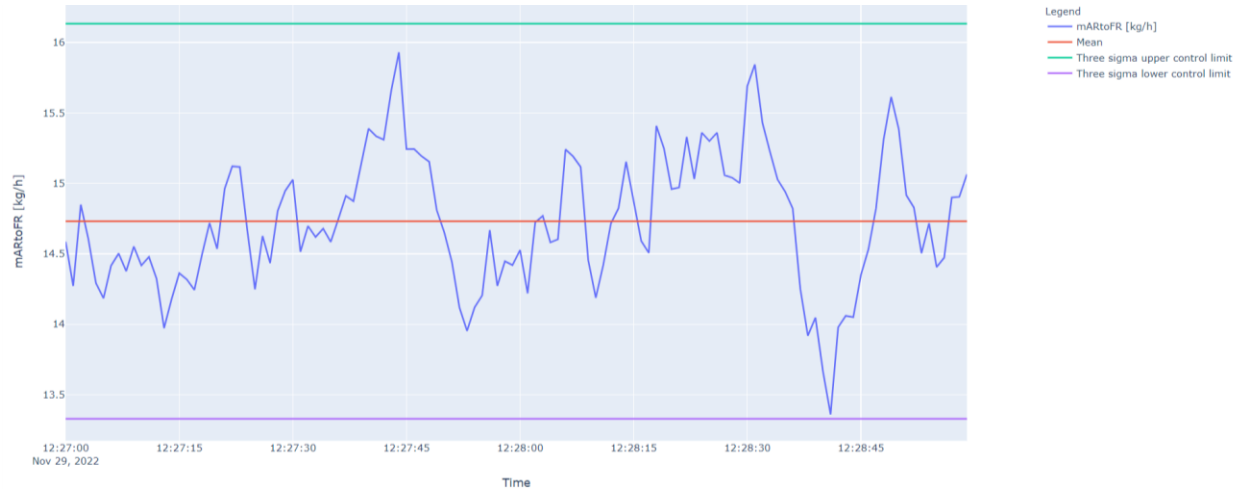

Figure 94. Timeseries graphs for air reactor to fuel reactor gas leakage at the 0.125 m weir opening height condition (second repeat).

Figure 95. Timeseries graphs for fuel reactor to air reactor gas leakage at the 0.125 m weir opening height condition (first repeat).

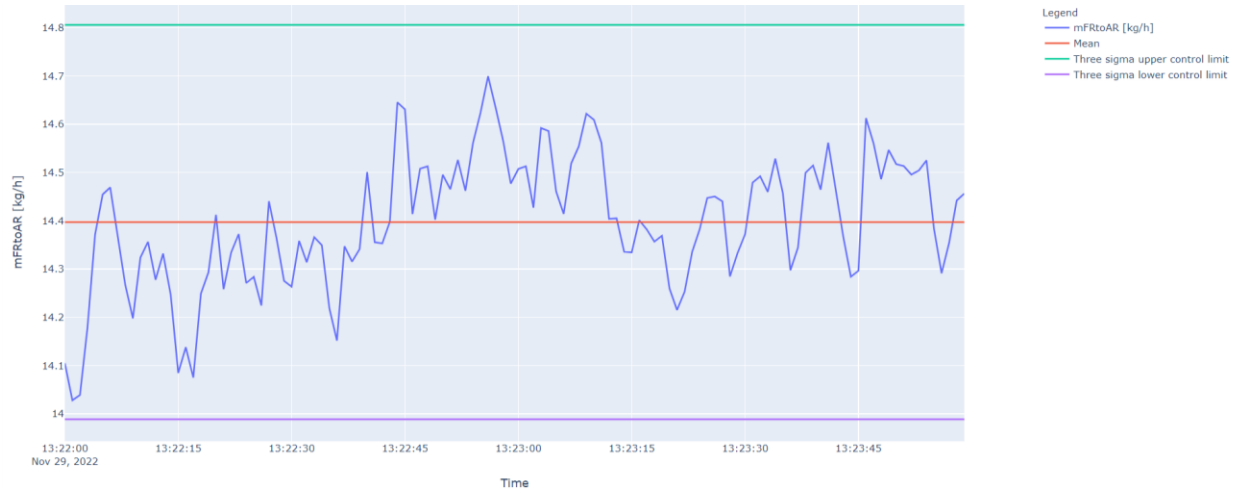

Figure 96. Timeseries graphs for fuel reactor to air reactor gas leakage at the 0.125 m weir opening height condition (second repeat).

Figure 97. Timeseries graphs fate of the amount of AR/FR purge gas that remained in the air reactor at the 0.125 m weir opening height condition (first repeat).

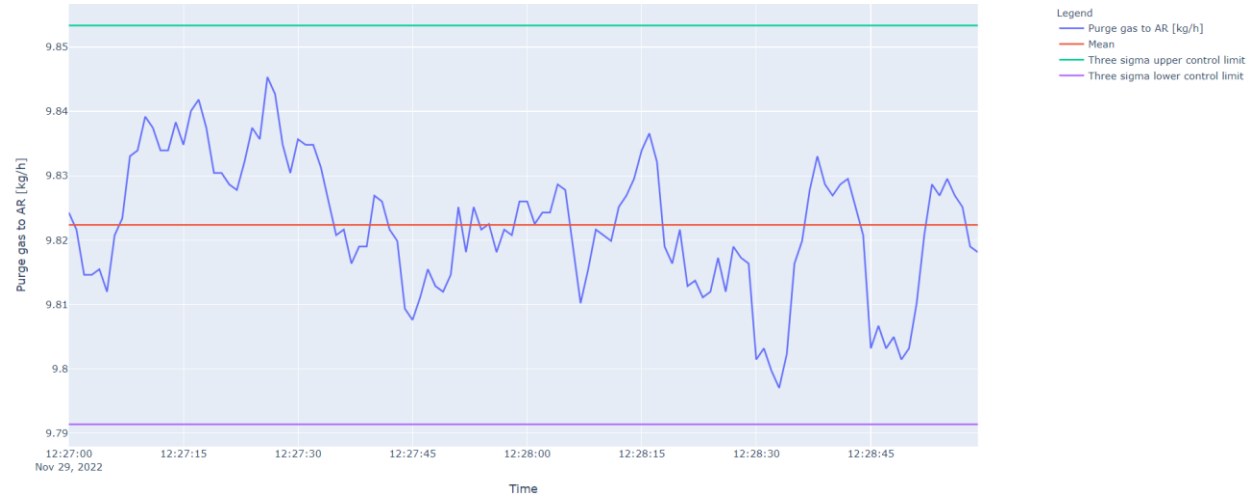

Figure 98. Timeseries graphs fate of the amount of AR/FR purge gas that remained in the air reactor at the 0.125 m weir opening height condition (second repeat).

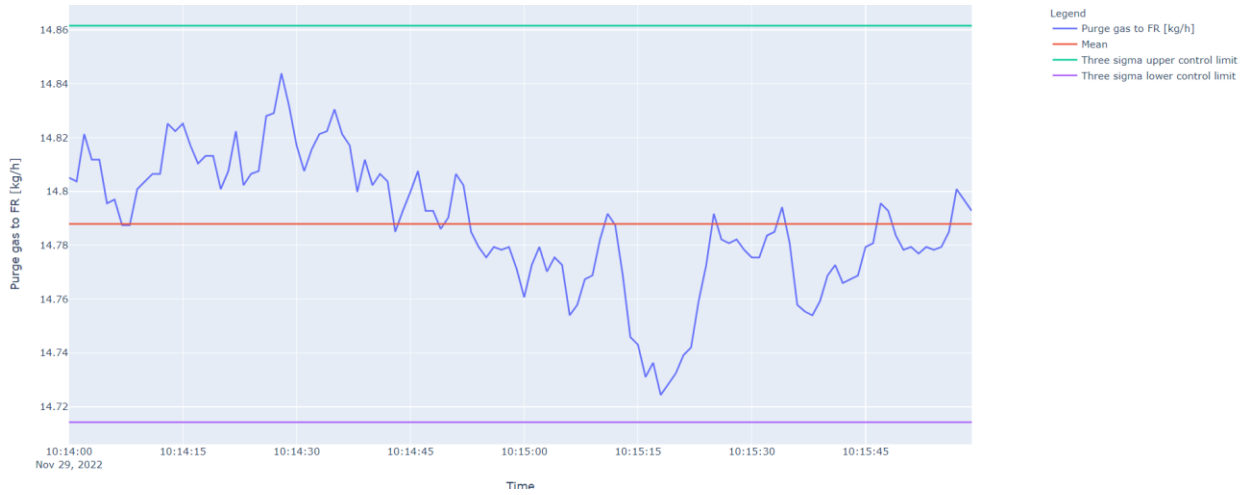

Figure 99. Timeseries graphs fate of the amount of AR/FR purge gas that moved to the fuel reactor at the 0.125 m weir opening height condition (first repeat).

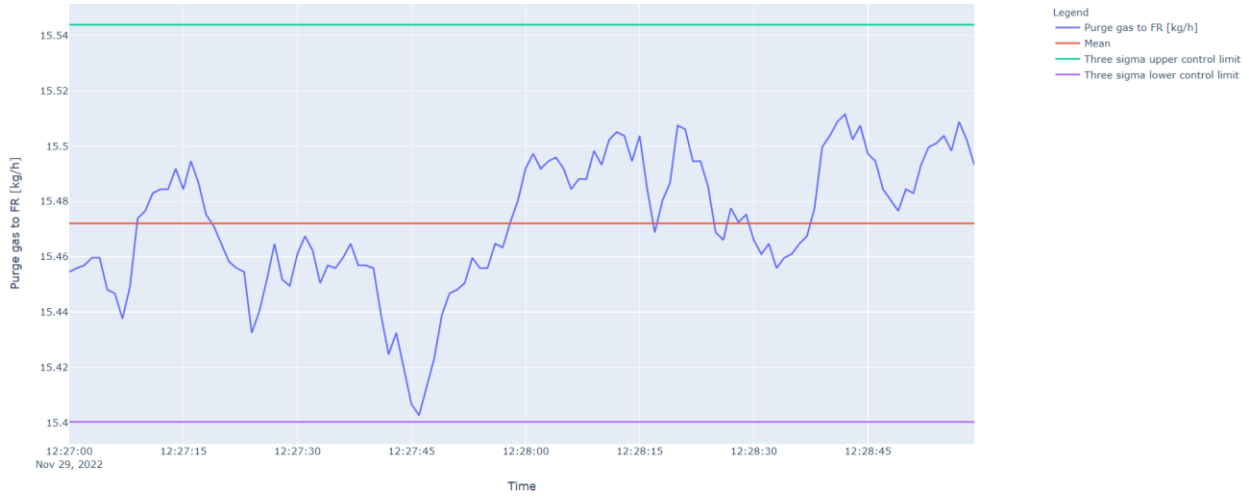

Figure 100. Timeseries graphs fate of the amount of AR/FR purge gas that moved to the fuel reactor at the 0.125 m weir opening height condition (second repeat).

Figure 101. Timeseries graphs fate of the amount of FR/AR purge gas that moved to the air reactor at the 0.125 m weir opening height condition (first repeat).

Figure 102. Timeseries graphs fate of the amount of FR/AR purge gas that moved to the air reactor at the 0.125 m weir opening height condition (second repeat).

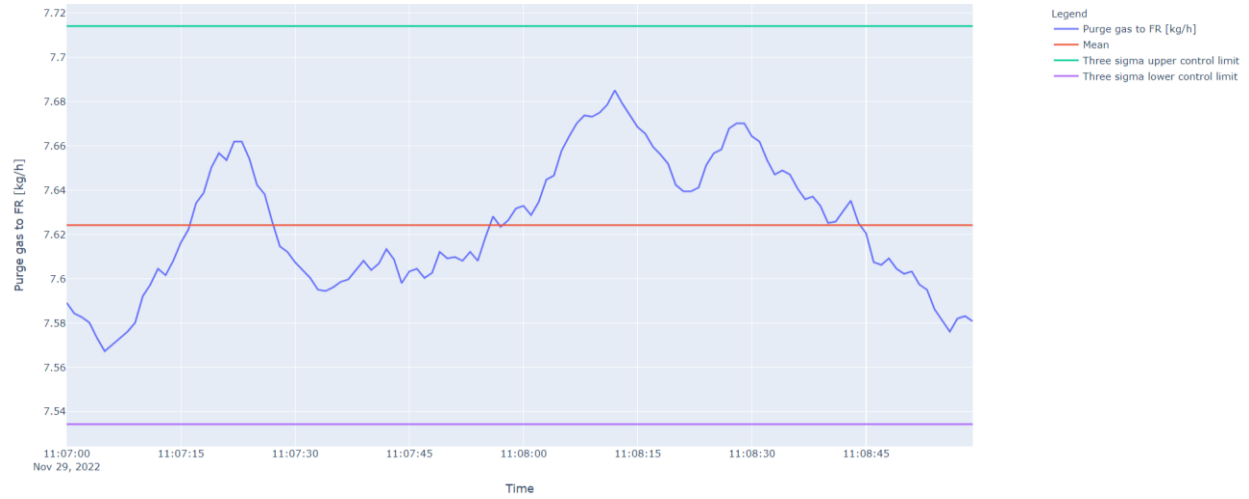

Figure 103. Timeseries graphs fate of the amount of FR/AR purge gas that remained in the fuel reactor at the 0.125 m weir opening height condition (first repeat).

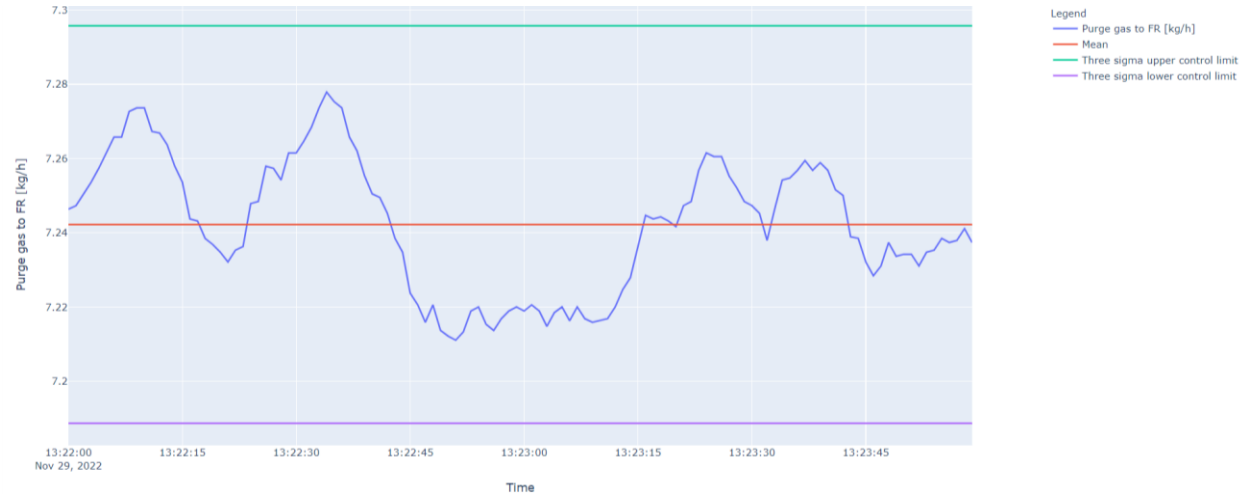

Figure 104. Timeseries graphs fate of the amount of FR/AR purge gas that remained in the fuel reactor at the 0.125 m weir opening height condition (second repeat).

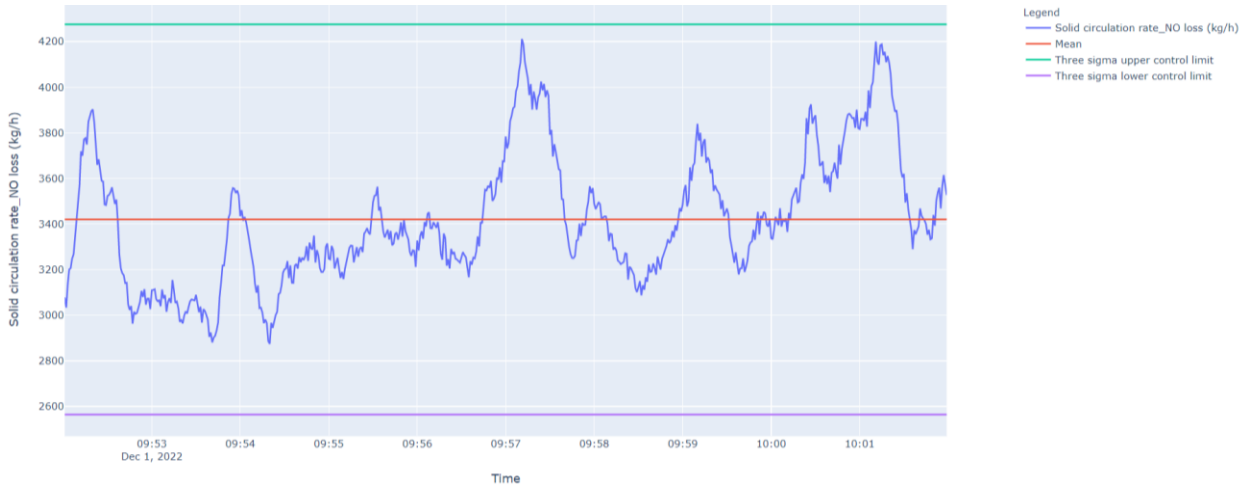

Figure 105. Timeseries graphs for solid circulation rate at the 0.15 m weir opening height condition (first repeat).

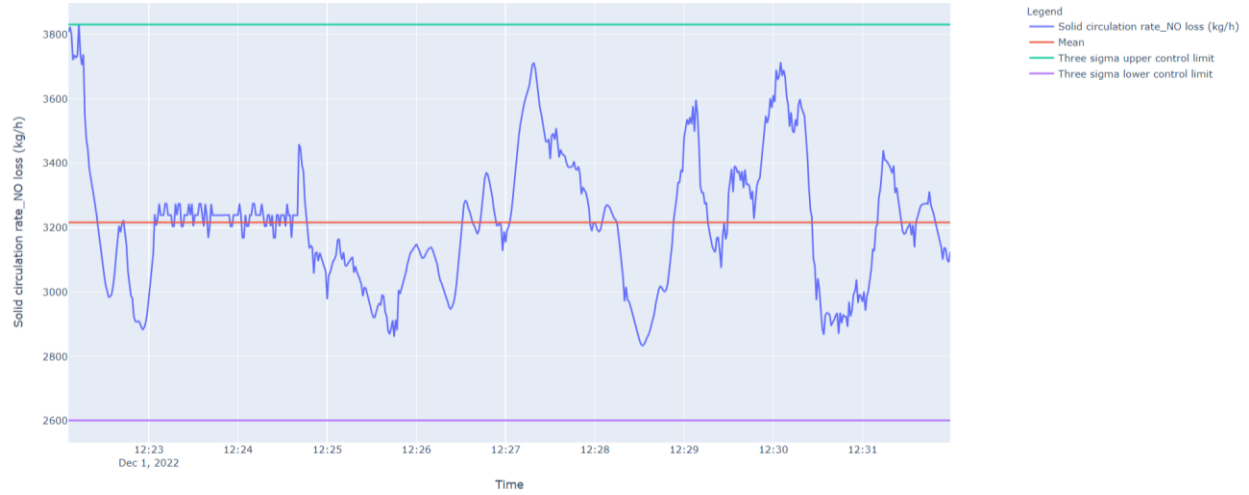

Figure 106. Timeseries graphs for solid circulation rate at the 0.15 m weir opening height condition (second repeat).

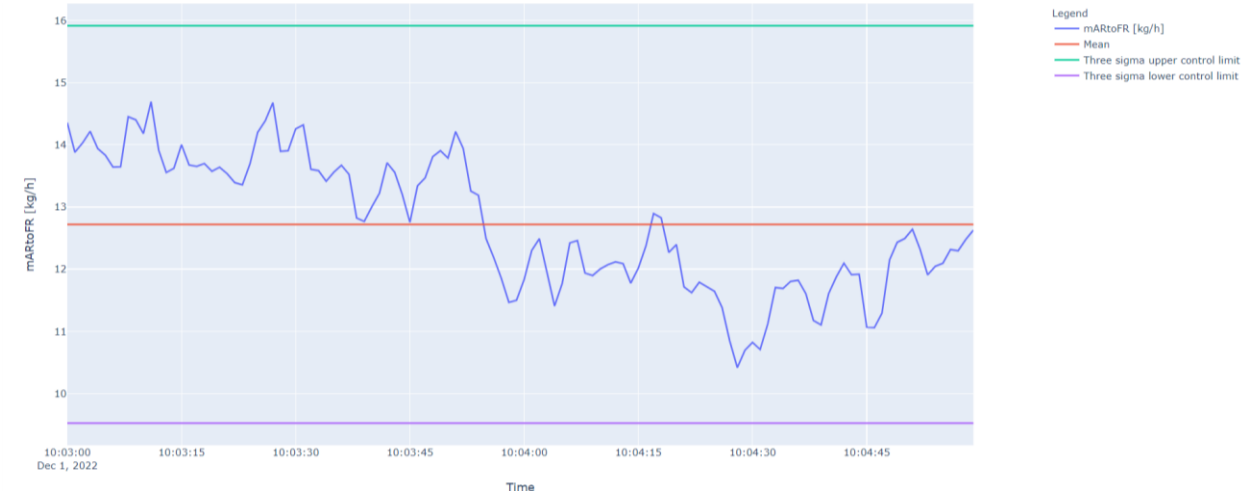

Figure 107. Timeseries graphs for air reactor to fuel reactor gas leakage at the 0.15 m weir opening height condition (first repeat).

Figure 108. Timeseries graphs for air reactor to fuel reactor gas leakage at the 0.15 m weir opening height condition (second repeat).

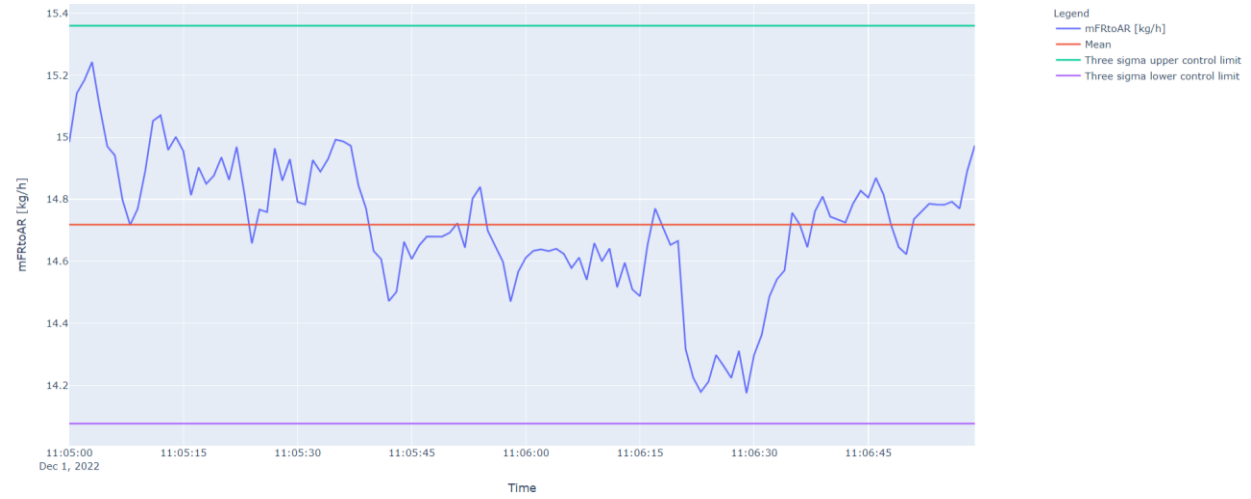

Figure 109. Timeseries graphs for fuel reactor to air reactor gas leakage at the 0.15 m weir opening height condition.

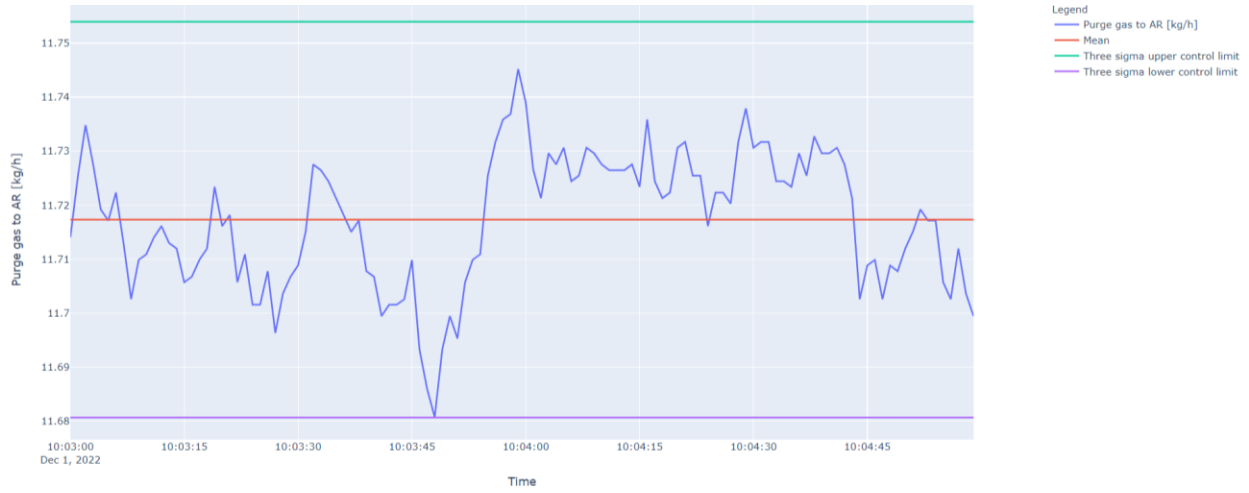

Figure 110. Timeseries graphs fate of the amount of AR/FR purge gas that remained in the air reactor at the 0.15 m weir opening height condition (first repeat).

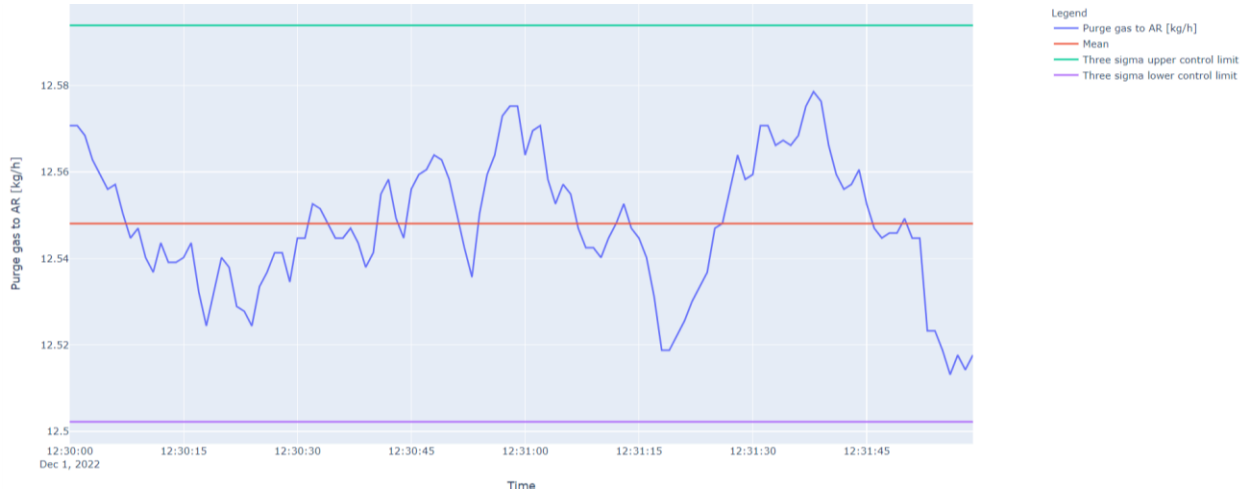

Figure 111. Timeseries graphs fate of the amount of AR/FR purge gas that remained in the air reactor at the 0.15 m weir opening height condition (second repeat).

Figure 112. Timeseries graphs fate of the amount of AR/FR purge gas that moved to the fuel reactor at the 0.15 m weir opening height condition (first repeat).

Figure 113. Timeseries graphs fate of the amount of AR/FR purge gas that moved to the fuel reactor at the 0.15 m weir opening height condition (second repeat).

Figure 114. Timeseries graphs fate of the amount of FR/AR purge gas that moved to the air reactor at the 0.15 m weir opening height condition.

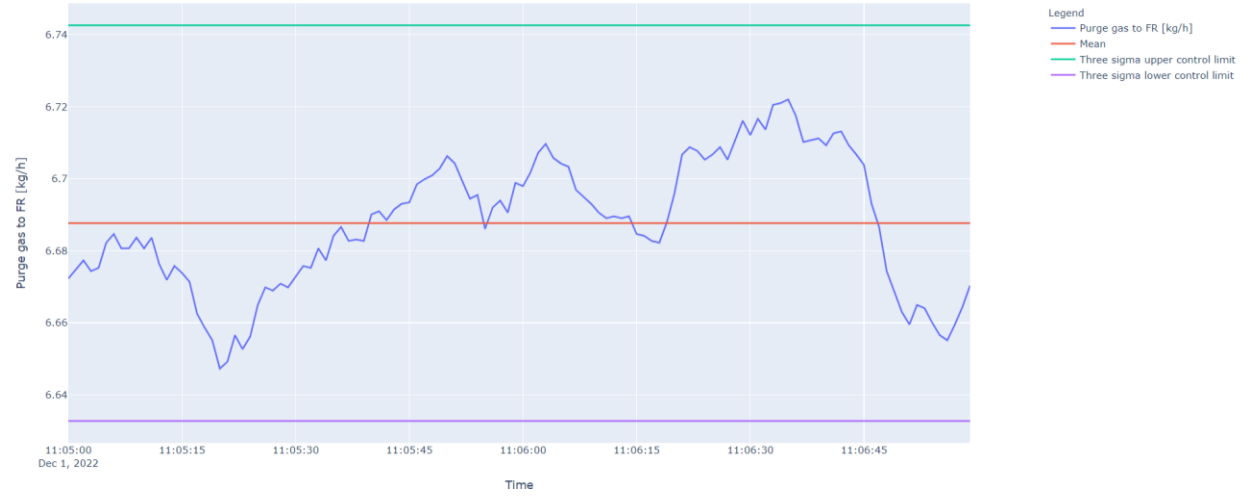

Figure 115. Timeseries graphs fate of the amount of FR/AR purge gas that remained in the fuel reactor at the 0.15 m weir opening height condition.

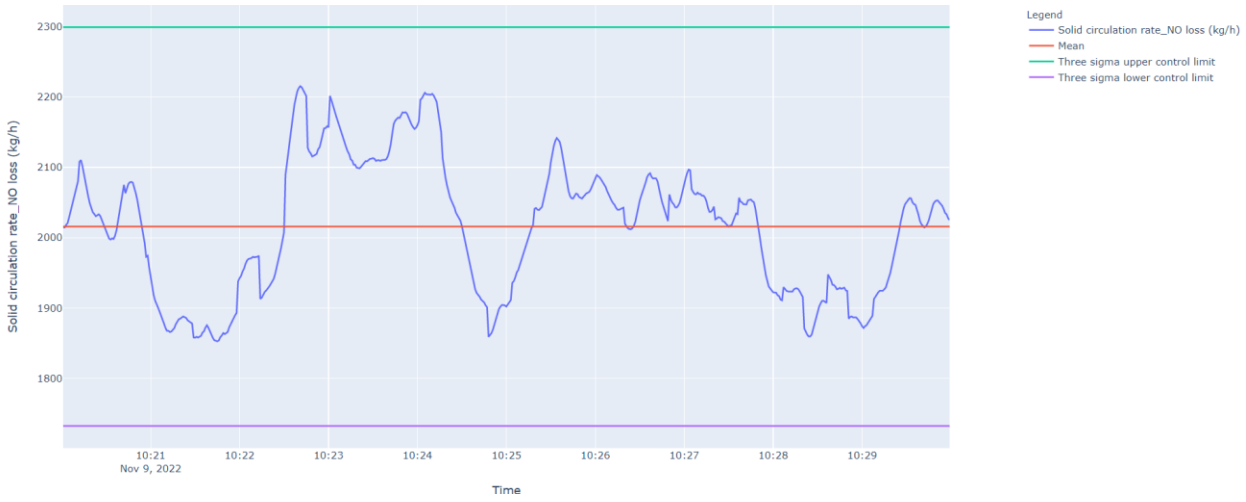

Figure 116. Timeseries graphs for solid circulation rate at the no purge tuyere condition (first repeat).

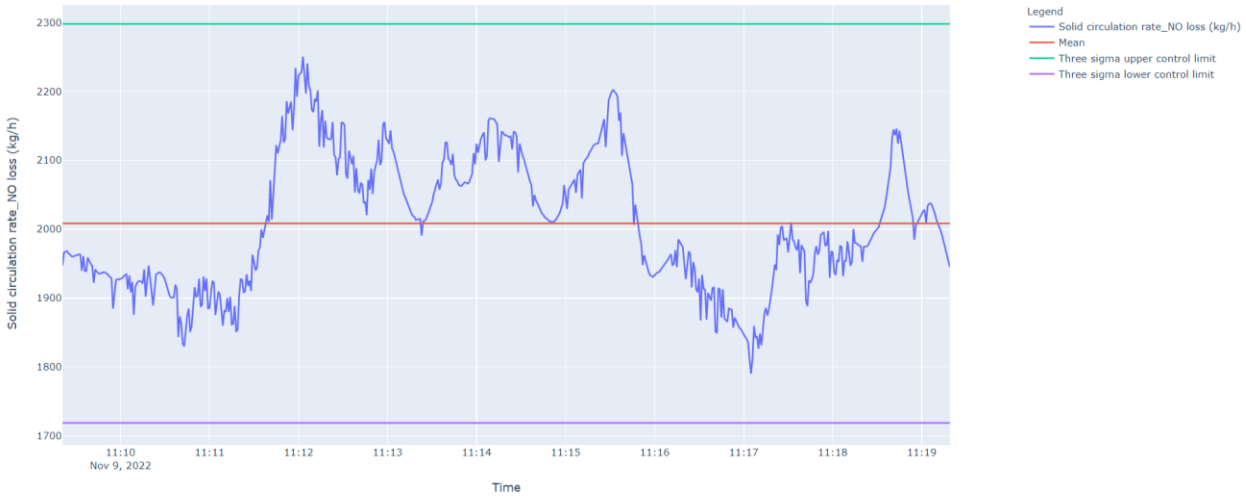

Figure 117. Timeseries graphs for solid circulation rate at the no purge tuyere condition (second repeat).

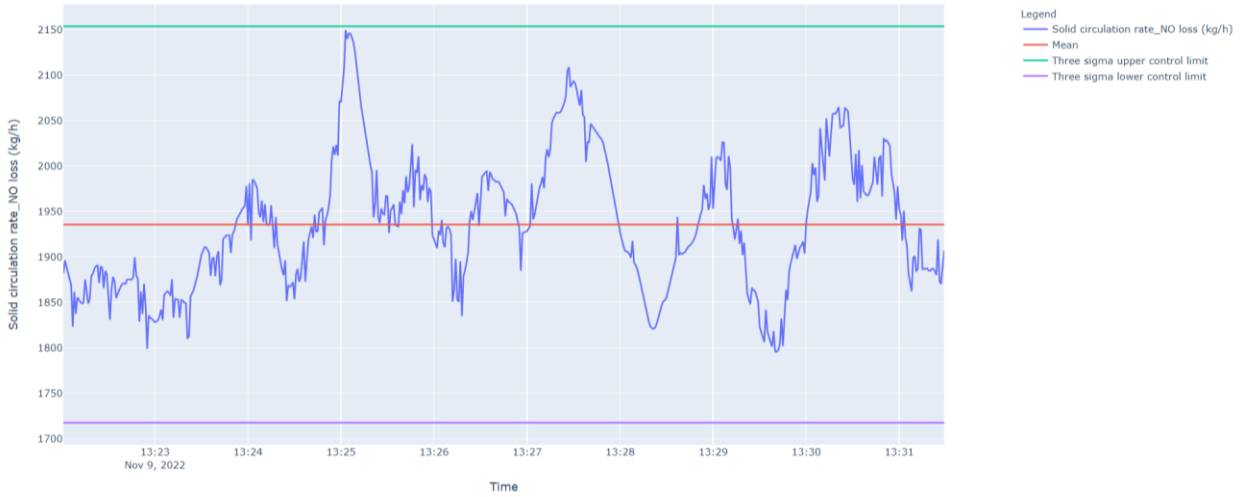

Figure 118. Timeseries graphs for solid circulation rate at the no purge tuyere condition (third repeat).

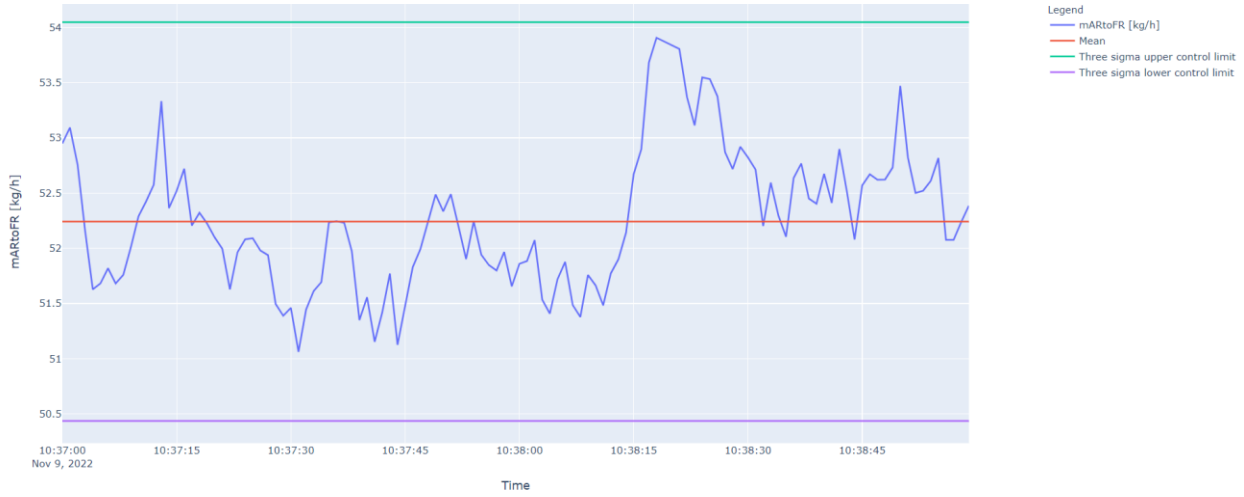

Figure 119. Timeseries graphs for air reactor to fuel reactor gas leakage at the no purge tuyere condition (first repeat).

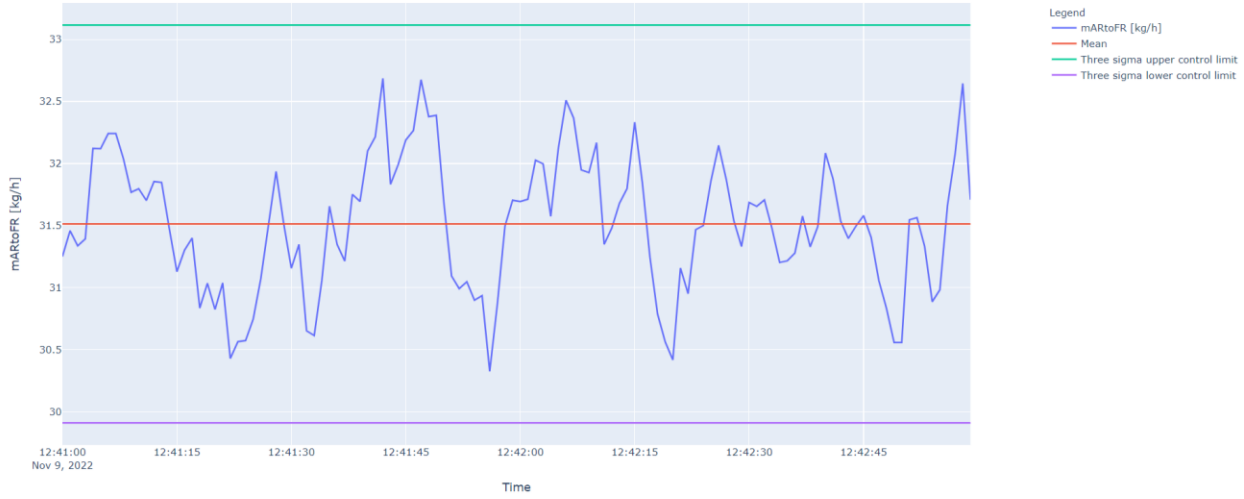

Figure 120. Timeseries graphs for air reactor to fuel reactor gas leakage at the no purge tuyere condition (second repeat).

Figure 121. Timeseries graphs for fuel reactor to air reactor gas leakage at the no purge tuyere condition (first repeat).

Figure 122. Timeseries graphs for fuel reactor to air reactor gas leakage at the no purge tuyere condition (second repeat).

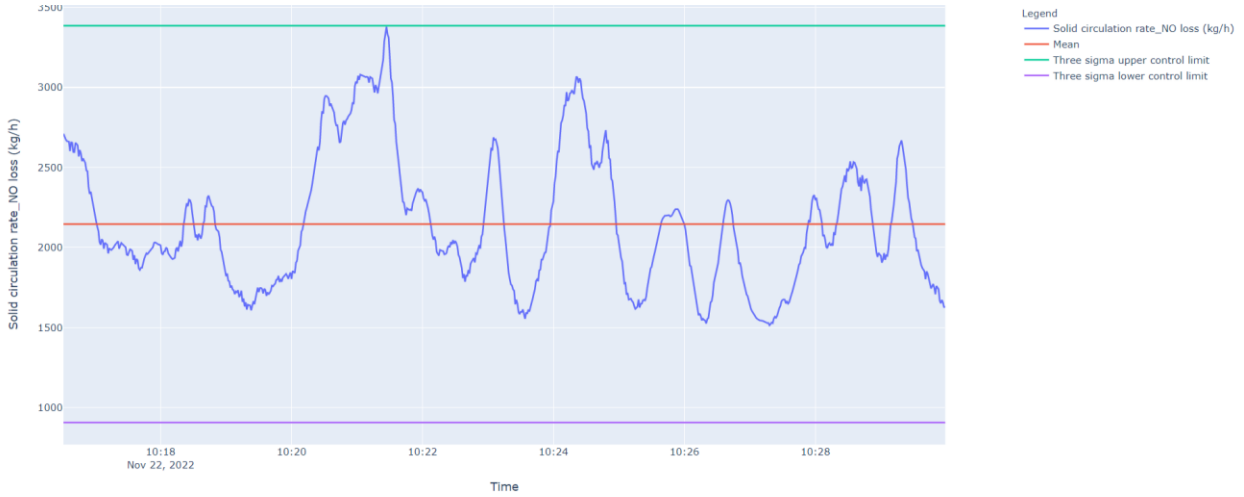

Figure 123. Timeseries graphs for solid circulation rate at the blank purge tuyere condition (first repeat).

Figure 124. Timeseries graphs for solid circulation rate at the blank purge tuyere condition (second repeat).

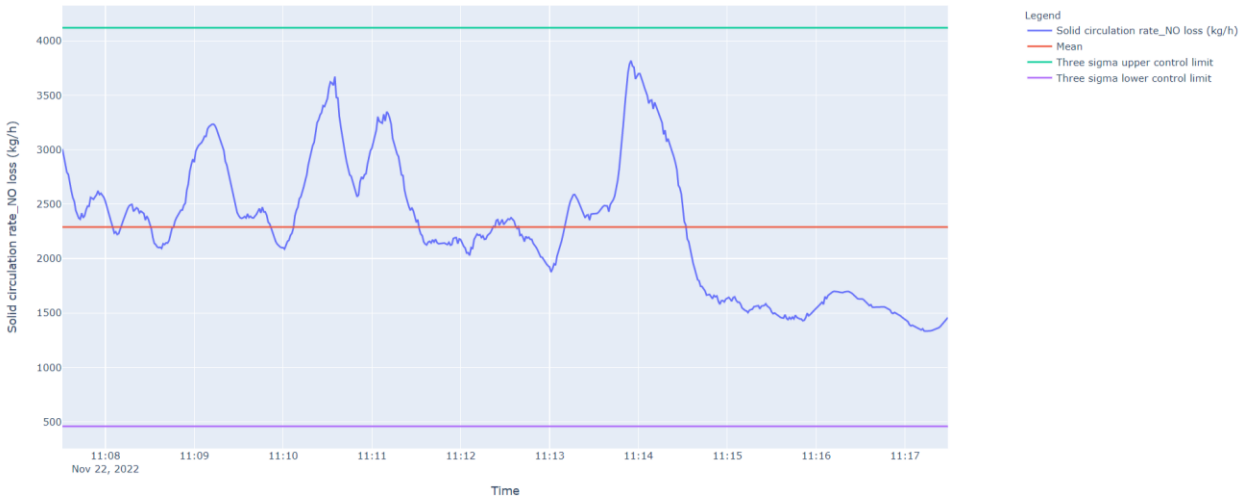

Figure 125. Timeseries graphs for solid circulation rate at the blank purge tuyere condition (third repeat).

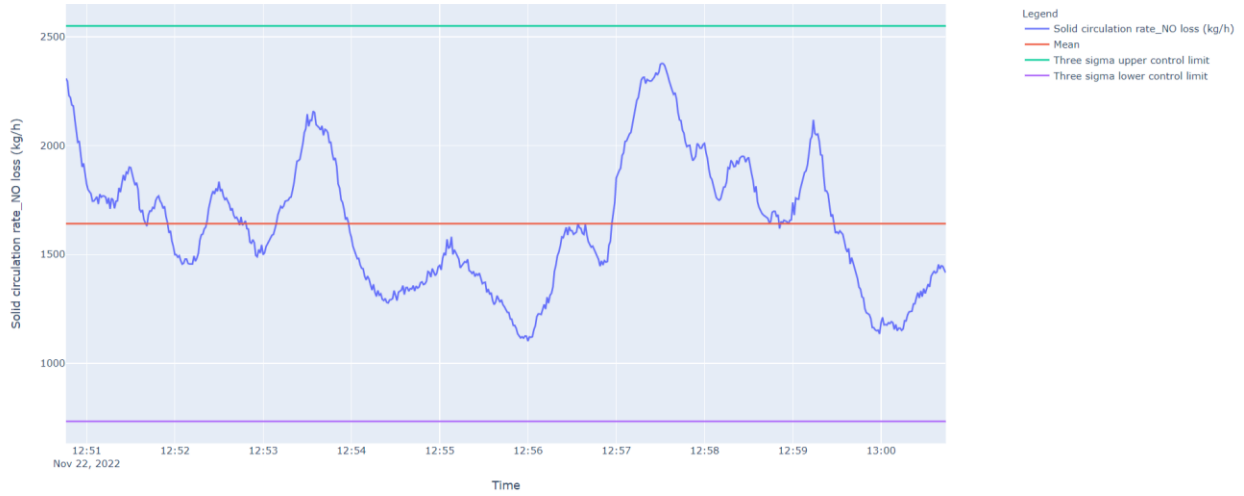

Figure 126. Timeseries graphs for solid circulation rate at the blank purge tuyere condition (forth repeat).

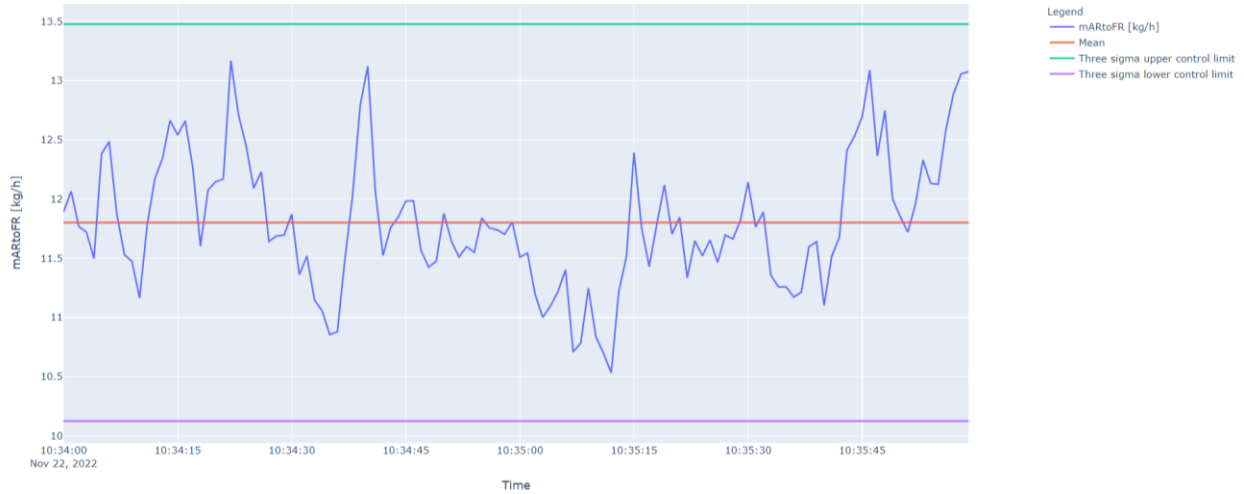

Figure 127. Timeseries graphs for air reactor to fuel reactor gas leakage at the blank purge tuyere condition (first repeat).

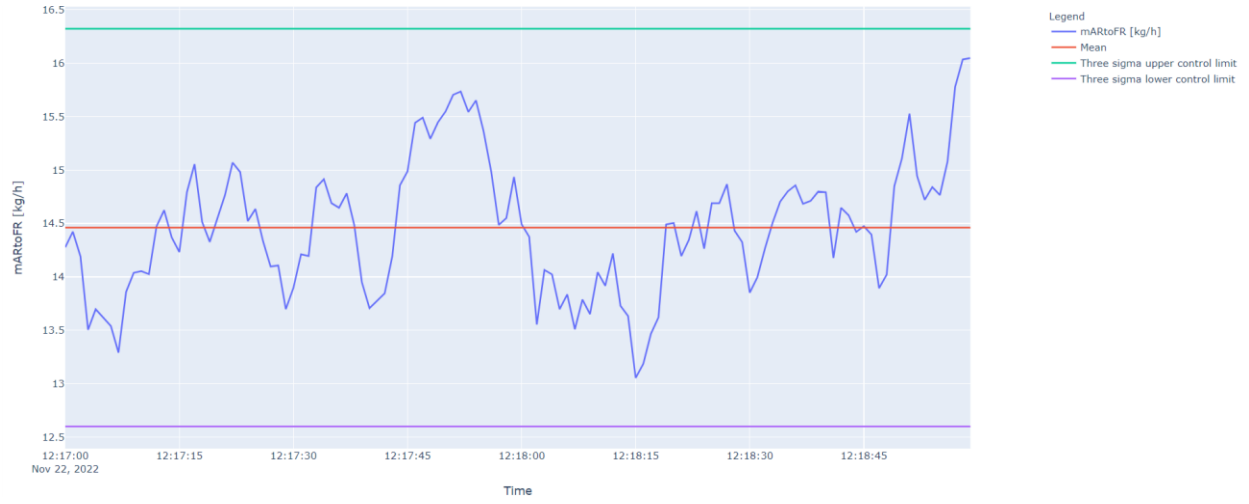

Figure 128. Timeseries graphs for air reactor to fuel reactor gas leakage at the blank purge tuyere condition (second repeat).

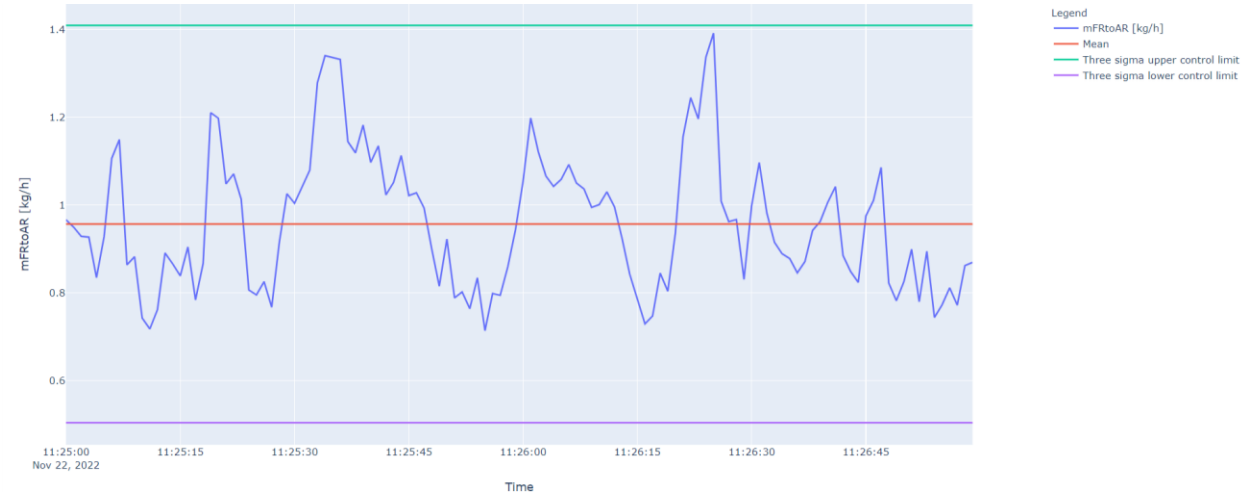

Figure 129. Timeseries graphs for fuel reactor to air reactor gas leakage at the blank purge tuyere condition (first repeat).

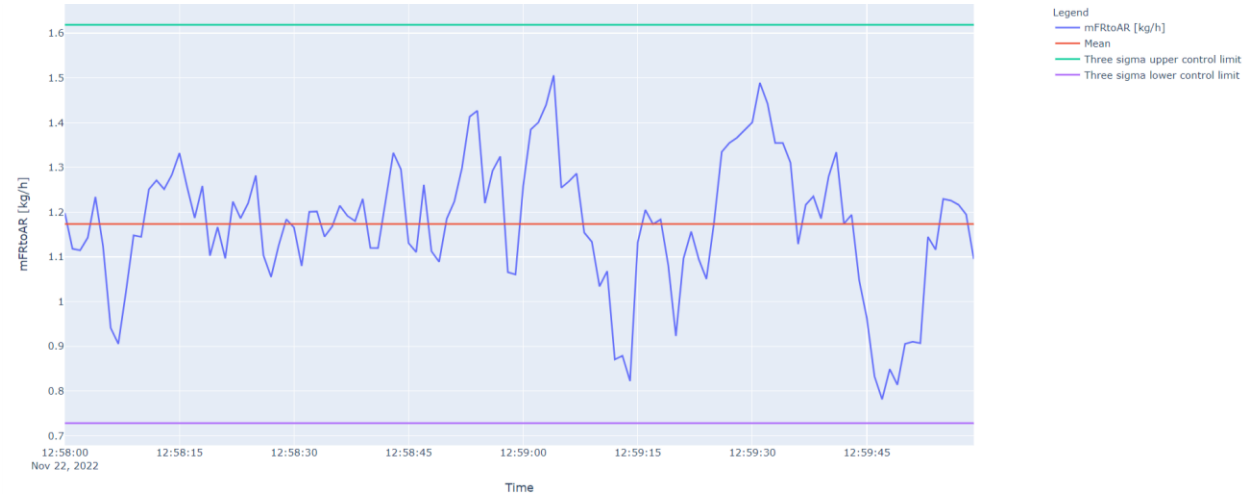

Figure 130. Timeseries graphs for fuel reactor to air reactor gas leakage at the blank purge tuyere condition (second repeat).

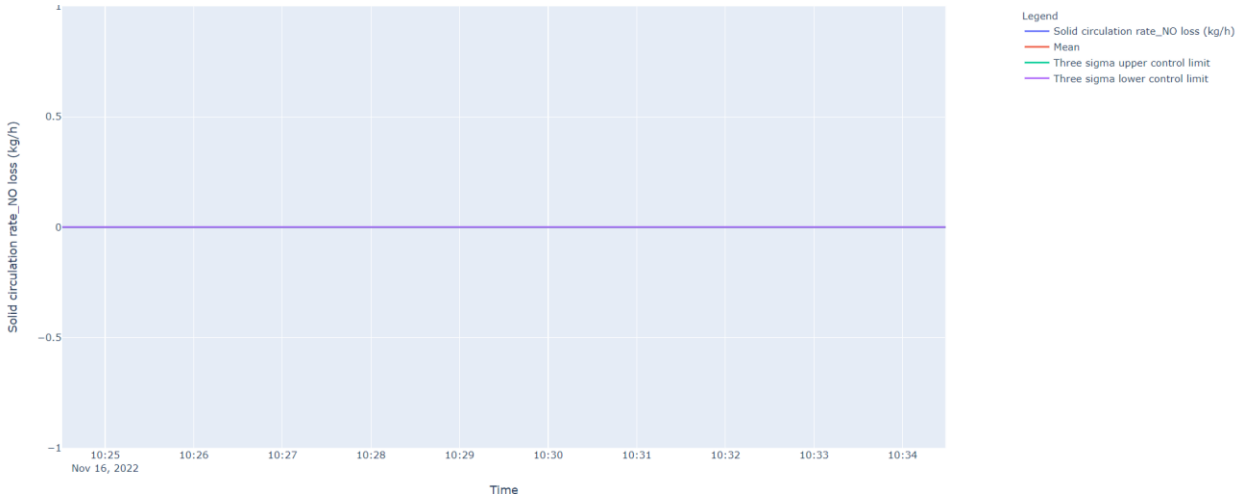

Figure 131. Timeseries graphs for solid circulation rate at the vertical purge tuyere condition (first repeat).

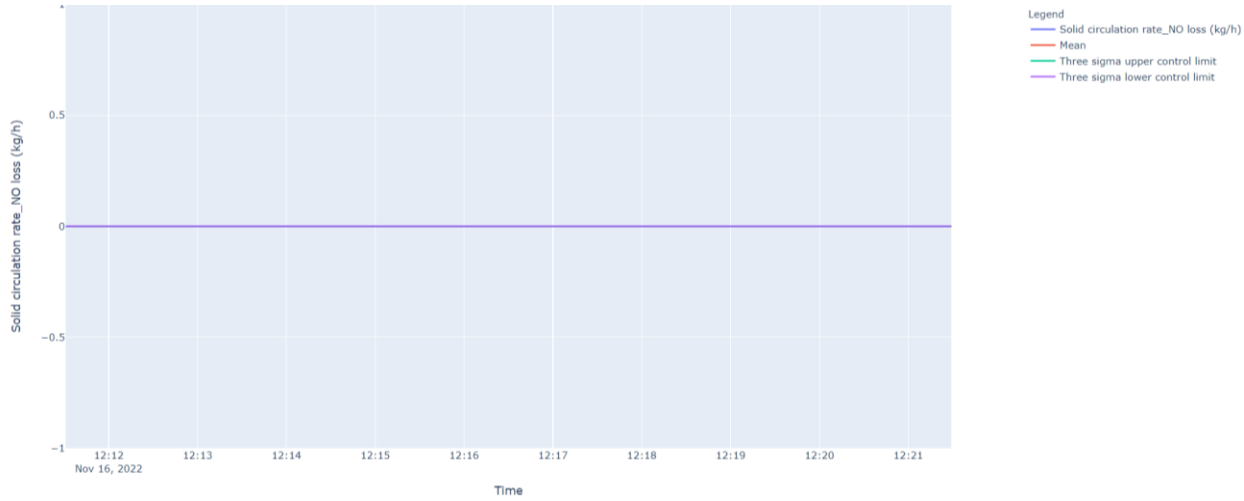

Figure 132. Timeseries graphs for solid circulation rate at the vertical purge tuyere condition (second repeat).

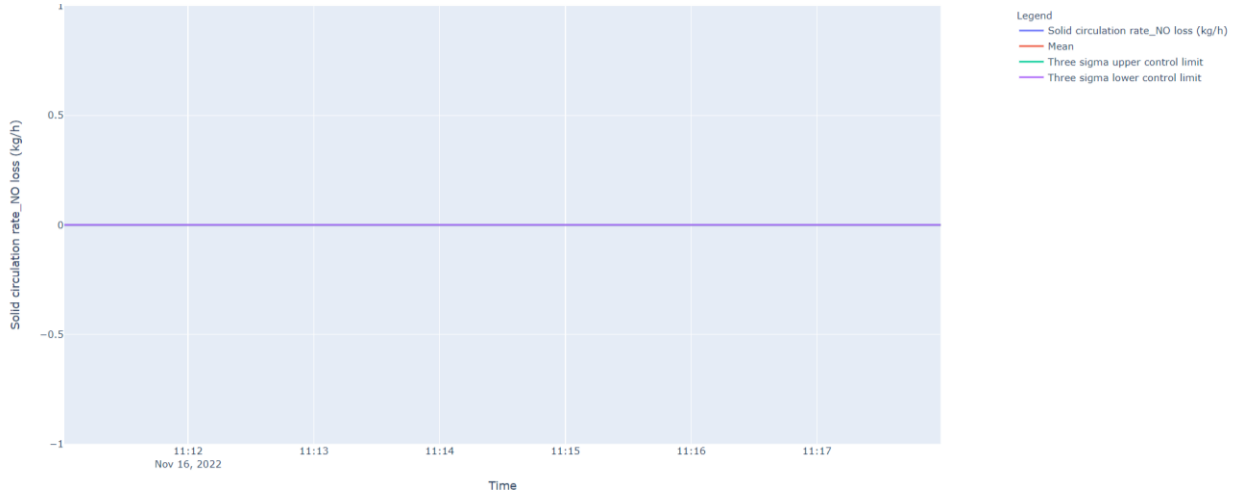

Figure 133. Timeseries graphs for solid circulation rate at the vertical purge tuyere condition (third repeat).

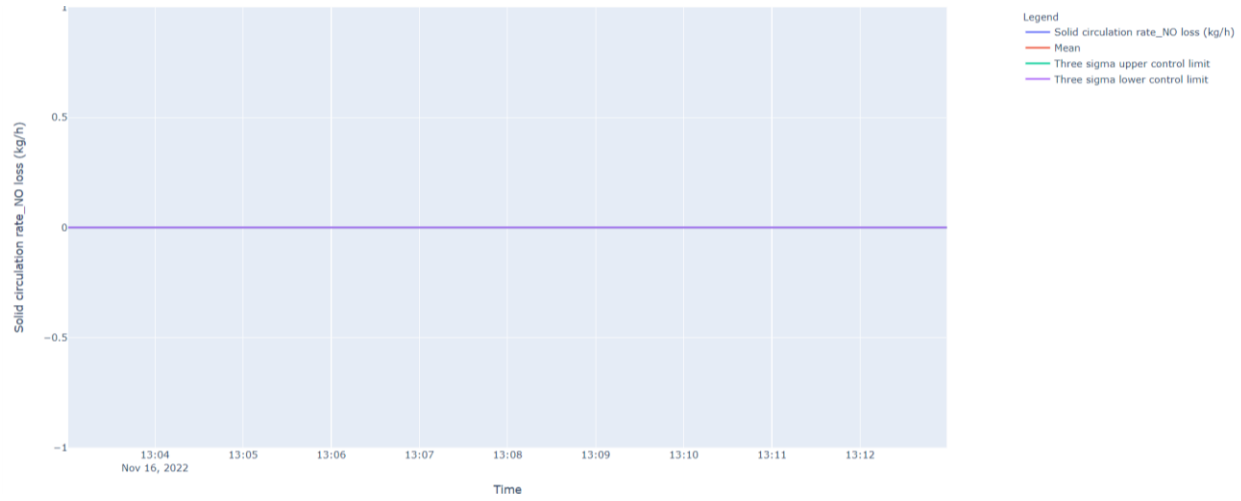

Figure 134. Timeseries graphs for solid circulation rate at the vertical purge tuyere condition (forth repeat).

Figure 135. Timeseries graphs for air reactor to fuel reactor gas leakage at the vertical purge tuyere condition (first repeat).

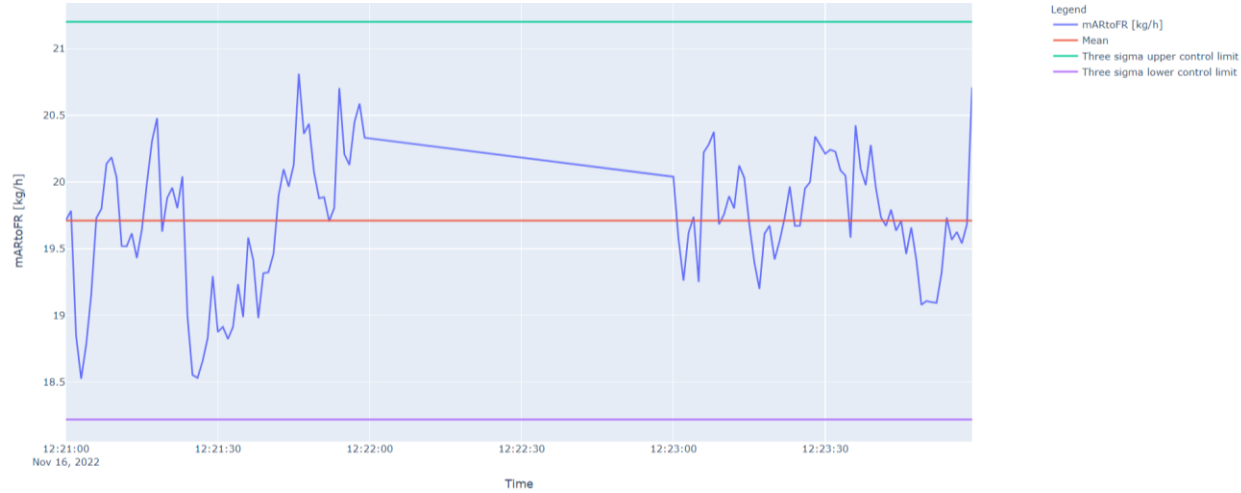

Figure 136. Timeseries graphs for air reactor to fuel reactor gas leakage at the vertical purge tuyere condition (second repeat).

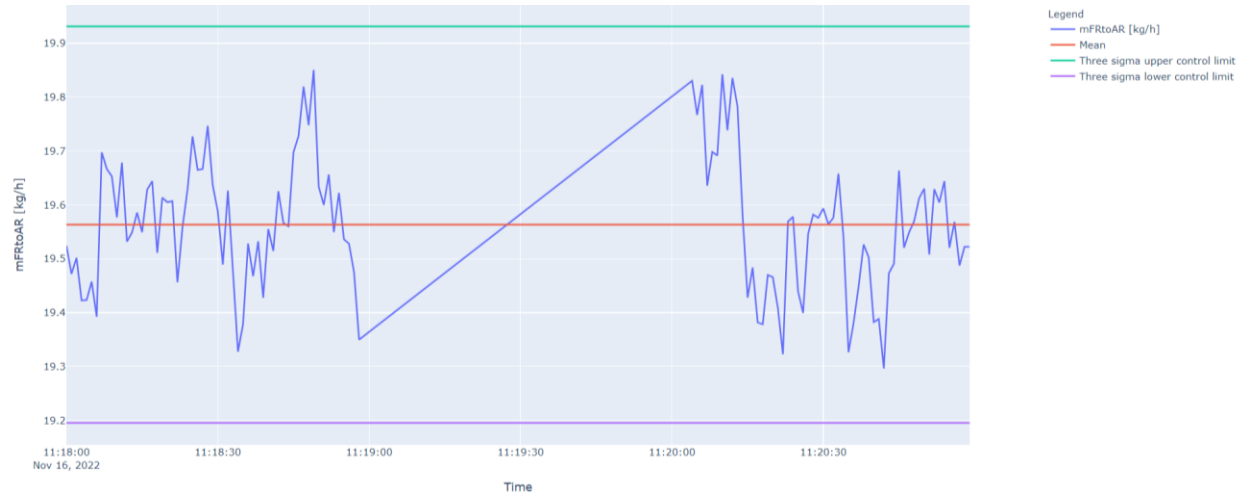

Figure 137. Timeseries graphs for fuel reactor to air reactor gas leakage at the vertical purge tuyere condition (first repeat).

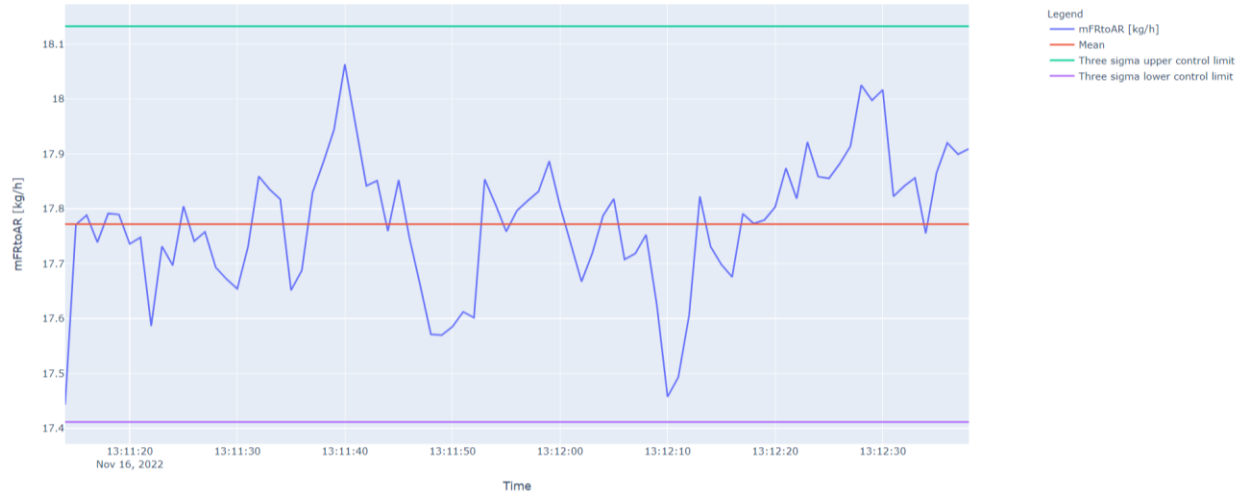

Figure 138. Timeseries graphs for fuel reactor to air reactor gas leakage at the vertical purge tuyere condition (second repeat).

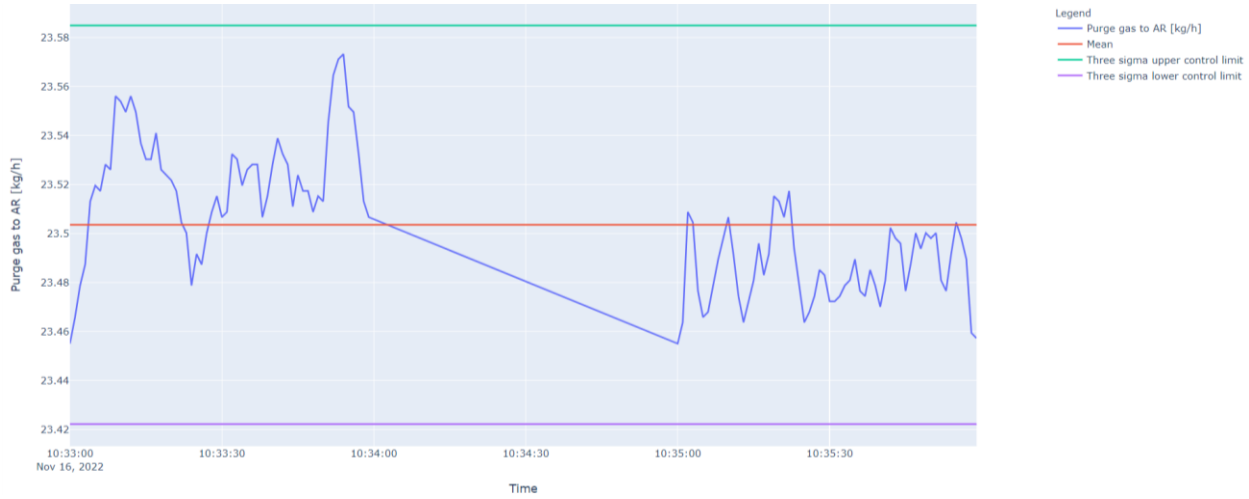

Figure 139. Timeseries graphs fate of the amount of AR/FR purge gas that remained in the air reactor at the vertical purge tuyere condition (first repeat).

Figure 140. Timeseries graphs fate of the amount of AR/FR purge gas that remained in the air reactor at the vertical purge tuyere condition (second repeat).

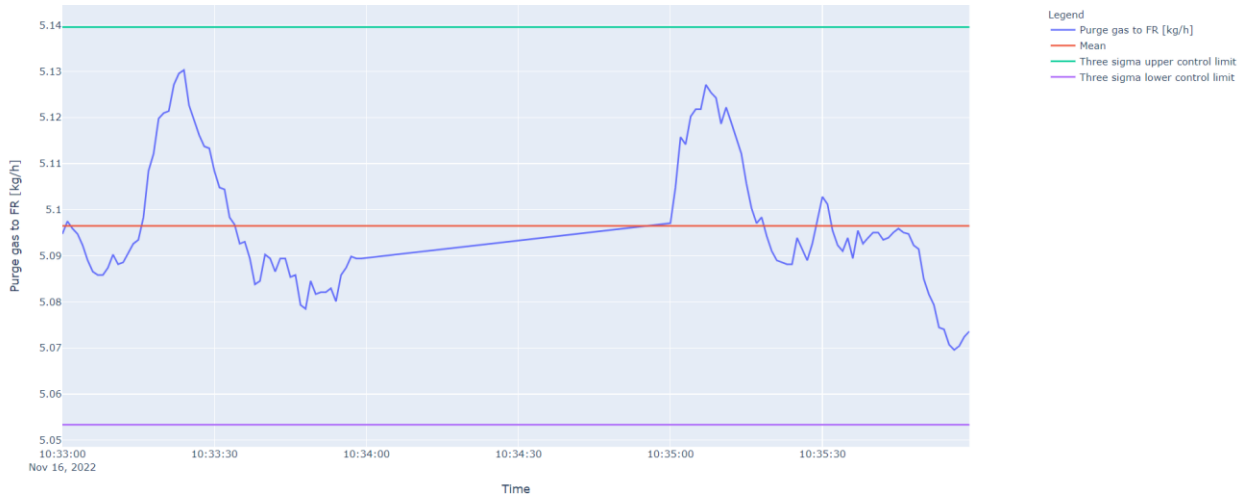

Figure 141. Timeseries graphs fate of the amount of AR/FR purge gas that moved to the fuel reactor at the vertical purge tuyere condition (first repeat).

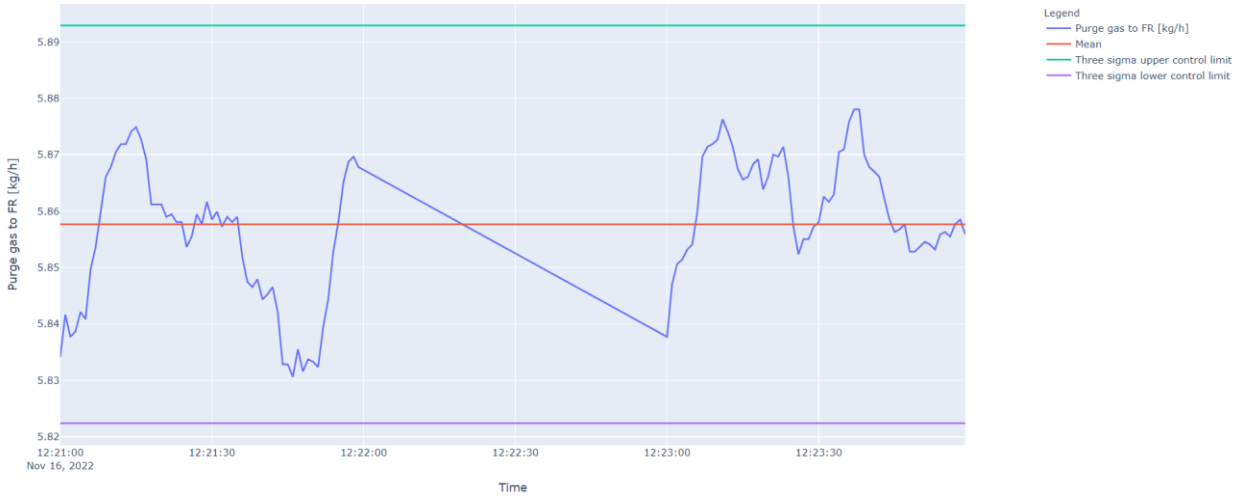

Figure 142. Timeseries graphs fate of the amount of AR/FR purge gas that moved to the fuel reactor at the vertical purge tuyere condition (second repeat).

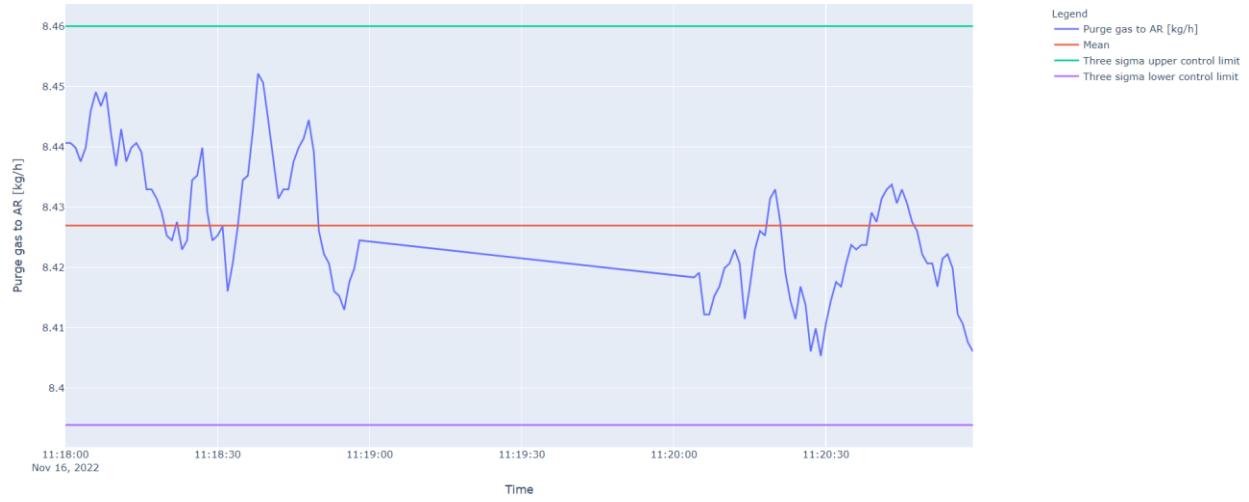

Figure 143. Timeseries graphs fate of the amount of FR/AR purge gas that moved to the air reactor at the vertical purge tuyere condition (first repeat).

Figure 144. Timeseries graphs fate of the amount of FR/AR purge gas that moved to the air reactor at the vertical purge tuyere condition (second repeat).

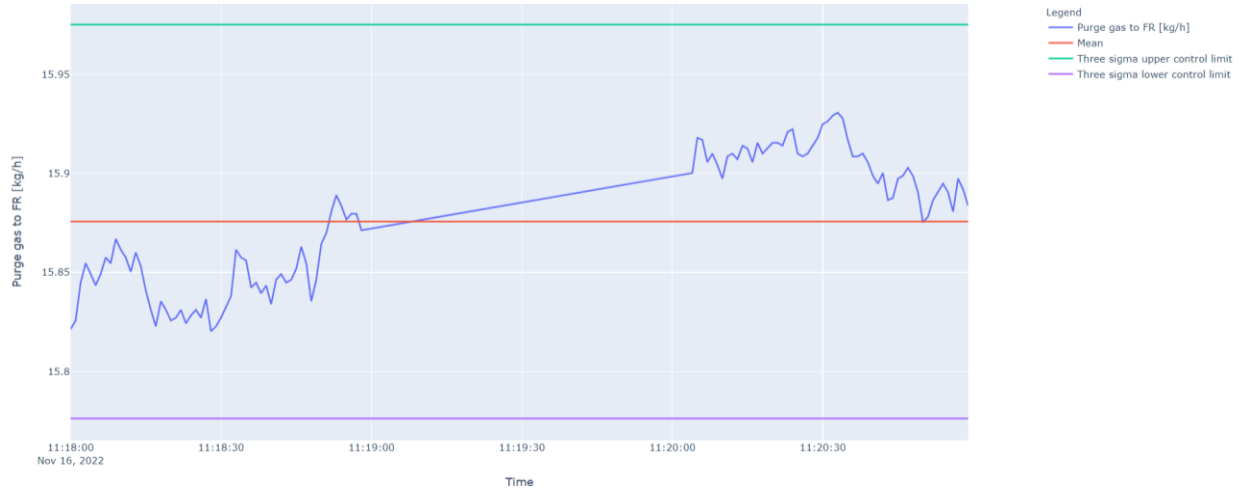

Figure 145. Timeseries graphs fate of the amount of FR/AR purge gas that remained in the fuel reactor at vertical purge tuyere condition (first repeat).

Figure 146. Timeseries graphs fate of the amount of FR/AR purge gas that remained in the fuel reactor at vertical purge tuyere condition (first repeat).

Figure 147. Timeseries graphs for solid circulation rate at the two AR/FR purge tuyere condition (first repeat).

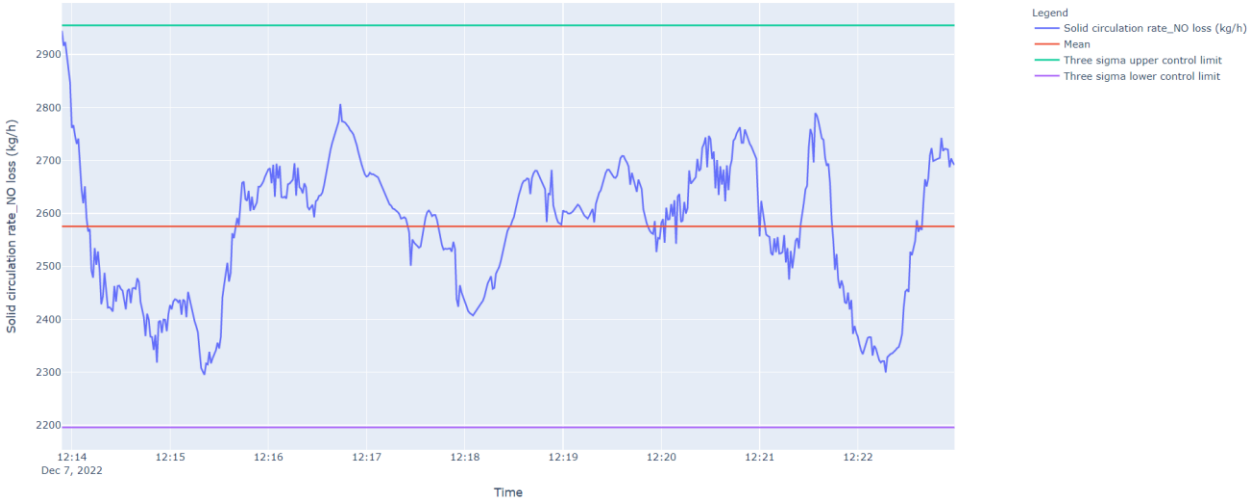

Figure 148. Timeseries graphs for solid circulation rate at the two AR/FR purge tuyere condition (second repeat).

Figure 149. Timeseries graphs for solid circulation rate at the two AR/FR purge tuyere condition (third repeat).

Figure 150. Timeseries graphs for solid circulation rate at the two AR/FR purge tuyere condition (forth repeat).

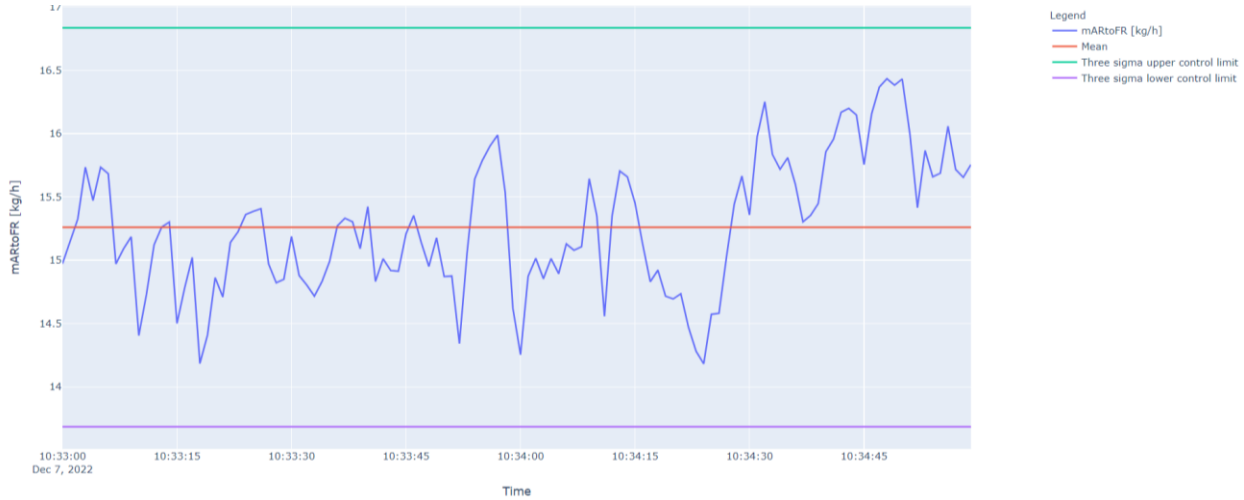

Figure 151. Timeseries graphs for air reactor to fuel reactor gas leakage at the two AR/FR purge tuyere condition (first repeat).

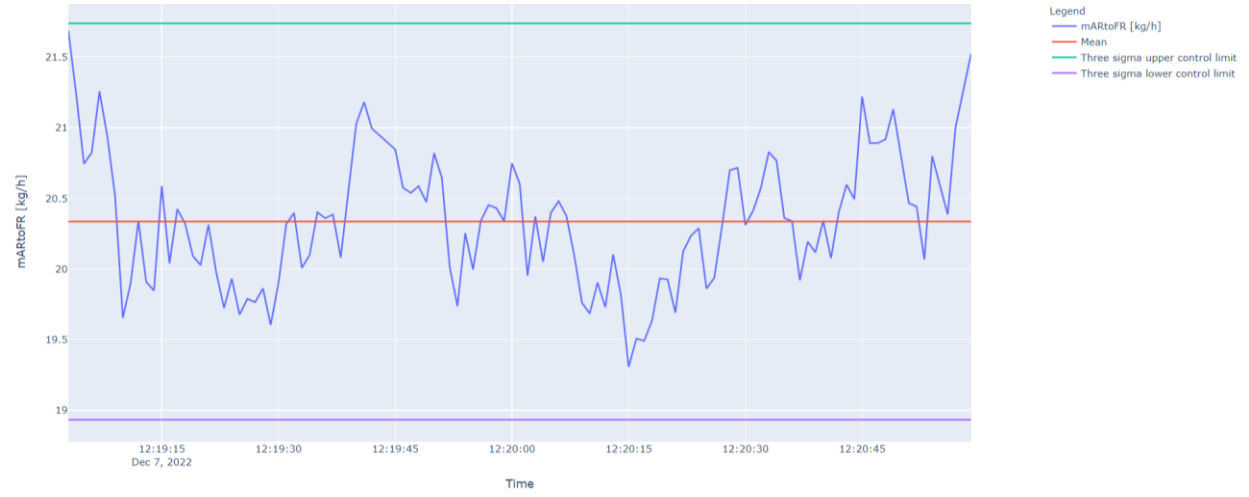

Figure 152. Timeseries graphs for air reactor to fuel reactor gas leakage at the two AR/FR purge tuyere condition (second repeat).

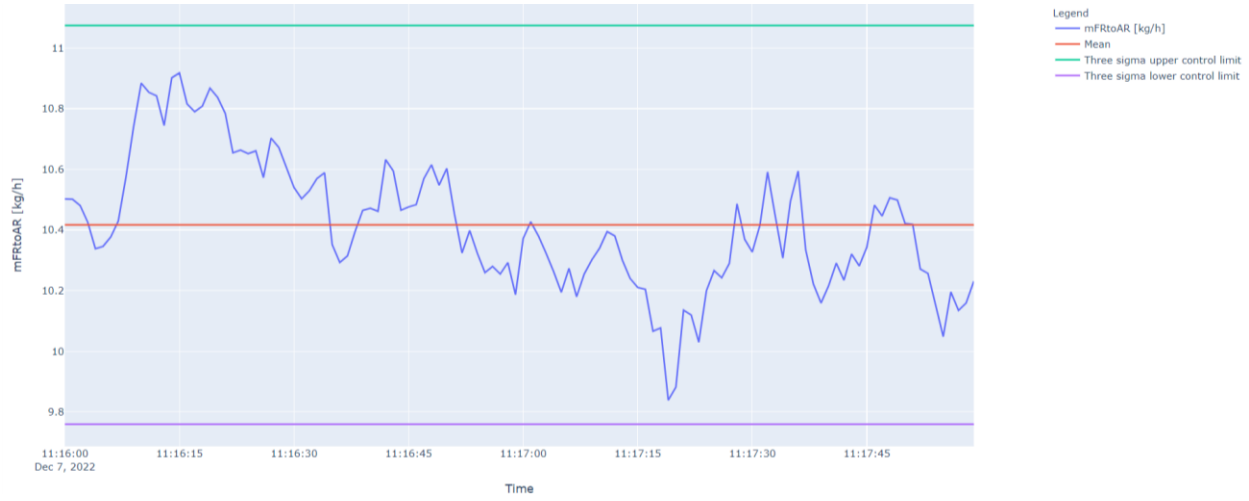

Figure 153. Timeseries graphs for fuel reactor to air reactor gas leakage at the two AR/FR purge tuyere condition (first repeat).

Figure 154. Timeseries graphs for fuel reactor to air reactor gas leakage at the two AR/FR purge tuyere condition (second repeat).

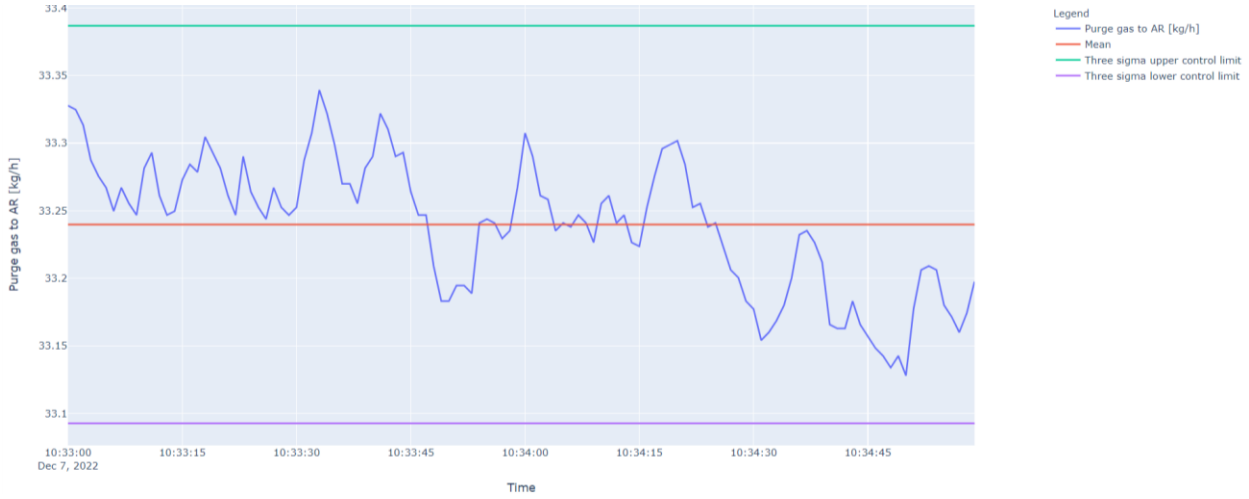

Figure 155. Timeseries graphs fate of the amount of AR/FR purge gas that remained in the air reactor at the two AR/FR purge tuyere condition (first repeat).

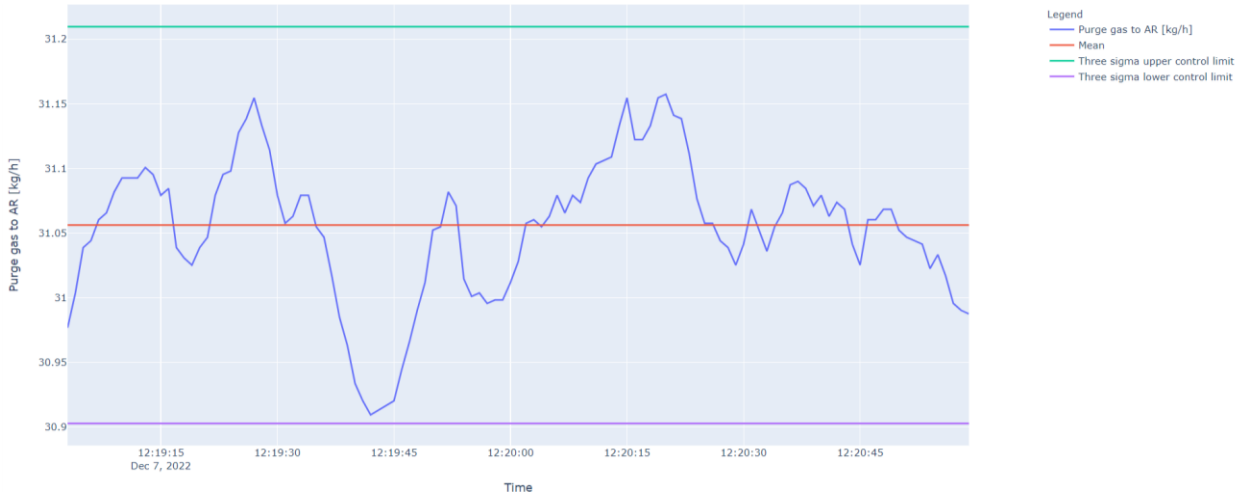

Figure 156. Timeseries graphs fate of the amount of AR/FR purge gas that remained in the air reactor at the two AR/FR purge tuyere condition (second repeat).

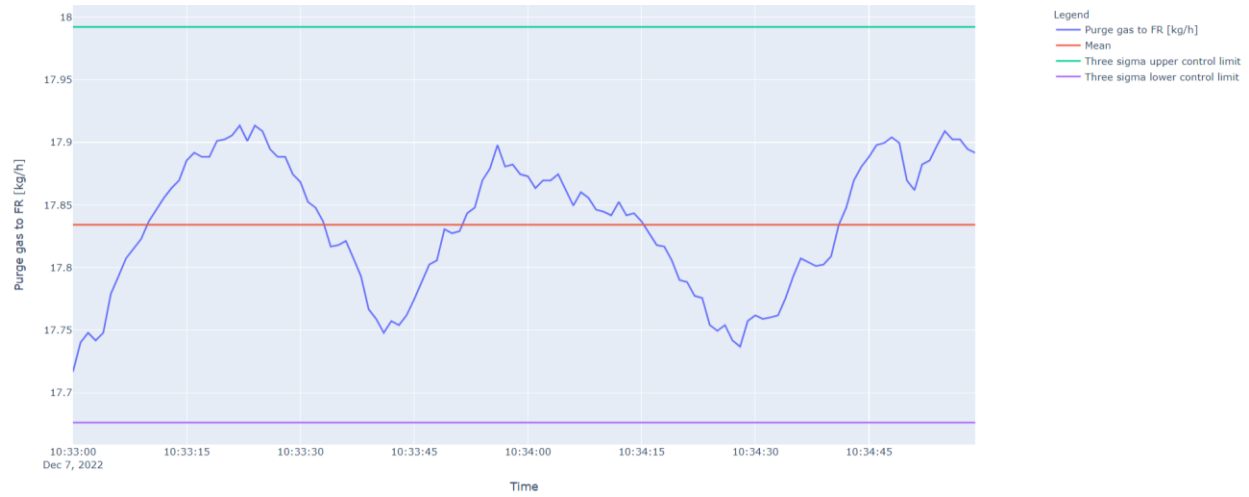

Figure 157. Timeseries graphs fate of the amount of AR/FR purge gas that moved to the fuel reactor at the two AR/FR purge tuyere condition (first repeat).

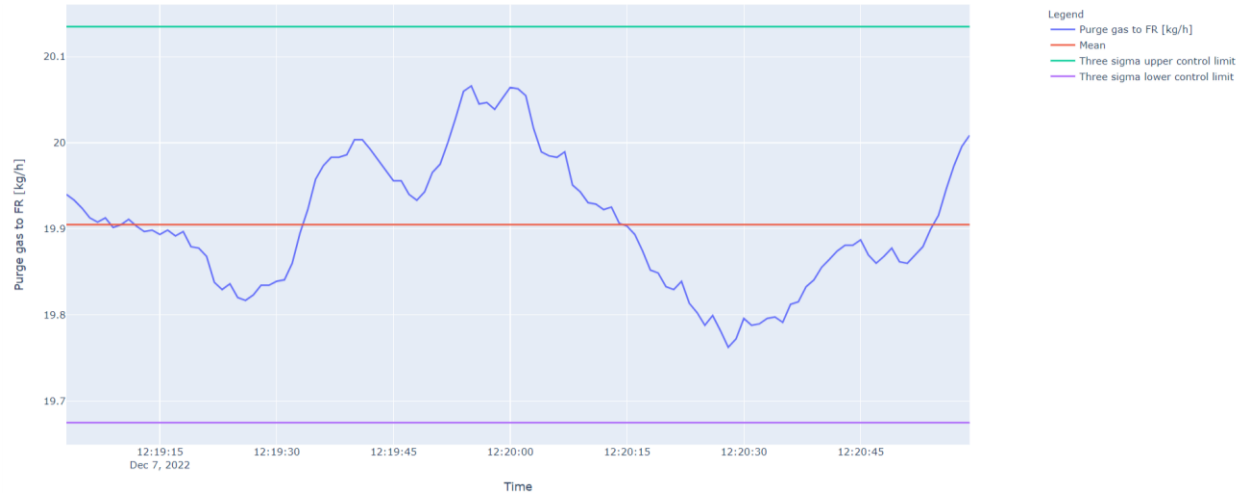

Figure 158. Timeseries graphs fate of the amount of AR/FR purge gas that moved to the fuel reactor at the two AR/FR purge tuyere condition (second repeat).

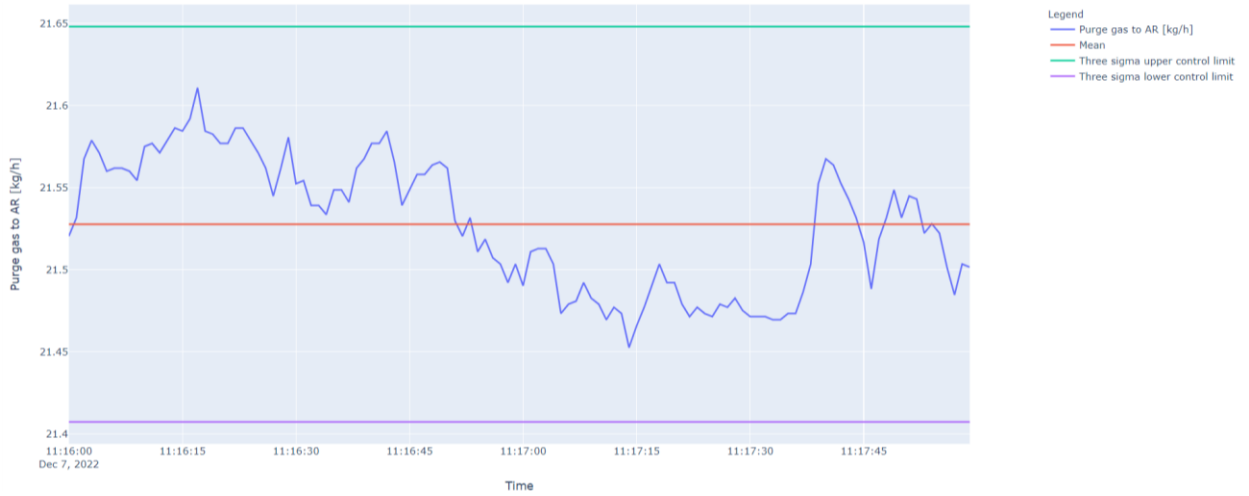

Figure 159. Timeseries graphs fate of the amount of FR/AR purge gas that moved to the air reactor at the two AR/FR purge tuyere condition (first repeat).

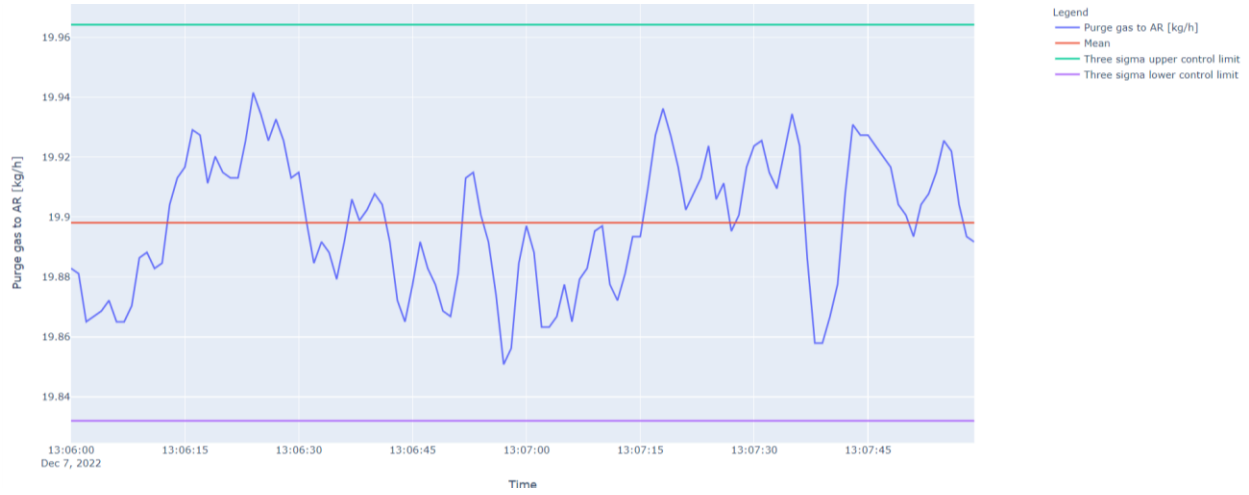

Figure 160. Timeseries graphs fate of the amount of FR/AR purge gas that moved to the air reactor at the two AR/FR purge tuyere condition (second repeat).

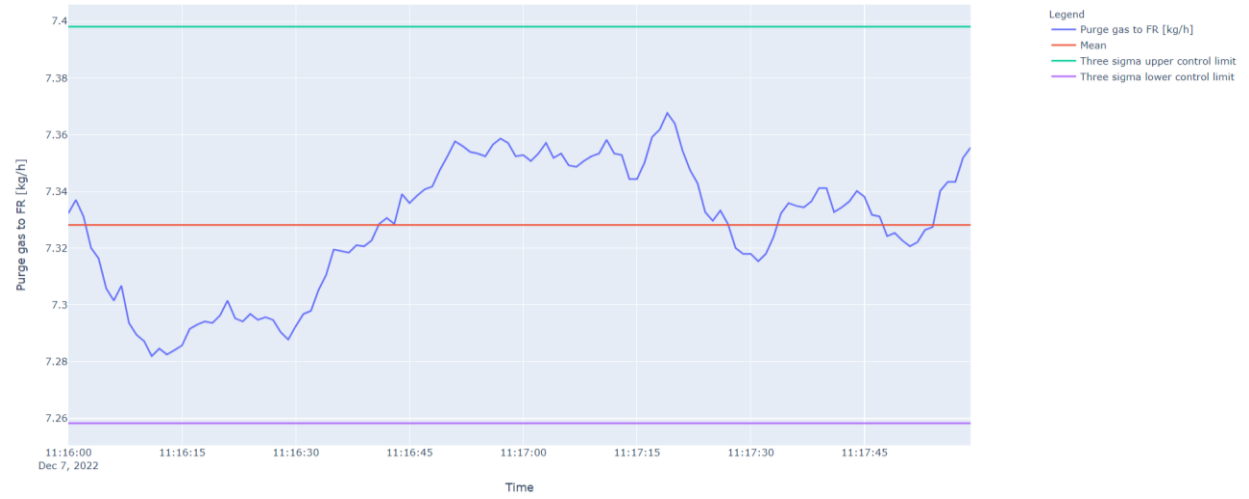

Figure 161. Timeseries graphs fate of the amount of FR/AR purge gas that remained in the fuel reactor at two AR/FR purge tuyere condition (first repeat).

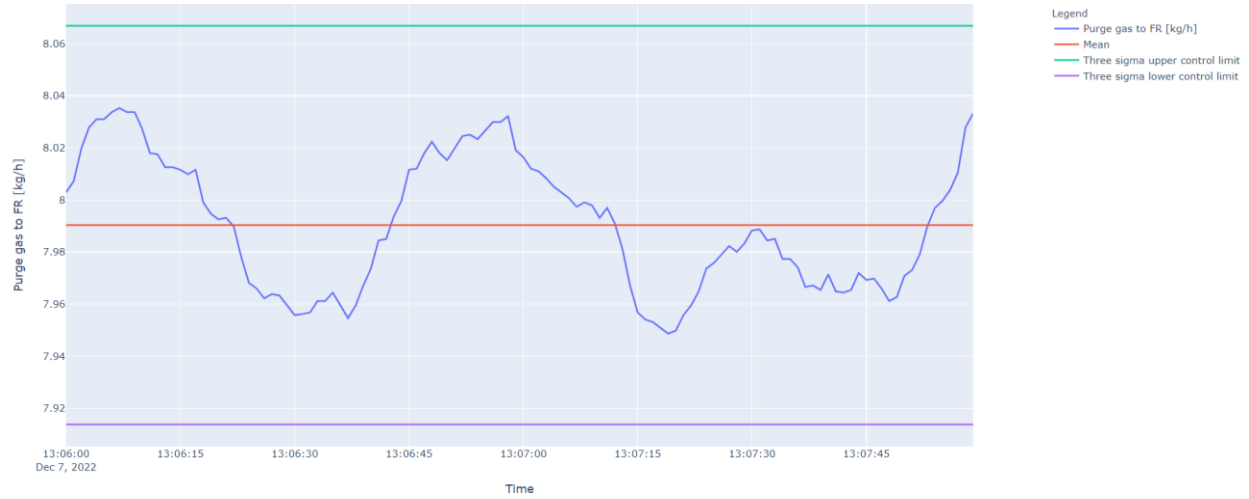

Figure 162. Timeseries graphs fate of the amount of FR/AR purge gas that remained in the fuel reactor at two AR/FR purge tuyere condition (first repeat).

Mean and population standard deviation for all data points

Table 16. Mean and population standard deviation of timeseries for solid circulation rate across all conditions.

Condition	Solid circulation rate [kg/h]	
	Mean	Standard deviation
Base case	2971	161
Base case	2966	197
Base case	2981	177
Base case	3302	159
Base case	3113	133
0.15 m bed height	4008	267
0.15 m bed height	3992	206
0.25 m bed height	3239	221
0.25 m bed height	3060	217
0.35 m bed height	3025	172
0.35 m bed height	3083	218
0.05 m weir opening height	1684	60
0.05 m weir opening height	1791	68
0.05 m weir opening height	1989	72
0.05 m weir opening height	1917	113
0.05 m weir opening height	1677	78
0.125 m weir opening height	2662	211
0.125 m weir opening height	2926	142
0.125 m weir opening height	2910	205
0.15 m weir opening height	3420	285
0.15 m weir opening height	3208	195
No purge	2016	94
No purge	2008	97
No purge	1936	73
Blanked purge	2146	413
Blanked purge	1902	473
Blanked purge	2290	610
Blanked purge	1641	303
Vertical purge	0	0
Vertical purge	0	0
Vertical purge	0	0
Vertical purge	0	0
Two AR/FR purge	2577	141
Two AR/FR purge	2575	127
Two AR/FR purge	2095	109
Two AR/FR purge	1983	104

Table 17. Mean and population standard deviation of timeseries for absolute gas leakage across all conditions.

Condition	Air reactor to fuel reactor gas leakage [kg/h]		Fuel reactor to air reactor gas leakage [kg/h]	
	Mean	Standard deviation	Mean	Standard deviation
Base case	23.6	0.5	11.9	0.2
Base case	31.0	0.6	16.8	0.2
Base case	N/A	N/A	9.8	0.3
0.15 m bed height	16.3	0.6	10.7	0.6
0.25 m bed height	16.2	0.6	11.4	0.7
0.35 m bed height	17.0	0.8	10.6	1.1
0.05 m weir opening height	11.7	0.7	8.2	0.1
0.05 m weir opening height	11.6	0.6	8.2	1.0
0.125 m weir opening height	13.4	0.9	14.6	0.4
0.125 m weir opening height	14.7	0.5	14.4	0.1
0.15 m weir opening height	12.7	1.1	14.7	0.2
0.15 m weir opening height	17.9	0.6	N/A	N/A
No purge	52.2	0.6	11.6	0.1
No purge	31.5	0.5	11.3	0.1
Blanked purge	11.8	0.6	1.0	0.2
Blanked purge	14.5	0.6	1.2	0.1
Vertical purge	23.5	0.5	19.6	0.1
Vertical purge	19.7	0.5	17.8	0.1
Two AR/FR purge	15.3	0.5	10.4	0.2
Two AR/FR purge	20.3	0.5	7.7	0.2

Table 18. Mean and population standard deviation of timeseries for percent of gas leakage across all conditions.

Condition	Air reactor to fuel reactor gas leakage [%]		Fuel reactor to air reactor gas leakage [%]	
	Mean	Standard deviation	Mean	Standard deviation
Base case	8.7	0.2	28.7	0.4
Base case	11.5	0.2	40.2	0.4
Base case	N/A	N/A	24.5	0.5
0.15 m bed height	6.2	0.2	25.6	1.1
0.25 m bed height	6.0	0.2	26.7	1.2
0.35 m bed height	6.3	0.3	26.2	2.2
0.05 m weir opening height	4.4	0.2	19.8	0.3
0.05 m weir opening height	4.3	0.2	19.8	2.0
0.125 m weir opening height	5.1	0.3	35.6	0.7
0.125 m weir opening height	5.5	0.2	34.1	0.2
0.15 m weir opening height	4.8	0.4	34.9	0.4
0.15 m weir opening height	6.7	0.2	N/A	N/A
No purge	19.7	0.2	28.3	0.2
No purge	11.8	0.2	27.3	0.3
Blanked purge	4.4	0.2	2.3	0.4
Blanked purge	5.4	0.2	2.8	0.3
Vertical purge	8.9	0.2	46.4	0.2
Vertical purge	7.6	0.2	42.8	0.2
Two AR/FR purge	5.7	0.2	24.8	0.4
Two AR/FR purge	7.5	0.2	19.0	0.4

Table 19. Mean and population standard deviation of timeseries for absolute AR/FR purge gas fate across all conditions.

Condition	AR/FR Purge that remained in air reactor [kg/h]		AR/FR Purge that moved to fuel reactor [kg/h]	
	Mean	Standard deviation	Mean	Standard deviation
Base case	8.24	0.01	16.36	0.05
0.15 m bed height	27.26	0.02	15.85	0.02
0.25 m bed height	11.11	0.01	16.42	0.03
0.35 m bed height	7.58	0.01	16.07	0.04
0.05 m weir opening height	7.25	0.01	17.12	0.03
0.05 m weir opening height	5.17	0.01	18.07	0.06
0.125 m weir opening height	11.48	0.02	14.79	0.02
0.125 m weir opening height	9.82	0.01	15.47	0.02
0.15 m weir opening height	11.72	0.01	14.75	0.03
0.15 m weir opening height	12.55	0.02	13.88	0.03
Vertical purge	23.50	0.03	5.10	0.01
Vertical purge	23.62	0.03	5.86	0.01
Two AR/FR purge	33.24	0.05	17.83	0.05
Two AR/FR purge	31.06	0.05	19.90	0.08

Table 20. Mean and population standard deviation of timeseries for percent AR/FR purge gas fate across all conditions.

Condition	AR/FR Purge that remained in air reactor [%]		AR/FR Purge that moved to fuel reactor [%]	
	Mean	Standard deviation	Mean	Standard deviation
Base case	33.49	0.04	66.51	0.21
0.15 m bed height	63.23	0.05	36.77	0.05
0.25 m bed height	40.36	0.04	59.64	0.10
0.35 m bed height	32.06	0.04	67.94	0.15
0.05 m weir opening height	29.75	0.03	70.25	0.14
0.05 m weir opening height	22.23	0.03	77.77	0.26
0.125 m weir opening height	43.70	0.06	56.30	0.09
0.125 m weir opening height	38.83	0.04	61.17	0.09
0.15 m weir opening height	44.26	0.05	55.74	0.11
0.15 m weir opening height	47.48	0.06	52.52	0.12
Vertical purge	82.18	0.09	17.82	0.05
Vertical purge	80.13	0.09	19.87	0.04
Two AR/FR purge	65.08	0.10	34.92	0.10
Two AR/FR purge	60.94	0.10	39.06	0.15

Table 21. Mean and population standard deviation of timeseries for absolute FR/AR purge gas fate across all conditions.

Condition	FR/AR Purge that moved to air reactor [kg/h]		FR/AR Purge that remained in fuel reactor [kg/h]	
	Mean	Standard deviation	Mean	Standard deviation
Base case	22.97	0.03	6.19	0.02
Base case	23.02	0.03	4.58	0.02
Base case	23.83	0.04	5.58	0.02
0.15 m bed height	24.75	0.03	3.60	0.01
0.25 m bed height	26.26	0.03	5.63	0.01
0.35 m bed height	21.73	0.03	5.59	0.02
0.05 m weir opening height	21.11	0.03	6.68	0.02
0.05 m weir opening height	21.30	0.04	6.30	0.03
0.125 m weir opening height	22.44	0.04	7.62	0.03
0.125 m weir opening height	21.52	0.03	7.24	0.02
0.15 m weir opening height	20.44	0.03	6.69	0.02
Vertical purge	8.43	0.01	15.88	0.03
Vertical purge	7.58	0.01	16.99	0.04
Two AR/FR purge	21.53	0.04	7.33	0.02
Two AR/FR purge	19.90	0.02	7.99	0.03

Table 22. Mean and population standard deviation of timeseries for percent FR/AR purge gas fate across all conditions.

Condition	FR/AR Purge that moved to air reactor [%]		FR/AR Purge that remained in fuel reactor [%]	
	Mean	Standard deviation	Mean	Standard deviation
Base case	78.77	0.09	21.23	0.06
Base case	83.40	0.11	16.60	0.05
Base case	81.02	0.13	18.98	0.05
0.15 m bed height	87.30	0.12	12.70	0.02
0.25 m bed height	82.34	0.09	17.66	0.03
0.35 m bed height	79.54	0.13	20.46	0.07
0.05 m weir opening height	75.96	0.10	24.04	0.06
0.05 m weir opening height	77.17	0.16	22.83	0.09
0.125 m weir opening height	74.64	0.13	25.36	0.10
0.125 m weir opening height	74.82	0.10	25.18	0.06
0.15 m weir opening height	75.35	0.12	24.65	0.07
Vertical purge	34.67	0.04	65.33	0.13
Vertical purge	30.86	0.02	69.14	0.17
Two AR/FR purge	74.60	0.14	25.40	0.08
Two AR/FR purge	71.35	0.08	28.65	0.09

Tukey's HSD test results tables

Table 23. In-depth results from Tukey's HSD test for multiple comparisons comparing the effect of static bed height on solid circulation rate. The p value is reported, followed by the 95% confidence interval in square brackets.

	0.15 m	**0.25 m**	**0.35 m**	**0.5 m**
0.15 m	-	0.0009	0.0005	0.0002
		[-1249.4, -451.3]	[-1345.0, -546.9]	[-1267.0, -599.3]
0.25 m	0.0009	-	0.86	0.84
	[-1249.4, -451.3]		[-494.6, 303.5]	[-416.6, 251.1]
0.35 m	0.0005	0.86	-	1.0
	[-1345.0, -546.9]	[-494.6, 303.5]		[-321.1, 346.7]
0.5 m	0.0002	0.84	1.0	-
	[-1267.0, -599.3]	[-416.62, 251.1]	[-321.1, 346.7]	

Table 24. In-depth results from Tukey's HSD test for multiple comparisons comparing the effect of weir opening height on solid circulation rate. The p value is reported, followed by the 95% confidence interval in square brackets.

	0.05 m	**0.1 m**	**0.125 m**	**0.15 m**
0.05 m	-	0.0 [981.1, 1528.9]	0.0 [704.8, 1337.3]	0.0 [1140.1, 1864.7]
0.1 m	0.0 [981.1, 1528.9]	-	0.18 [-550.2, 82.3]	0.23 [-114.9, 609.7]
0.125 m	0.0 [704.8, 1337.3]	0.18 [-550.2, 82.3]	-	0.017 [86.0, 876.7]
0.15 m	0.0 [1140.1, 1864.7]	0.23 [-114.9, 609.7]	0.017 [86.0, 876.7]	-

Table 25. In-depth results from Tukey's HSD test for multiple comparisons comparing the effect of purge configuration on solid circulation rate. The p value is reported, followed by the 95% confidence interval in square brackets.

	No purge row	**One blank purge row**	**One purge row**	**Two AR/FR purge rows, one FR/AR purge row**	**One vertical purge row**
No purge row	-	1.0 [-489.8, 473.7]	0.0 [619.3, 1540.6]	0.29 [-160.7, 802.9]	0.0 [-2468.4, -1504.8]
One blank purge row	1.0 [-489.8, 473.7]	-	0.0 [648.7, 1495.0]	0.24 [-133.9, 759.1]	0.0 [-2440.7, -1548.6]
One purge row	0.0 [619.3, 1540.6]	0.0 [648.7, 1495.0]	-	0.0005 [-1182.0, -335.7]	0.0 [-3489.7, -2643.4]
Two AR/FR purge rows, one FR/AR purge row	0.29 [-160.7, 802.9]	0.24 [-133.9, 759.1]	0.0005 [-1182.0, -335.7]	-	0.0 [-2753.7, -1861.7]
One vertical purge row	0.0 [-2468.4, -1504.8]	0.0 [-2440.7, -1548.6]	0.0 [-3489.7, -2643.4]	0.0 [-2753.7, -1861.7]	-

Table 26. In-depth results from Tukey's HSD test for multiple comparisons comparing the effect of weir opening height on air to fuel reactor gas leakage. The p value is reported, followed by the 95% confidence interval in square brackets.

	0.05 m	**0.1 m**	**0.125 m**	**0.15 m**
0.05 m	-	0.03	0.87	0.69
		[2.5, 28.8]	[-10.7, 15.6]	[-9.5, 16.9]
0.1 m	0.028	-	0.049	0.07
	[2.5, 28.8]		[-26.4, -0.1]	[-25.1, 1.2]
0.125 m	0.87	0.049	-	0.98
	[-10.7, 15.6]	[-26.4, -0.1]		[-11.9, 14.4]
0.15 m	0.69	0.07	0.98	-
	[-9.5, 16.9]	[-25.1, 1.2]	[-11.9, 14.4]	

Table 27. In-depth results from Tukey's HSD test for multiple comparisons comparing the effect of purge configuration on fuel reactor to air reactor gas leakage. The p value is reported, followed by the 95% confidence interval in square brackets.

	No purge row	**One blank purge row**	**One purge row**	**Two AR/FR purge rows**	**One vertical purge row**
No purge row	-	0.02	1.0	0.8	0.10
		[1.7, 19.0]	[-6.4, 9.2]	[-11.0, 6.2]	[-1.4, 15.8]
One blank purge	0.02	-	0.008	0.07	0.002
row	[1.7, 19.0]		[4.0, 19.6]	[-0.6, 16.6]	[9.0, 26.2]
One purge row	1.0	0.008	-	0.44	0.15
	[-6.4, 9.2]	[4.0, 19.6]		[-11.6, 4.0]	[-2.0, 13.6]
Two AR/FR purge	0.8	0.07	0.44	-	0.03
rows	[-11.0, 6.2]	[-0.6, 16.6]	[-11.6, 4.0]		[1.0, 18.2]
One vertical	0.10	0.002	0.15	0.03	-
purge row	[-1.4, 15.8]	[9.0, 26.2]	[-2.0, 13.6]	[1.0, 18.2]	

Table 28. In-depth results from Tukey's HSD test for multiple comparisons comparing the effect of weir opening height on percent of AR/FR purge gas that moved into the fuel reactor. The p value is reported, followed by the 95% confidence interval in square brackets.

	0.05 m	**0.1 m**	**0.125 m**	**0.15 m**
0.05 m	-	0.50	0.08	0.04
		[-30.5, 15.5]	[-34.0, 3.5]	[-38.6, -1.1]
0.1 m	0.50	-	0.48	0.22
	[-30.5, 15.5]		[-30.7, 15.2]	[-35.3, 10.6]
0.125 m	0.08	0.48	-	0.67
	[-34.0, 3.5]	[-30.7, 15.2]		[-23.4, 14.1]
0.15 m	0.04	0.22	0.67	-
	[-38.6, -1.1]	[-35.3, 10.6]	[-23.4, 14.1]	

Table 29. In-depth results from Tukey's HSD test for multiple comparisons comparing the effect of weir opening height on percent of FR/AR purge gas that moved into the air reactor. The p value is reported, followed by the 95% confidence interval in square brackets.

	0.05 m	**0.1 m**	**0.125 m**	**0.15 m**
0.05 m	-	0.14	0.72	0.93
		[-1.8, 10.8]	[-8.7, 5.1]	[-9.7, 7.2]
0.1 m	0.14	-	0.049	0.13
	[-1.8, 10.8]		[-12.6, 0.0]	[-13.7, 2.3]
0.125 m	0.72	0.05	-	0.99
	[-8.7, 5.1]	[-12.6, 0.0]		[-7.8, 9.1]
0.15 m	0.93	0.13	0.99	-
	[-9.7, 7.2]	[-13.7, 2.3]	[-7.8, 9.1]	

Table 30. In-depth results from Tukey's HSD test for multiple comparisons comparing the effect of purge fate on percent of AR/FR purge gas that moved into the fuel reactor. The p value is reported, followed by the 95% confidence interval in square brackets.

	One purge row	**Two AR/FR purge rows**	**One vertical purge row**
One purge row	-	0.02 [-46.2, -12.9]	0.006 [-64.3, -31.0]
Two AR/FR purge rows	0.02 [-46.2, -12.9]	-	0.03 [-31.8, -4.5]
One vertical purge row	0.02 [-46.2, -12.9]	0.03 [-31.8, -4.5]	-

Table 31. In-depth results from Tukey's HSD test for multiple comparisons comparing the effect of purge fate on percent of FR/AR purge gas that moved into the air reactor. The p value is reported, followed by the 95% confidence interval in square brackets.

	One purge row	**Two AR/FR purge rows**	**One vertical purge row**
One purge row	-	0.05 [-16.0, -0.2]	0.0001 [-56.2, -40.4]
Two AR/FR purge rows	0.05 [-16.0, -0.2]	-	0.0002 [-48.8, -31.6]
One vertical purge row	0.0001 [-56.2, -40.4]	0.0002 [-48.8, -31.6]	-

Appendix B: Solid circulation rate methods that were considered

To determine the solid circulation rate in the PFIR column, several solid circulation rate methods were considered: inductance particle tracking, magnetic particle tracking, radioactive particle tracking, and heated particle tracking. Ideally, the chosen solid circulation rate measurement technique would be simple to implement, non-invasive, have a tracer that is similar to the bed material, and be robust.

The first technique that was considered, was inductance particle tracking. Inductance particle tracking is generally a non-invasive bulk particle tracking technique. The tracer particles are generally ferromagnetic particles, that fluidize similarly to the particle of interest [19]–[23]. The sensor is a coil that detects the tracer concentration by responding to changes in the coil's magnetic field caused by the presence of the tracer. Inductance is a property of an inductor that indicates the amount of energy that can be stored as a magnetic field. Furthermore, self-inductance occurs when a changing current in a wire alters the voltage in that wire. The inductance of an inducer varies with its geometry and the permeability of its core. Permeability is a magnetic property related to a material's ability to form an internal magnetic field. These properties can change the impedance of a coil, allowing for a quantitative way to determine the amount of magnetic material present in or near the coil.

In this method, the coil inductance is correlated with a concentration of tracer. Since this method uses ferromagnetic and/or conductive tracer particles, there can be no metal in the vicinity of the coil, or it will cause the noise floor in the signal to increase. In previous work, the coil is wrapped around an area of interest, such as a loop seal [23] or the entire bed[21], [22], or directly inserted into the fluidized bed [19], [20]. Unfortunately, in the PFIR column, there was no place to wrap a coil near the weir openings. Instead of wrapping the coil, a flat coil could be placed on the inner and outer walls of the annulus, with some number of flat coils in the middle of the flow path. The flat coils would be placed parallel to the solids flow path to prevent affecting the solid circulation. After some tests, it was determined that using a flat coil introduces a distance dependence to the inductance measurement[24]. Decoupling concentration and distance would be a large research and development endeavour, so it was at this point it was decided to not continue with this method.

The next method that was considered was magnetic particle tracking. Magnetic particle tracking is also typically a non-invasive method, but tracks a single particle instead of a packet of tracer particles. The tracer is a single magnet that can be encased in epoxy to better ensure that the magnetic tracer particle acts similarly in a fluidized bed [25]–[27]. The sensors used for magnetic particle tracking is anisotropic

magnetoresistive sensors. These sensors measure the change in magnetic field due to the location of the tracer magnet. With several sensors and a large enough magnet, the position of the tracer can be triangulated with good precision. It also requires that there are no ferromagnetic materials near the sensors or the PFIR column to prevent interference with the tracer. Typically, magnetic particle tracking is used to track larger particles, such as fuel particles, and is not used to track the bed material itself [25], [26]. In the cold-flow PFIR column, the bulk bed material needs to be tracked, so a micro magnet must be used to ensure they fluidize similarly compared to the bed material. Due to their small volume, the signal strength is significantly decreased and sensors must be placed at the inner and outer wall of the PFIR column as well as inside the flow path at the weir opening to detect the passage of the magnet [28]. Developing sensors that can be placed within the PFIR column requires a considerable time and money investment, so this measurement method was not pursued further.

The third solid circulation rate measurement that was considered was radioactive particle tracking. Radioactive particle tracking is a non-invasive single particle tracking technique that tracks the particle throughout the entire column with enough sensors. It requires increased safety precautions compared to the other techniques and has a more involved data analysis as the signal strength of the tracer decreases with time. The tracer is a radioactive particle, and the sensors are scintillation detectors [29]. The tracer particle is typically used to replace large particles and are encased to ensure the tracer fluidizes similarly [30]. The scintillation detectors detect ionizing radiation from the tracer particle and correlates the number of photons it receives to a tracer particle position and distance [30]. For the cold-flow PFIR column, very small particles are needed, which will decrease the amount of ionizing radiation compared to larger particles. On the other hand, this technique is normally performed with metal reactors, rather than plastic, which means the signal will be far less attenuated in the PFIR column compared to a similarly sized metal column[31]. For this reason, radioactive particle tracking could be implemented into the PFIR column, but the logistics of getting the proper paperwork completed and getting this test work done would take too much time to complete, so radioactive particle tracking was not pursued further.

The final method that was considered was heated particle tracking. Heated particle tracking is a more invasive bulk particle tracking method that is very simple to implement. It uses a heater to heat particles in the fuel reactor and RTDs to measure the temperature of the solids and gas entering and exiting the fuel reactor. An energy balance can be used to calculate the solid circulation rate. This method does have a slightly higher uncertainty compared to the other methods, especially radioactive particle tracking, but

this method can give a coarse idea of solid circulation rate. Since the overall goal of the cold-flow PFIR column is to validate the CPFD model, a coarse idea of the solid circulation rate is sufficient.